NAFEMS

Conference Proceedings

MULTIPHYSICS Conference 2024

21-23 October 2024 | Singapore

NAFEMS

Conference Sponsors

ALTAIR

Ansys

BETA SIMULATION SOLUTIONS

DASSAULT SYSTEMES

QUANSCIENT

ISBN 978-1-83979-235-9

THE INTERNATIONAL ASSOCIATION FOR THE ENGINEERING MODELLING, SIMULATION, AND ANALYSIS COMMUNITY.

ORGANIZED BY

THE INTERNATIONAL ASSOCIATION FOR THE ENGINEERING MODELLING, SIMULATION, AND ANALYSIS COMMUNITY.

ISBN 978-1-83979-235-9

EXHIBITORS


ALTAIR


Ansys


BETA
SIMULATION SOLUTIONS


CADIT


DASSAULT SYSTEMES


DAZZTECH
Empowering Smart Digital Twins


NAFEMS


QUANSCIENT


SCx
Solutions
HEXAGON

CONTENTS

Contents

Conference Sponsors

Altair is a global leader in computational intelligence that provides software and cloud solutions in simulation, high-performance computing (HPC), data analytics, and AI. Altair enables organizations across all industries to compete more effectively and drive smarter decisions in an increasingly connected world – all while creating a greener, more sustainable future. To learn more, please visit:

www.altair.com

Ansys, Inc. is an American multinational company with its headquarters based in Canonsburg, Pennsylvania. It develops and markets engineering simulation software for product design, testing, manufacturing, and operation and offers its products and services to customers worldwide across industries. When visionary companies need to know how their world-changing ideas will perform, they close the gap between design and reality with Ansys simulation. For more than 50 years, Ansys software has enabled innovators across industries to push boundaries by using the predictive power of simulation. From sustainable transportation to advanced semiconductors, from satellite systems to life-saving medical devices, the next great leaps in human advancement will be powered by Ansys. 50 Years of Simulation , Innovation and Leadership

www.ansys.com

BETA is an engineering simulation solutions provider, dedicated to the development of state of the art software systems. For more than 30 years, we have been developing software and delivering services for the front runners of numerous sectors, by listening to their needs and taking up even the most demanding challenges. Committed to our mission to enable engineers to deliver results of high value, we continue to offer state-of-the-art, high-performance software and best-in-class services. Our simulation solutions liberate low risk and high Return-On-Investment innovation. The ground-breaking technology, the excellent services and our high standards of business ethics are the three pillars on which BETA was founded and grows since then.

www.beta-cae.com

Conference Sponsors

Dassault Systèmes is a catalyst for human progress. We provide businesses and people with collaborative virtual environments to imagine sustainable innovations. By creating 'virtual experience twins' of the real world with our 3DEXPERIENCE platform and applications, our customers push the boundaries of innovation, learning and production. Dassault Systèmes' 20,000 employees are bringing value to more than 270,000 customers of all sizes, in all industries, in more than 140 countries. For more information, visit:

www.3ds.com

QUANSCIENT

Quanscient Allsolve is a cloud-based FEM multiphysics simulation software allowing our users to solve 10x more accurate multiphysics simulations 10x faster. With proven speedups from weeks to hours in large-scale multiphysics simulations and the ability to run hundreds of simulations in parallel, Quanscient Allsolve has helped our customers accelerate their design cycle saving months in product development time compared to existing alternatives through more accurate simulations in sheer massive scale powered by the cloud. This enables faster and more efficient analyses of large-scale 3D simulations with up to hundreds of millions of degrees of freedom, saving our customers money in both the simulations themselves as well as through a faster go-to-market with new products. Quanscient Allsolve: FEM Multiphysics in the cloud.

www.quanscient.com

The Role of Multiphysics in the Digital Transformation of the Vehicle Design Cycle

Alfred Svobodnik (Mvoid Group);

Mario J. Felice (Virsoltec/NAFEMS Technical Fellow, formerly Ford)

Solder Joint Reliability Workflow Automation for a Ball-Grid Array (BGA) Package

Kajal Khan, Rajesh Meena, Akhil KS, Bharat Deorukhkar (Ansys Software Pvt. Ltd., India)

Abstract: Solder joint reliability is a critical aspect of electronic packaging, and accurate simulation is essential for ensuring product performance and durability. This work presents an automated workflow developed for solder joint reliability simulation of a ball-grid array (BGA) package using multiple Ansys tools. The major challenge for solder joint reliability simulation is the expertise required for multiple tools and the extensive time needed for an end-to-end manual workflow, which is typically in the order of 3-4 weeks. The proposed workflow streamlines the simulation process by automating key steps such as ECAD to MCAD conversion in Ansys Sherlock, geometry preparation in Ansys Discovery, mesh generation, material assignment, boundary condition, setup, and post-processing in Ansys Mechanical. Additionally, temperature from Ansys Icepak can be read into the workflow to define accurate thermal cycling. The newly developed solder fatigue application features a sophisticated user interface built using the PySide6 module, ensuring a user-friendly and intuitive experience. To secure the source code and enable unique deployment, the entire application is packaged as a binary extension (.wbex) file created with the Ansys ACT framework. This design facilitates seamless PyAnsys deployment and adoption, integrating open-source technologies to support a scalable workflow. The application interfaces with multiple Ansys products, including Ansys Workbench, Ansys Sherlock, Ansys Discovery, and Ansys Mechanical, leveraging PyAnsys modules such as pyworkbench, pysherlock, pyansysgeometry, and pymechanical. This backend integration ensures robust functionality, allowing the application to be easily integrated into various environments and invoked from any interface, providing a comprehensive solution for solder fatigue analysis. This automated workflow eliminates the need for specialized expertise and reduces turnaround time by at least 10X.

Keywords: Workflow Automation, Multiphysics, Electronics Reliability, Ball grid array (BGA), Thermo-Mechanical analysis, Material nonlinearity, PyAnsys

1 Introduction

The increasing use of electronic components across industries is well recognized, driven by advancements in smart, connected products and their integration into digital innovations like the Internet of Things (IoT) [1]. As a result, these components are now being utilized in much harsher environments, with rising power densities contributing to more complex challenges. Stricter environmental regulations also promote the adoption of eco-friendly materials, such as lead-free solder alloys for solder balls. These harsher conditions and new material requirements necessitate a comprehensive understanding of the behavior of electronic components at multiple levels to ensure robustness and reliability in design [2, 3]. One critical failure mode for which design studies are done is the thermo-mechanical fatigue of the solder balls. Various standards like the JESD22-A104C [4] prescribe accelerated cyclic thermal testing for fatigue. These tests simulate the cyclical thermal variations experienced by the assembly, ranging from low temperatures (~ -40°C) to high temperatures (~ 125°C), with dwell periods at both extremes. This aggressive thermal testing enables the testing of the material behavior which is function of temperature. The stresses and strains that develop during the cycling initiate cracks inside the solder and over time cause failure [5]. In this paper, a finite element approach is used to model the solder joint failure in an electronics assembly consisting of a ball grid array (BGA) package. This work introduces an automated workflow designed for solder joint reliability simulation of a ball-grid array (BGA) package using multiple Ansys tools. One of the main challenges in such simulations is the need for expertise across different tools and the considerable time required to manually complete the process, typically taking 3-4 weeks. The proposed workflow addresses these issues by automating key steps, significantly streamlining the simulation process. Lifing models are finally used to correlate the stress and strain field to cycles to failure of the BGA package.

2 Workflow Automation for Finite Element Modeling of BGA Package

A printed circuit board (PCB) assembly along with the cross-sectional view of the BGA package considered for the present study has been presented in Figure 1(a). In this study, one ball grid array

(BGA) package with 256 solder balls is modeled using a commercial finite element software ANSYS® [6]. Figure 1(b) shows the cross-section of the BGA package with different components. This solution is generic and not limited to only this PCB assembly.

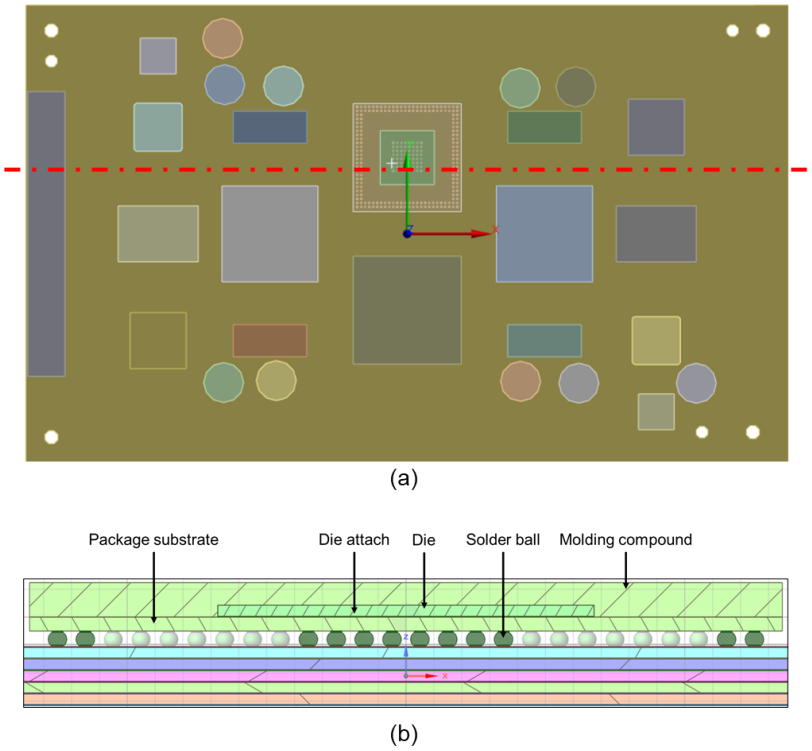

Figure 1 (a) Printed circuit board (PCB) assembly (b) Cross-sectional view of the BGA package.

The detailed cross-section of a corner solder ball is shown in Figure 2. It consists of a SMD pad on the package side and an NSMD pad on the PCB side. The solder ball is split into three halves for the calculation of damage corresponding to the possible failure locations which are near the interface of the copper pads.

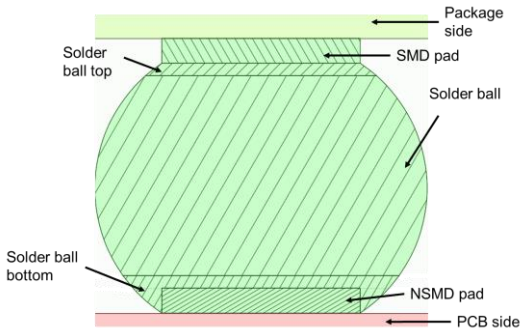

Figure 2 Cross-sectional view of an SMD-NSMD solder ball.

Linear elastic material models are used for all these components except for the solder balls. Multilinear isotropic hardening (MISO) along with a rate-dependent Generalized Garofalo creep material model is used for the solder balls. Trace mapping feature of Ansys is used to consider the copper traces in the PCB. It helps to capture the accurate material properties in the PCB without much increase in the computational effort. The assembly is meshed with linear hexahedral elements (Solid185) with shared nodes between most of the parts as show in Figure 3. Bonded contacts are used in places where shared node is difficult to generate. The automatically generated finite element mesh consists of 1.1 million nodes and 0.9 million elements. The PCB is fixed in all directions at the four corner holes and a thermal cycle boundary condition is applied with 4 thermal cycles with a temperature range of -40 to 85 °C and a cycle time of 1 hour.

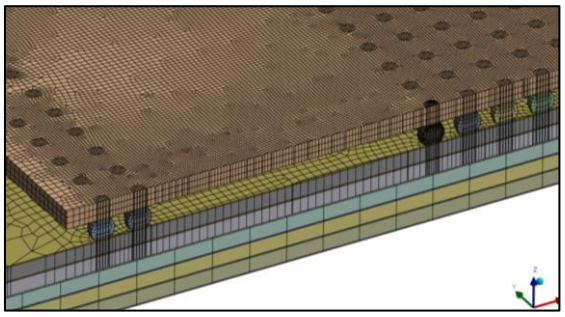

Figure 3 Sectional view of the finite element mesh of the PCB assembly.

Figure 4 shows the steps and approximate manual efforts in each of the steps involved in the solder joint fatigue workflow which shows a typical turnaround time of around 3-4 weeks. This workflow also involves multiple tools which requires expertise for different tools. In this present work, the workflow is automated using PyAnsys framework as shown in Figure 5.

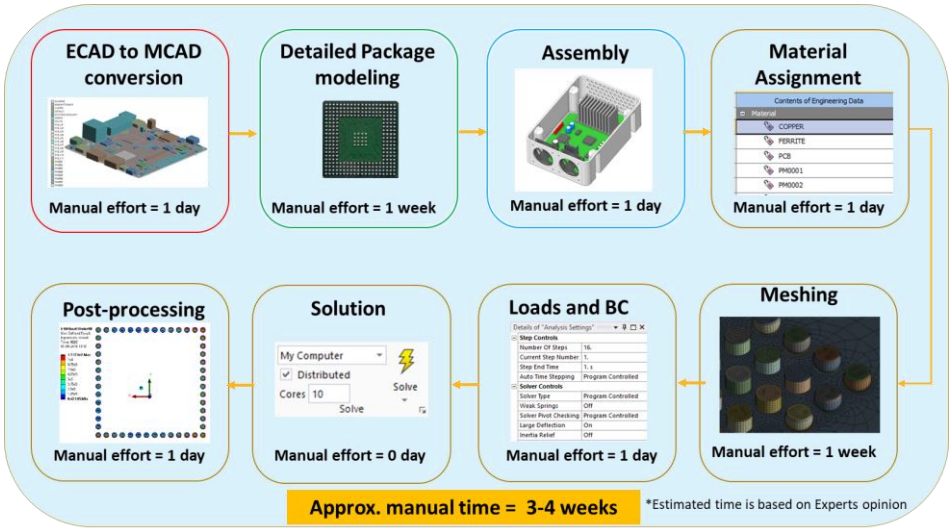

Figure 4 Summary of a typical solder joint reliability workflow.

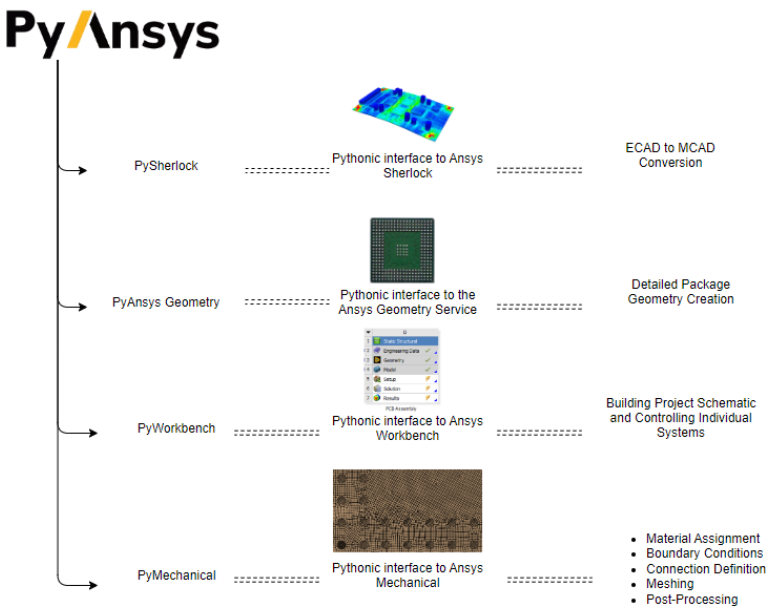

Figure 5 Summary of a typical solder joint reliability workflow.

Figure 6 shows the graphical user interface (GUI) of the application which shows different steps and the inputs required. Figure 7 shows the fatigue life postprocessing using Darveaux method [7] which shows the crack initiation life and the crack propagation life for different thermal cycles.

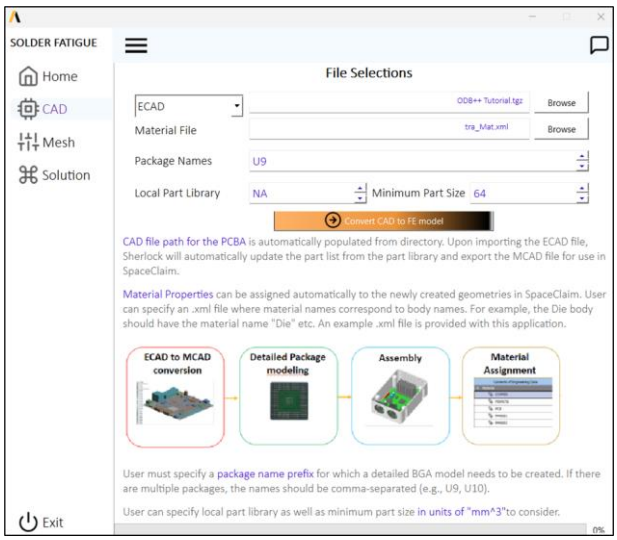

Figure 6 User interface of the developed application.

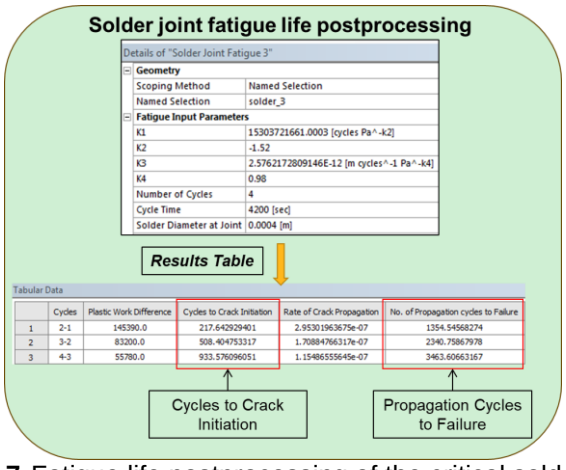

Figure 7 Fatigue life postprocessing of the critical solder joint.

3 Conclusions

In this research, an automated workflow is developed to simulate solder joint reliability for ball-grid array (BGA) packages using various Ansys tools. Key stages of the process, such as ECAD to MCAD conversion in Ansys Sherlock, geometry preparation in Ansys Discovery, and mesh generation, material assignment, boundary condition setup, and post-processing in Ansys Mechanical, are all streamlined through automation. This automation eliminates the requirement for specialized expertise and reduces the total simulation time by a factor of 10, greatly enhancing efficiency and reducing manual effort.

4 References

[1] S.Cheng, C.M.Huang, M.Pecht “A review of lead-free solders for electronics applications”, Microelectronics Reliability, Vol. 75, pp. 77-95, 2017.
[2] O.O.Ogbomo, E.H.Amalu, N.N.Ekere, P.O.Olagbegi “Effect of operating temperature on degradation of solder joints in crystalline silicon photovoltaic modules for improved reliability in hot climates”, Solar Energy, Vol.170, pp. 682-693, 2018.
[3] K.Choi, D.Y.Yu, S.Ahn, et al. “Joint reliability of various Pb-free solders under harsh vibration conditions for automotive electronics”, Microelectronics Reliability, Vol. 86, pp. 66-71, 2018.
[4] JEDEC, Standard. "Jesd22-a104c temperature cycling," JEDEC Solid State Technology Association, 2005.
[5] K.Khan, R. Meena, P.Andrade. “ Thermo-Mechanical Fatigue Life Prediction of Lead-Free Solder Balls in Electronics Packaging”, NAFEMS India Regional Conference on Engineering Modelling, Analysis, Simulation and 3D-Printing (NIRC-2018), 20 – 21 July 2018, Bengaluru, Karnataka, India.
[6] ANSYS, Inc. “Theory Reference for ANSYS 19.0”, Canonsburg, PA, 2018.
[7] R.Darveaux “Effect of Simulation Methodology on Solder Joint Crack Growth Correlation and Fatigue Life Prediction”, Journal of Electronic Packaging, Transactions of the ASME., Vol. 124(3), pp. 147-154, 2002.

An Integrated Workflow for Power Module Development

Wilfried Wessel, Florian Bauer, Rod Dudzinski (Siemens EDA)

John Parry, Hon Wong (Siemens Digital Industry Software)

1 Summary

This extended abstract describes a comprehensive automation of a power module design and verification process. State-of-the-art design and verification tools are combined in a novel way to achieve full automatic optimisation of a real industry use case. The abstract presents significant electrical and thermal performance benefits.

2 Introduction

In the next three years, the market for power modules will grow with a CAGR of 10.5% [1]. This high growth rate demands novel development methods. This is because it is not possible to employ engineers at the same rate as the CAGR. On top of that, growing highly competent employees proportional to the market growth rate is not sustainable. There are multiple reasons for this. Firstly, these employees are not available in the market. Secondly, adding more engineers to a project does not linearly increase productivity. The pressure for those engineers would still be high, which leads experiencewise to long working hours and stress.

The method we describe accommodates the bottleneck of experts. Using novel optimisation technologies, as described in this paper, increases the performance and quality of power modules but also has a significant effect on the environment [4]. The current work method of manufacturing a design idea and validating the physical prototype takes material resources and labour hours. Even if other state-of-the-art methods, such as [5], are available, they are not widely used. This is because fragmented simulation tools need to be glued together. In such a workflow, a huge amount of engineering resources is required to synchronise between the thermal, mechanical and electrical domains [5].

Another major disadvantage is that the literature confused optimisation with manual design adjustment and simulation. This manual process is repeated until a sufficient design has been found. The novel approach in this paper proves that full-automatic optimisation is possible, and the manual steps of design adjustments and synchronising domains can be eliminated from the workflow. Paper [6] shows a typical optimisation of a power module with a high count of parallel SiC FETs. The paper concludes with a good improvement in the overall module performance. This clearly illustrates that the outcome is highly dependent on engineering expertise. The human in the process is the limiting factor in processing simulated data and making an optimal design decision. Of course, the design will most likely fulfil the specifications, but it is unclear if it is the best possible design.

3 Approach Taken

Revolving around the utilisation of the Siemens EDA toolchain, the novel core of the paper is to fully integrate, connect and automate power module design and simulation. This ensures that all requirements, including manufacturing parameters, electrical, thermal, and mechanical parameters, can be verified and fulfilled. This paper describes a full automatic multiobjective optimisation to overcome the disadvantages, including electrical and thermal parameters. The novel approach to enhancing power modules' electrical and thermal performance uses an enhanced analytics search algorithm called SHERPA [2].

The method is applied to a power module used in solar inverters of the Vincotech power module. Comprising multiple SiC MOSFETs in parallel, this design serves as a representative platform for demonstrating the effectiveness of the proposed methodology.

The main reason for parallelising is to extend the power module's power range. Therefore, equal current sharing is crucial among all devices. Because the current imbalance has significant effects on reliability and product lifetime. Paper [13] describes the effect of higher temperatures on SiC MOSFET devices. It concludes that higher temperatures led to faster switching and decreased gate-source voltage for the same drain current. This behaviour can cause a negative feedback loop if electrical and thermal parameters are not optimised for all parallel devices. The method used is capable of performing this kind of design optimisation. The time needed for this task is two days compared to the four weeks usually required.

4 Details of the Approach

Rather than focus on the Vincotech example, which has been reported elsewhere and given the simulation focus of NAFEMS events, this abstract focuses on the methodology.

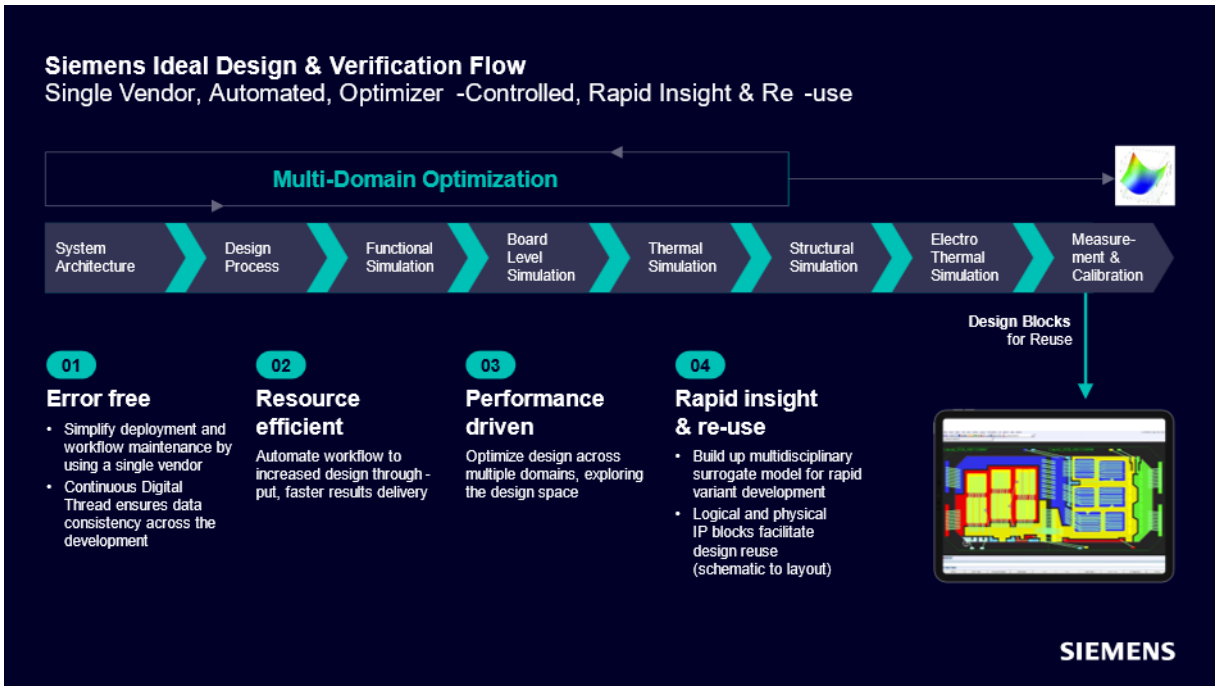

Fig. 1. Architectural view of Siemens automated power module design flow.

Siemens DI SW has solutions for PLM, CAD, EDA, CAE and physical testing, and have spent several years increasing the connectivity between these domains to deliver digital threads that support both data continuity and a single source of truth for data. This is what has been achieved with our power module workflow.

In our power module workflow this starts with system architecture, for example a system simulation model of an electric vehicle, where the required battery, inverter and motor performances conbine and are traded off. The inverter performance provides requirements for the power modules at its heart. The next step is the design process, which starts with the electrical schematic and the physical layout. This complete, functional simulation is an electrical simulation of the idealized circuit, to check the circuit works. Board-level simulation uses the physical layout to predict the currents, voltage drops, loop inductance, etc. and extract these electrical parasitic effects, which are then automatically back-annotated into the circuit simulation to show how the circuit will actualy perforn based on the physical design. Up to this point the simulations are isothermal. Thermal simulation is needed because temperature affects the electrical performance, and temperature changes during operation contribute to wear-out damage that affects the modules lifetime. Layout affects thermal performance and so the layout needs to be assesed. Once the temperature distribution is known, this can be used as the thermal load for a structural simulation to understand the thermomechanical performance of the module, which can be used to predict warpage, stress and strain within the solder die attach and sintered copper attachment of the direct bonded copper (DBC) substate to the housing.

A particular challenge is simulating electronics products or semiconductor devices, is how to make the circuit simulation temperature-aware. Powers are needed as a boundary condition for the thermal simulation, but power dissipations are affected by temperature, so how to get accurate powers ahead of the thermal design? This contention is broken by including thermal ROMs in the circuit simulation that are themselves boundary condition independent (BCI).

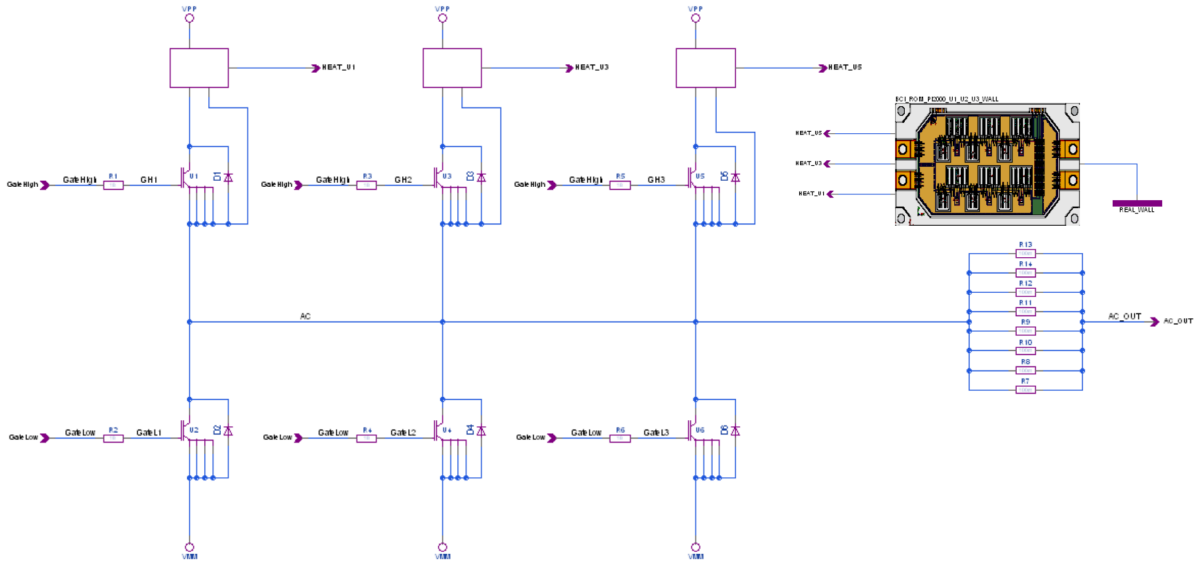

Fig 2. BCI-ROM thermal model of power module incorporated into circuit simulation.

The workflow is completed by the use of thermal characterization hardware to measure the performance of a physical implementation of the optimized design, and fully-automated active power cycling equipment to measure cycles to failure under different powering conditions, with real-time monitoring of the changes in electrical parameters that occur e.g. when wire bonds break, coupled with periodic assessments of the thermal performance of the structure with diagnostics to indicate where structural changes are occuring, e.g. delamination or cracking of the die attach solder.

5 Some Specific Features of the Workflow

Some further comment on Figure 1 is needed. The individual steps are shown as connected with light blue arrows, as workflow automation software takes outputs from one tool as input to others in the sequence. As this can be done right across the workflow all simulations can be performed without human intervention in the process, allowing the whole process to be put under the control of an optimizer. The user defines what the cost function the optimizer is to minimize contains, and the relative weighting of these terms. SHERPA fully expores the design space, with technology built in to prevent the optimization getting stuck in a local minima. In the example below, over 250 design points are simulated, taking about 2 days. This provides a large set of design performance data to which to fit a surrogate model for each simulated performance. Once the design space has been explored, designs optimized for a different balance of parameters in the cost function can be achieved very rapidly using surogate models not full 3D CAE simulations.

6 Worked Example: PI3000 Design

Positions of die U2 and U4, along with their bond wires, and the bond wires of J1-M are varied. With the objective of illustrating the process and understanding how the design performs, a series of separate optimizations have been performed. Had the objective been to produce the best design variant, which would be the case for a manufacturer, all design parameters should be varied as part of a single design space exploration search. The presentation will show the results of the optimization steps performed, discuss the workflow and its automation in more detail, and discuss how the workflow can be extended further.

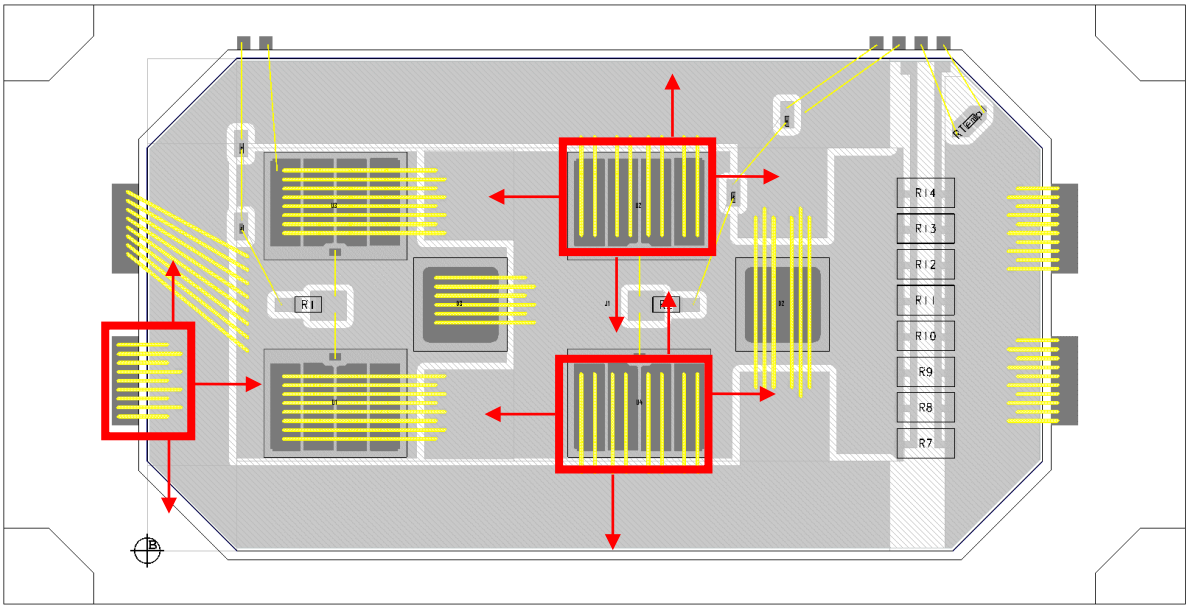

Fig. 3. IP3000 demonstrator design showing parameters varied

7 Conclusions

Typical power module development workflows are hampered by the use of many good point solutions from different vendors, for CAD, circuit simulation, low-frequency electromagnetics, etc. that do not allow seamless and complete data transfer across the development workflow. Many individuals each with experience with one or more tools are needed to complete one design iteration and simulate its performance. Manually entering missing data into multiple tools introduces errors in addition to being resource intensive and time-consuming.

Our power module design flow utilizes design connectivity found in EDA suites, that combine schematic capture, layout, circuit simulation and electromagnetic performance into one platform as the foundation of the workflow. Seamless connectivity between the EDA and CAD domains allows process automation with Simcenter CAE solutions, thereby including thermal and mechanical performance to be included in the cost function that the optimizer minimizes to produce the optimally performing design.

8 References

[1] Dr. S. Agarwal, ‘Status of the Power Module Packaging Industry 2021’,2021, www.yole.fr, pp. 17.

[2] L. Hertel, J. Collado, P. Sadowski, J. Ott, and P. Baldi, ‘Sherpa: Robust hyperparameter optimization for machine learning’, SoftwareX, vol. 12, p. 100591, Jul. 2020, doi: 10.1016/j.softx.2020.100591.

[4] S. Wilke, ‘Treibhausgasminderungsziele Deutschlands’, Umweltbundesamt. Accessed: Apr. 01, 2024. [Online]. Available: https://www.umweltbundesamt.de/daten/klima/treibhausgasminderungsziele-deutschlands

[5] Y. Yang, Y. Ge, Z. J. Wang, and Y. Kang, ‘An Automated Electro-Thermal-Mechanical Co-Simulation Methodology Based on PSpice-MATLAB-COMSOL for SiC Power Module Design’, in 2021 IEEE Workshop on Wide Bandgap Power Devices and Applications in Asia (WiPDA Asia), Aug. 2021, pp. 499–503. doi: 10.1109/WiPDAAsia51810.2021.9656074

[6] W. Li, S. Mao, H. Liu, J. Fan, and K. Zeng, ‘Current Uniformity Optimization of Multi-Chip SiC Module for High-Power Applications’, presented at the 2022 IEEE International Power Electronics and Application Confer-ence and Exposition (PEAC), Guang-zhou,Guangdong, China: IEEE, Nov. 2022, pp. 545–550. doi: 10.1109/PEAC56338.2022.9959680.

[13] A. J. Lelis, D. B. Habersat, R. Green, and N. Goldsman, ‘Temperature-Dependence of SiC MOSFET Threshold-Voltage Instability’, MSF, vol. 600–603, pp. 807–810, Sep. 2008, doi: 10.4028/www.scientific.net/MSF.600-603.807.

Enhancing Safety Assessments for CO_2 Pipelines with a Validated Fluid-Structure Interaction Model

Aida Nonn (Aixima GmbH), Philipp Marx (Aixima GmbH)

1 Summary

Despite global efforts to combat climate change, the pace of decarbonization remains insufficient, resulting in a critical "decarbonization gap." Solutions such as Carbon Capture, Utilization, and Storage (CCUS) technology are essential to reducing CO_2 emissions. However, the scaling up of these technologies has been hindered by outdated standards for CO_2 pipeline fracture control. These standards often necessitate expensive full-scale testing, limiting their applicability and efficiency.

Here we present a validated, fully coupled fluid-structure interaction (FSI) model designed as a digital twin of a CO_2 pipeline. The digital twin allows for rapid virtual testing and efficient fracture propagation assessment, eliminating the need for extensive full-scale testing. Using rigorously calibrated material models and high-quality data from small-scale tests, including instrumented Drop-Weight-Tear (DWTT) tests, the model accurately simulates fracture propagation, arrest and related phenomena such as 3D pressure distributions, pipe deformation, wall thinning and crack tip opening angles.

The FSI model fills critical data gaps in current standards and serves as a foundation for developing new guidelines, enabling more efficient design and safety assessments for CO_2 pipelines, thereby accelerating the realization of CCUS projects.

2 Introduction

As global efforts to combat climate change progress, CO_2 and H_2 pipelines are essential for advancing CCUS technologies. Managing running ductile fracture (RDF) in high-pressure CO_2 pipelines is critical, requiring higher steel toughness due to the unique decompression behavior of dense-phase CO_2. The traditional Battelle Two-Curve Method (BTCM) [1] is inadequate for CO_2 pipelines, prompting the development of improved models through projects like CO2PIPETRANS [2] and COOLTRANS [3]. The CO_2 Safe-Arrest Joint Industry Project developed a new empirical model for fracture control, now included in DNV-RP-F104 [4], but it remains limited by the narrow range of tested pipe types.

Numerical multiphysics models offer an alternative, simulating complex interactions between material properties, gas decompression, and backfill, though they face challenges like the need for extensive experimental calibration. Advances in ductile failure theories [5]-[7] and computational methods have facilitated the development of coupled Fluid-Structure Interaction (FSI) models, providing a robust alternative to full-scale testing.

The developed FSI model [8] [9], validated through full-scale CO_2 pipeline burst tests, accurately predicts fracture propagation, velocity, and arrest [10]. Acting as a digital twin, the FSI model enables virtual testing, helping to optimize pipeline design and ensure the safety of the pipe for reuse. This model is applied to varying industrial safety assessments, including basic, standard, and advanced levels, and generates synthetic data for machine learning integration, streamlining industrial workflows.

3 Modeling and Methodology

The FSI model is based on the following components:

- Structural model with plasticity and fracture description
- Fluid model with fluid description and thermodynamics of transported mixtures
- Backfill model of materials such as soil, silt, clay and loam in onshore and water in offshore applications

3.1 Material Model Calibration

The plasticity and fracture properties of API X52 pipeline material are characterized through a rigorous calibration process. This process leverages data from small-scale tests designed to cover a wide range of stress conditions. Additionally, instrumented Drop-Weight-Tear (DWTT) tests are conducted to validate the model's predictive capabilities. The Hill'48 quadratic yield function is used to describe plastic anisotropy, while the Modified Mohr-Coulomb (MMC) [5] damage model captures fracture

initiation and propagation. These material models are calibrated against experimental data to ensure accurate representation of the pipeline material's behavior under various loading conditions.

3.2 Fluid Dynamics and Thermodynamics

The FSI model integrates fluid and thermodynamic simulations using Euler equations and the GERG-2008 Reference Equation of State (EOS) to represent the behavior of dense-phase CO_2. The Euler domain is employed to solve the mass, momentum, and energy equations governing the transported CO_2 mixture, capturing the unique decompression wave propagation and two-phase flow characteristics typical of CO_2 pipelines.

3.3 Backfill and Soil Interaction Modeling

In onshore pipelines, soil backfill significantly influences pipe deformation and rupture behavior. The soil is modeled using the Mohr-Coulomb (MC) framework, which accurately simulates the effects of soil interaction on the pipeline's structural response. This model is particularly important for capturing the inertia and deformation behavior of the pipeline as it interacts with surrounding soil during a rupture event.

3.4 Coupled Fluid-Structure Interaction

The core of the FSI model is built using the Coupled Euler-Lagrange (CEL) method, which allows for large-deformation fluid-structure interaction simulations. The CEL method couples the structural response of the pipeline material with the fluid dynamics of the transported CO_2 mixture and the soil backfill. This approach provides detailed insights into the complex interactions between the pipeline, fluid, and environment during fracture propagation.

4 Results

The results from our Fluid-Structure Interaction (FSI) simulations show significant advantages over the DNV-RP-F104 empirical model. Unlike the DNV model, which provides only a binary assessment (arrest or no arrest), the fully coupled FSI model offers detailed insights into key parameters critical for accurate fracture control. The FSI model extracts 3D pressure distributions, crack tip opening angle (CTOA), and membrane stresses, along with other crucial factors such as wall thinning, see Fig. 1. This provides a much more comprehensive assessment of fracture propagation behavior by considering complex multiphysics interactions between structural, fluid, and backfill domains.

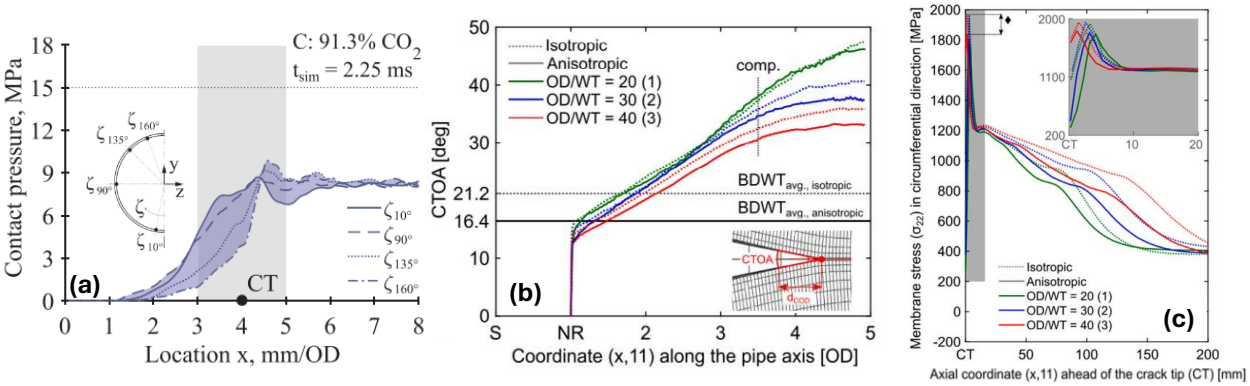

Fig. 1: Pressure load distributions in front of and behind the crack tip (CT) in (a) [8], CTOA evaluations along the crack length extracted from isotropic (dotted lines) and anisotropic (solid lines) pipe simulations with different pipe geometries in (b) [11], and principal circumferential stresses (membrane stress) as a function of x-coordinate in front of the CT in (c) [11]

5 Conclusions

- The validated fully-coupled Fluid-Structure Interaction (FSI) model provides accurate, reliable, and cost-effective predictions of pipeline behavior, reducing the need for full-scale testing.
- The FSI model effectively predicts key parameters such as crack propagation velocities and fracture arrest, making it a valuable tool for pipeline integrity management.
- Integrating state-of-the-art computational tools like the FSI model and AI can enhance pipeline safety and efficiency.
- The FSI model can be further improved with real-time monitoring and predictive analytics, optimizing pipeline integrity management.

- The model supports the broader deployment of carbon capture and storage (CCS) and hydrogen-based energy systems.

6 References

[1] W. A. Maxey, “Fracture Initiation, Propagation and Arrest,” in 5th Symposium on Line Pipe Research, Houston, Texas, 1974

[2] E. Aursand, S. Dumoulin, M. Hammer, H. I. Lange, A. Morin, S. T. Munkejord and H. O. Nordhagen, “Fracture propagation control in CO2 pipelines: Validation of a coupled fluid-structure model,” Engineering Structures, vol. 123, pp. 192-212, 2016

[3] V. Linton, B. H. Leinum, R. Newton and O. Fyrileiv, “CO2SAFE-ARREST: A full-scale burst test research program for carbon dioxide pipelines – Part 1 Project overview and outcomes of test 1,” in 2018 18th International Pipeline Conference, Calgary, Canada, 2018

[4] DNVGL-RP-F104: Recommended Practice - Design and operation of carbon dioxide pipelines,” DNV GL, 2017

[5] Y. Bai and T. Wierzbicki, “Application of extended Mohr–Coulomb criterion to ductile fracture,” International Journal of Fracture, pp. 1-20, 2010

[6] I. Scheider, A. Nonn, A.Völling, A. Mondry and C. Kalwa, “A damage mechanics based evaluation of dynamic fracture resistance in gas pipelines,” in Procedia Materials Science, vol. 3, pp. 1956-1964, 2014

[7] V. Keim, A. Nonn and S. Münstermann, “Application of the modified Bai-Wierzbicki model for the predition of ductile fracture in pipelines,” International Journal of Pressure Vessels and Piping, vol. 171, pp. 104-116, 2019

[8] V. Keim, P. Marx, A. Nonn and S. Münstermann, “Fluid-structure-interaction modeling of dynamic fracture propagation in pipelines transporting natural gases and CO2-mixtures,” Int. J. of Pressure Vessels and Piping, vol. 175, p. 103934, 2019

[9] V. Keim, M. Paredes, A. Nonn and S. Münstermann, “FSI-simulation of ductile fracture propagation and arrest in pipelines: Comparison with existing data of full-scale burst tests,” International Journal of Pressure Vessels and Piping, vol. 182, p. 104067, 2020

[10] P. Marx, and A. Nonn, “Advancing CO2 Pipeline Safety: Innovative Predictive Approaches and their Application in On- and Offshore Ductile Fracture Assessment,” in Proceedings of the 19th Pipeline Technology Conference, Berlin, Germany, 08-11 April 2024

[11] L. Xue, V. Keim, M. Paredes, A. Nonn and T. Wierzbicki, “Anisotropic effects on crack propagation in pressurized line pipes under running ductile fracture scenarios,” Engineering Fracture Mechanics, vol. 249, p. 107748, 2021

Fast Running Digital-Twin of a Multiphysics BEV Model Trained using ML

Ujjwal Chopra, Gautham Reddy (Gamma Technologies)

1 Summary

In this paper, a Multiphysics battery electric vehicle model is being created. Models consist of 1D longitudinal dynamics vehicle model being integrated with electrochemistry based P2D battery pack model and system level 1D thermal and cooling circuit for accurately capturing interdependencies and two-way coupling. This detailed physics-based model was run on various drive cycles City/rural/highway standard cycles and drive cycles generated using GT-RealDrive which considers live traffic condition, accurate road elevation and weather boundary conditions including wind and temperature. Physics based model was used as a data generator for training the NARX based dynamic neural network to create a fast-running metamodel which can be eventually useful for digital twin application to monitor temperature rise, battery degradation and accurately estimate range.

1.1 Vehicle Model

Vehicle model consists of a 4 wheeled rear wheel drive passenger vehicle modelled using 1D logitudinal dynamics model of GT-SUITE [4]. Vehicle model is used to accurately capture vehicle load inclusive of aerodynamic force (including effect of wind velocity and direction), rolling resistance, driveline losses, gradient forces and inertias. Motor is modelled using map-based model capturing motor electromechanical conversion efficiency and inverter losses and capable of performing both as a motor and generator. User needs to define drive cycle (standard & real-world cycles using GT-RealDrive [4]) in driver template (feedforward + feedback controller) which will calculate torque demand which will be passed onto motor generator. Motor then demands required electrical power from battery including motor & inverter losses [1].

1.2 Battery Model

Battery is being modelled using P2D electrochemical model using GT-AutoLion [4]. 5Ah Cylindrical cell with Anode as Graphite+Silicon and Cathode as NCM811 is being modelled. GT-AutoLion comes with a library of material properties and coin cells which can used as a starting point. Here, geometry calibration was done by taking the dimensions provided by the manufacturer. OCV, dynamic, and ageing calibrations were done using experimental data provided by the Southwest Research Institute's (SwRI) battery testing consortium, Electrified Vehicle and Energy Storage Evaluation (EVESE) [2].

1.3 Thermal Model

The Thermal Management model consists of 4 circuits: 2 cooling circuits (Dark and Light green), Refrigerant circuit (pink) and Cabin air circuit (blue). The power consumption of compressor, water pumps and lowers are added to get auxiliary loads (HV Loads). The Light green circuit consists of High temperature cooling circuit which cools all the Power electronics while the dark green circuit is a low temperature cooling circuit which cools the battery pack. All the moving parts (Compressor, Blowers, Pumps) have their own control strategy based on drive cycle and ambient temperature.

Thermal Management System

- HT cooling circuit
- LT cooling circuit
- Refrigerant circuit
- Cabin air circuit
- Underhood air circuit

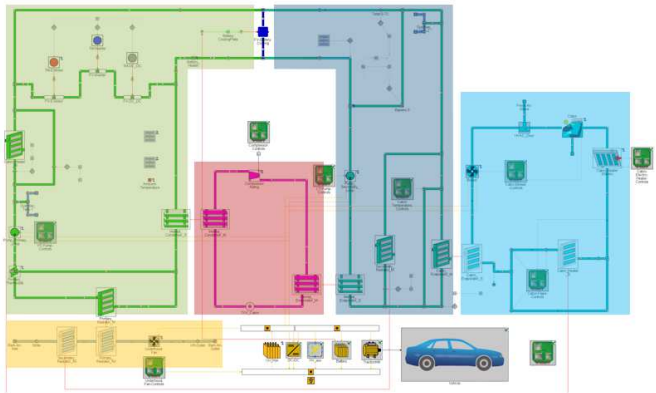

1.4 Metamodels aka Machine Learning Models

1.4.1 Vehicle Metamodels

Electrical power (Pm) demanded by motor from battery is a function of vehicle loads including aerodynamics force, rolling resistance, driveline losses, inertial loads and gradient forces. Heat generation (Qm) which includes motor and inverter losses is a product of efficiency and power hence following I/Os were considered for vehicle metamodel to predict Pm and Qm.

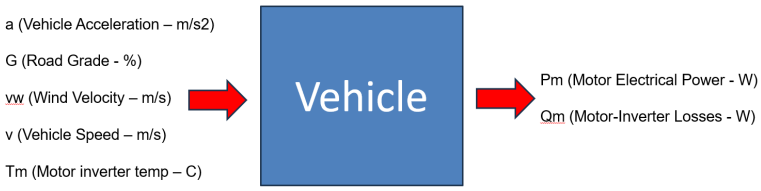

1.4.2 Battery Metamodels

Due to large interdependancies and to avoid higher machince learning computational cost and time, its is better to segregate the system into smaller subsystems wherever feasible. Hence the battery metamodle was subdivided into three: B1, B2 and B3 as described in next section. Global battery metamodel I/Os are as shown below:

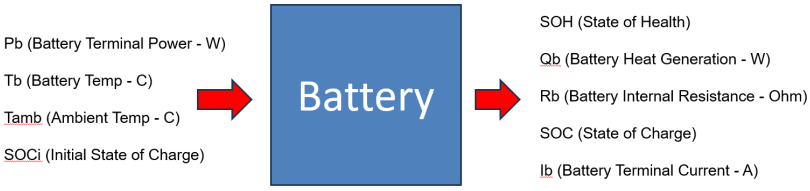

Interdepancies of these metamodels and I/Os of each is shown below:

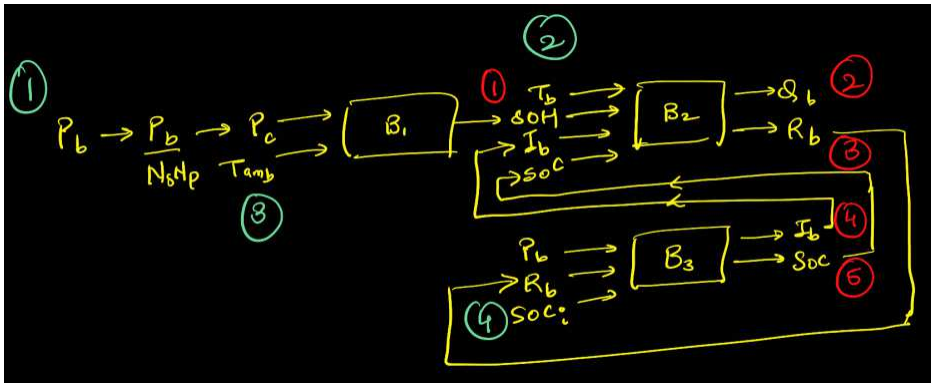

1.4.3 Thermal Metamodels

Thermal metamodel represents Vehicle thermal management including battery & motor coolant loop, cabin air circuit, refrigerant loop and underhood air circuit. High voltage (HV) loads include compressor, underhood fan, cabin blower/heater and pump consumptions.

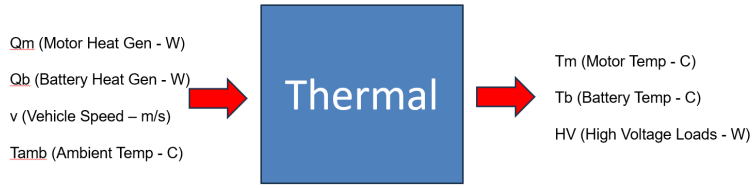

2 Metamodel Training Results

First step of metamodel creation is preprocessing. PACF (Partial Autocorrelation Function) and CCF (Cross-Correlation Function) plots are useful to identify factor and response delay values. Then a very small subset of entire data is chosen to identify right set of metamodel parameters using a step called grid search or hyperparameter study. Once we identify right hyperparameters, we include all the data which is being generated by running physics-based model over various operating conditions, standard

[4] and real world drive cycles [3]. Then the entire dataset was divided into training (75-80%), test (10-15%) and validation (10-15%). In case of lack of data, alternatively a 100% training with crossvalidation based approach was followed. Eventually, below are some of the training, test and validation results for the optimal machine learning model being derived after grid search. compared to physics-based model predictions.

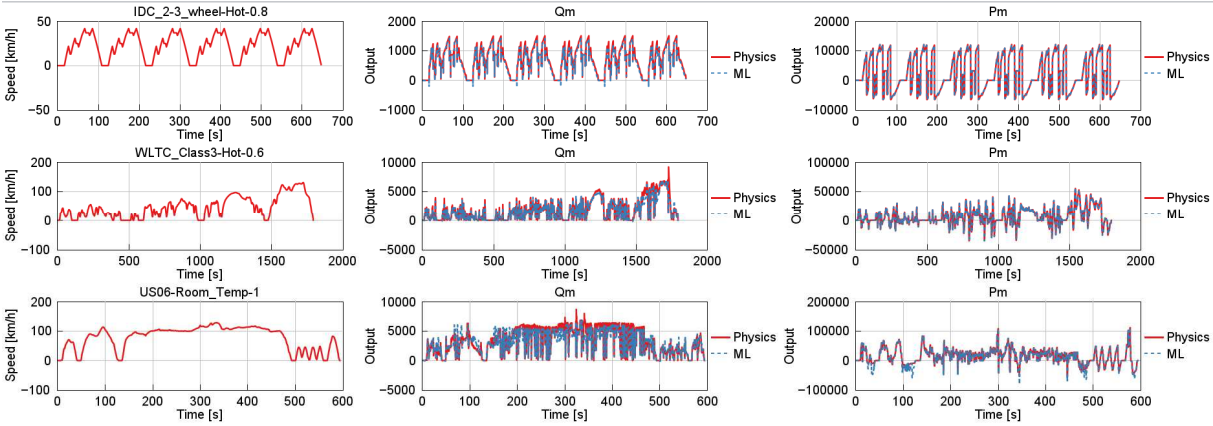

Fig. 1 Vehicle metamodel training results for motor heat generation (Qm in W) and motor-inverter electrical power demand (Pm in W).

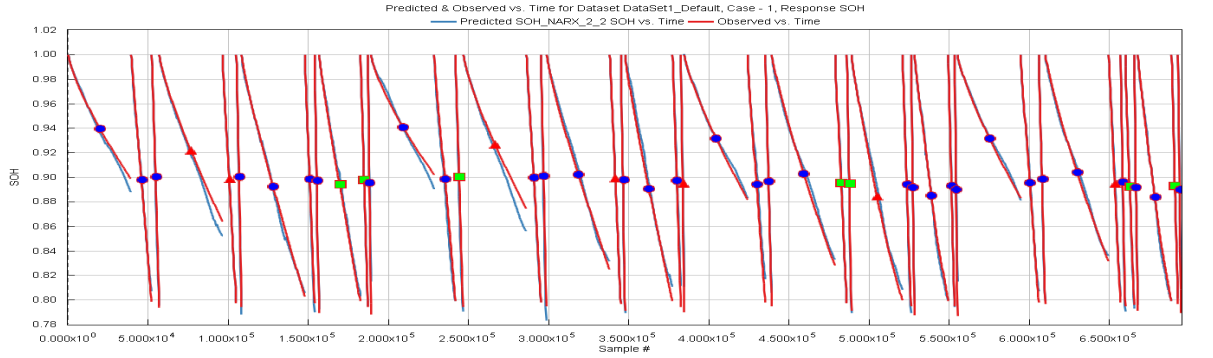

Fig. 2 Battery (B1) metamodel training results for state of health prediction (SOH in fraction).

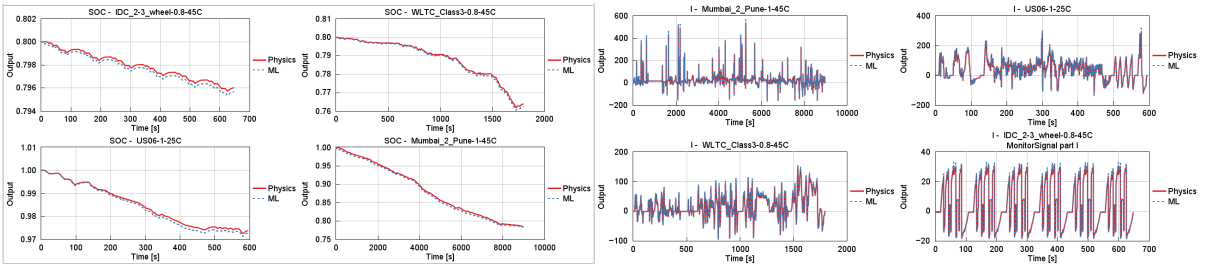

Fig. 3 Battery (B3) metamodel training results for state of charge (SOC in fraction) and current (I in A) prediction.

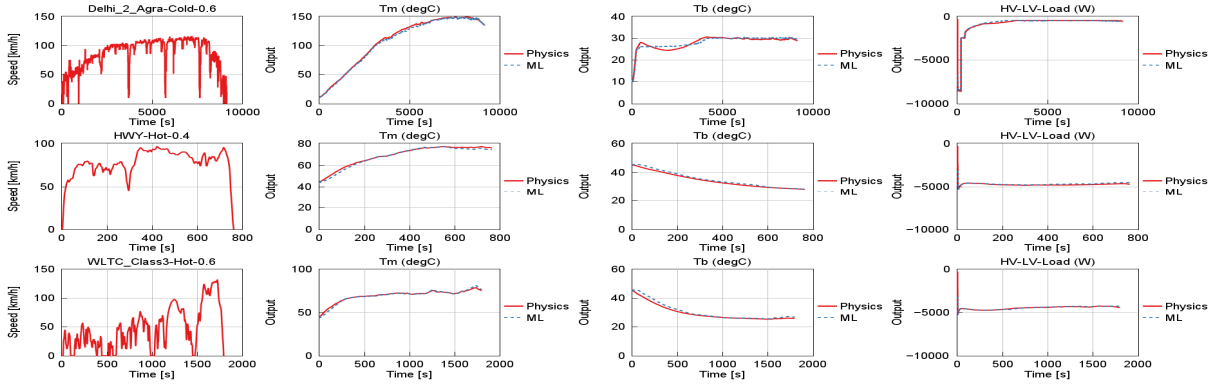

Fig. 4 Thermal metamodel training results for motor temp (Tm), battery temp (Tb) & high voltage loads (HV).

3 Metamodel Validation Results

Below are some validation results using fresh set of drive cycles (standard & real world) which were not involved during metamodel training.

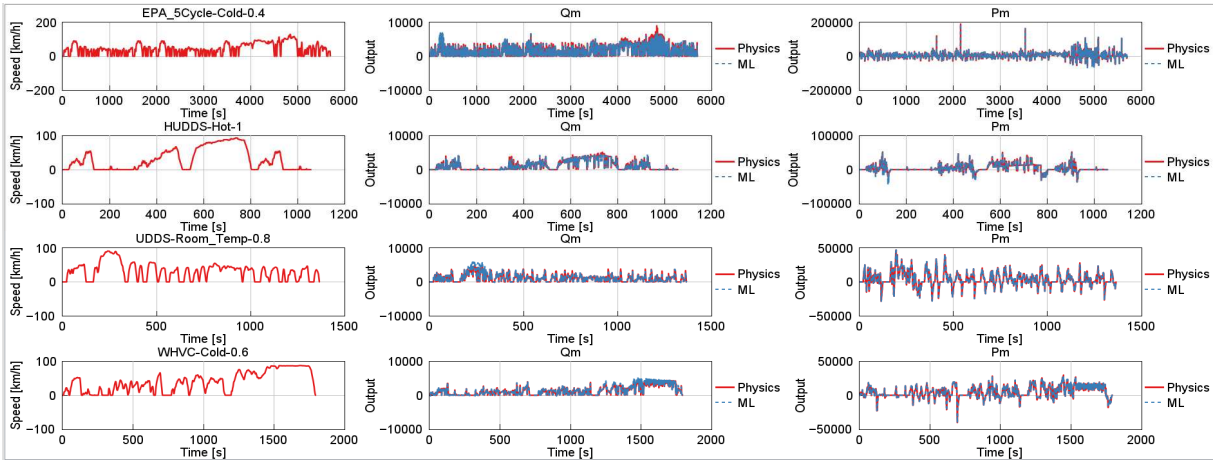

Fig. 5 Vehicle metamodel validation results for motor heat generation (Qm in W) and motor-inverter electrical power demand (Pm in W).

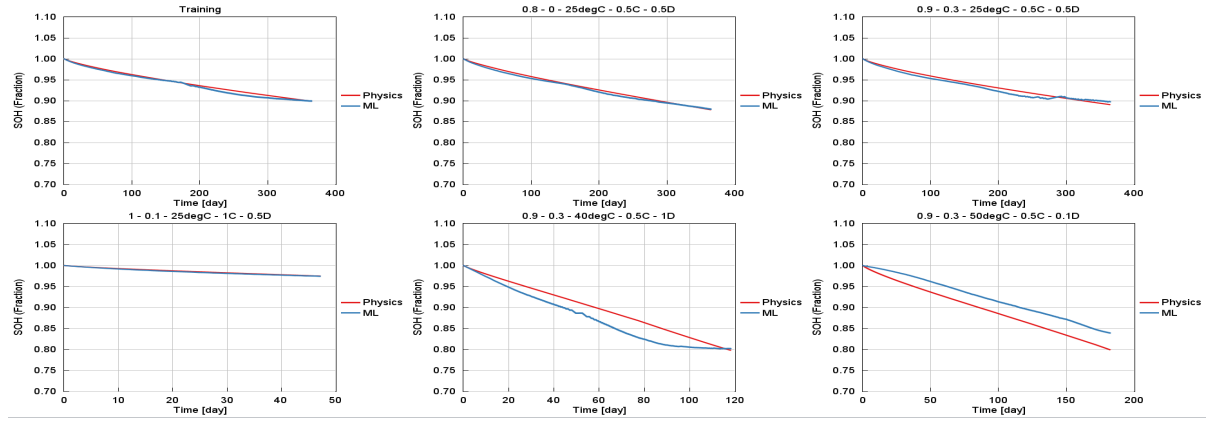

Fig. 6 Battery (B1) metamodel validation results for state of health prediction (SOH in fraction).

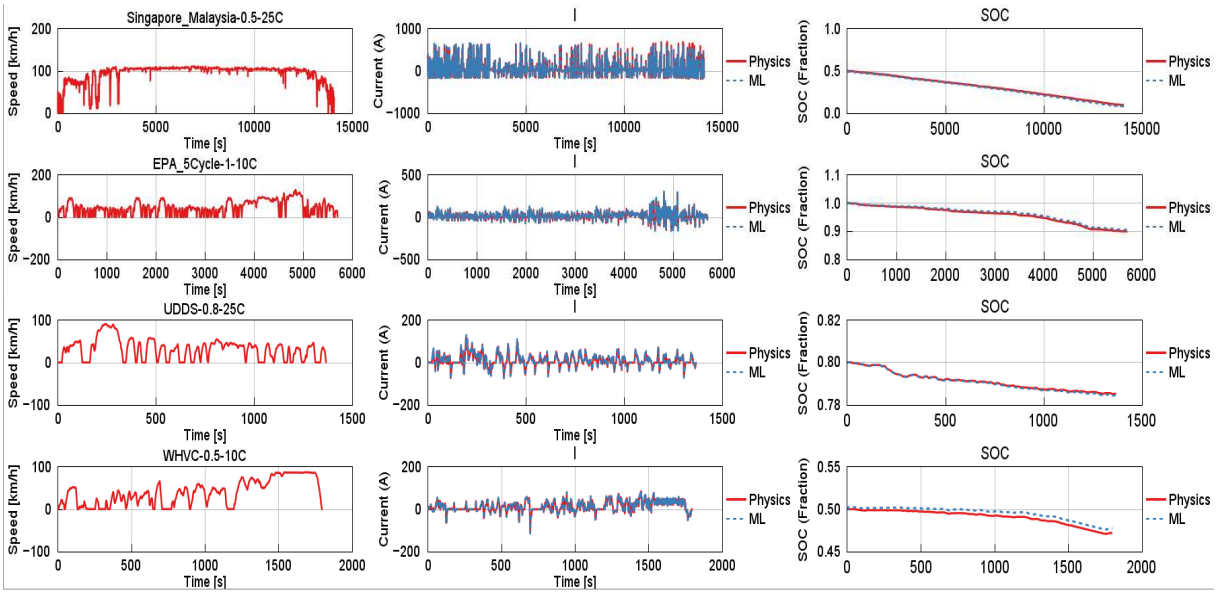

Fig. 7 Battery (B3) metamodel Validation results for state of charge (SOC in fraction) and current (I in A) prediction.

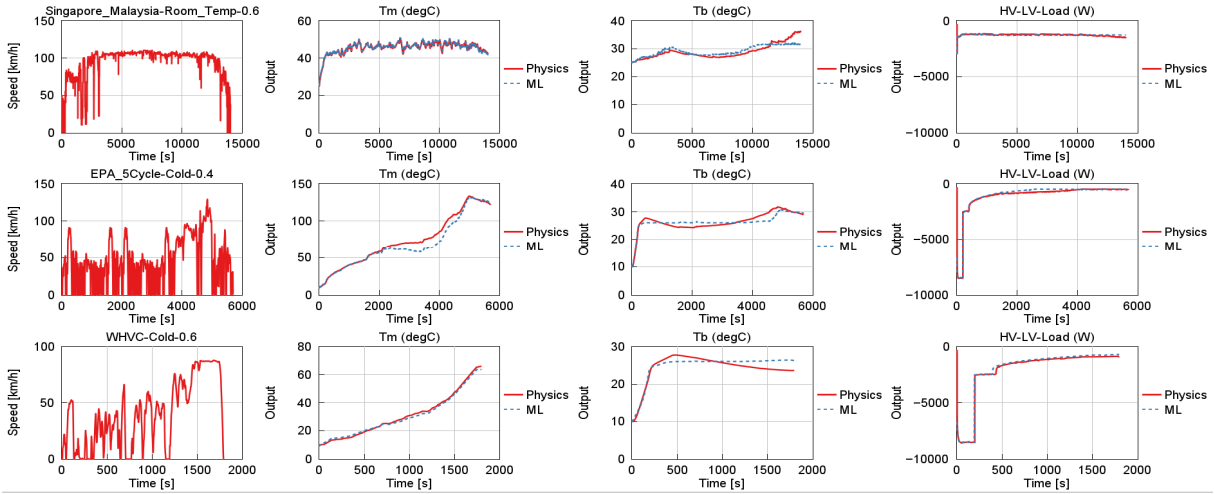

Fig. 8 Thermal metamodel validation results for motor temp (Tm), battery temp (Tb) & high voltage loads (HV).

4 Conclusions

In this analysis, we tried to create machine learning models using physics-based model as a data source/generator to reduce overall testing time and cost. Physics based models are accurate but can be challenging to deploy on physical hardware due to size constraints of microprocessors. Hence, we created metamodels representing different subsystems of a typical BEV including vehicle, battery and thermal to predict power consumptions, heat generation, temperature rise, SOC & SOH. Metamodels are in good agreement with physics-based models and are much faster and light.

5 References

1. Tesla Model 3 owner's manual accessed April 2024.
2. Electrified Vehicle and Energy Storage Evaluation, Southwest Research Institute, San-Antonio, personal communication, 2022
3. Here Technologies, "HERE Routing API v8" https://developer.here.com/documentation/routing-api/dev_guide/index.html, accessed Jan. 2023.
4. GT-SUITE (Version 2024), CAE software, Gamma Technologies, LLC, Westmont, Illinois, United States (HQ).

Pre-Compression Effect on Charge-Discharge Characteristics of Li-ion Batteries

Bhaskar Ramagiri[1], Youngwon Hahn[2], Matias Zielonka[2], Sonu Kumar Mishra[1], Nikhil Dhavale[1]

[1]Dassault Systèmes Solutions Lab, Rajiv Gandhi InfoTech Park Phase I, Pune, MH, India

[2]Dassault Systèmes SIMULIA Corp., 1301 Atwood Ave, Suite 101W, Johnston, RI, 02919, USA

Abstract

The growing demand for sustainable technologies is propelling the widespread adoption of rechargeable batteries across various sectors, from portable electronic devices to power grids. Battery technology is advancing swiftly, particularly in terms of energy density and safety, to meet the increasing requirements for electrification in recent years. Mathematical and numerical models play a crucial role in advancing this technology by offering insights into design improvements, especially when physical measurements are impractical. In our current study, we utilize a fully coupled thermal-electrochemical-mechanical model to examine the impact of pre-compression on the charge-discharge characteristics of Li-ion battery pouch cells. This model accounts for the stress interaction arising from swelling and external constraints confinement. In automotive battery packs, cells are organized into modules, which are then arranged to fulfill the pack's specifications. Within each module, cells are closely packed and pre-constrained to fit within geometrically constrained box sizes. The pre-stress affects the initial porosity, while mechanical constraints influence the electrochemical behavior of the cells during charge and discharge cycles. Our investigation focuses on thick pouch cells, commonly used in automotive applications, to analyze the effects of pre-compression and mechanical constraints.

Keywords

coupled thermal electrochemical and mechanical, li-ion battery, mechanically constrained pouch cell behavior, Newman model

1. Introduction

Over the years, rechargeable Li-ion battery technologies have undergone significant evolution, driven by numerous innovations from both industry and academic research. Concurrently, mathematical and numerical models for analyzing battery performance under different scenarios have also progressed. One commonly utilized numerical model for comprehending the performance of Li-ion batteries is the porous electrode theory initially proposed by Newman et al.[1], which has since been refined and enhanced by subsequent researchers.

Rechargeable Li-ion batteries consist of several components, including porous electrodes, current collectors, and a separator. The porous electrodes are composed of a solid skeleton with interconnected pores, which are filled with liquid electrolyte. The solid part of the electrode comprises active material and binder. The active material consists of particles held together by the binder. During charging, the particles in the anode undergo delithiation, while electrons simultaneously flow to the cathode through an external circuit. This process of delithiation and lithiation causes the electrodes to swell and contract. These changes in volume result in the evolution of the pore volume fraction, leading to fluid-pressure mediated electrolyte flow and the transport of Li-ions through the electrolyte medium. The cells under operation undergo charge-discharge cycles and are subjected to varying temperature and confining pressure conditions and these conditions significantly affect the performance of the cell. This behavior of li-ion cells can be studied through

fully coupled thermal electrochemical and mechanical (TECM) model. A fully coupled model implemented in ABAQUS is presented in detail Kulathu et al. [2].

Pouch cells are used in automobiles and other applications because of simplicity in construction and as they offer flexibility and lightweight advantage. In automobile applications, the cells are usually placed in modules and subjected to confinement pressure. Experimental and numerical studies examining the effects of external pressure or confinement have demonstrated that the response of the battery differs from that of unconstrained conditions [3], [4], [5]. In the current work the effect of pre-compression on the charge discharge behavior is studied specific to case of simple constant current charging followed by constant current discharge. The fully coupled model in ABAQUS is employed to determine if it can accurately capture the charge-discharge time response and reaction force observed in the literature for both confined and unconfined scenarios.

2. Motivation and Problem Statement:

In the current work, using fully coupled numerical framework we tried to understand the coupling between mechanical and electrochemical behavior. Yuan [6] has performed experimental study on charge-discharge behavior for two cases of with and without constraint condition. The research has observed decrease charge time (Fig 4C) and higher charge potential under mechanical constraint (Fig 2A). The research also showed the reaction force increasing with decreasing C-rate. The research has performed the numerical simulations to see if a coupled model can help understand the underlying coupling effect. In the current work, the charge discharge behavior specific to case of charge-discharge cycle definition was carried out to see if the fully coupled model can capture the change in charge time for the constrained and unconstrained case. Two simulation cases have been studied as shown in this section.

Case – 1 (Fix- Free case):

In the Fix-Free case, the bottom face of the pouch cell was fixed (displacements in X, Y, and Z are constrained). The top face of the pouch is free to move in all 3 degrees of freedom.

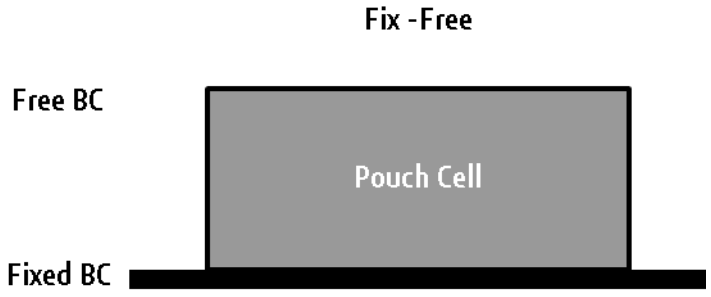

Fig 1: Fix-Free Case with bottom end constrained and top end free to expand.

Case -2 (Fix-Fix case):

In the Fix-Fix case, the bottom face of the pouch cell was fixed (displacements in X, Y, and Z are constrained). The top face of the pouch is displaced in step-1 of the analysis and constrained in position for the rest of the steps in the analysis.

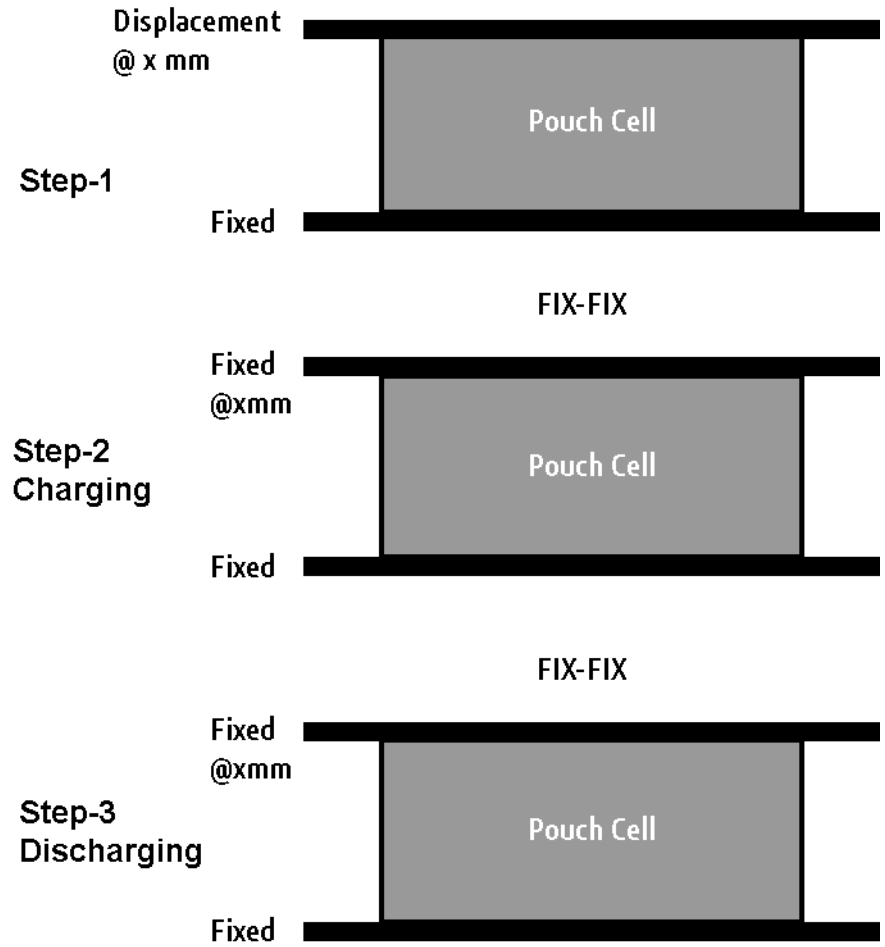

Fig 2: Fix- Fix case with bottom end constrained and top end that is displaced and constrained.

3. Finite Element Model

A pouch cell of length 101 mm and width 85 mm with thickness of 15.1mm was modelled using ABAQUS pouch cell modeler plugin. The meshed model is presented in Fig.3. The model contains 48 double electrode layers. The thickness of anode and cathode active layers are 73.7 µm and 54.5 µm respectively. The collectors are modelled with thickness of 10 µm and separator is modelled with 19 µm thickness. The layers are meshed with 3 elements through the thickness. The mesh is generated to share nodes at the interface between different layers of the pouch cell. Analytical rigid surfaces were modelled on the top and bottom surfaces of the pouch cell to apply the mechanical compression load. The analytical surfaces were tied to the top and bottom element surface faces of the pouch cell using surface-based contact pairs. QEC3D8 elements were assigned to all the elements of the pouch cell having a node count of 423888. The elements support 7 degree of freedom suitable to study the coupled electrochemical and mechanical scenario problems. The constitutive behavior of the coupled model implemented in ABAQUS that is used in the current work is presented in detail by Kulathu et al. [2]. The thermal and electrochemical material behavior for the electrodes and electrolyte are taken from the literature [7], [8], [9] .

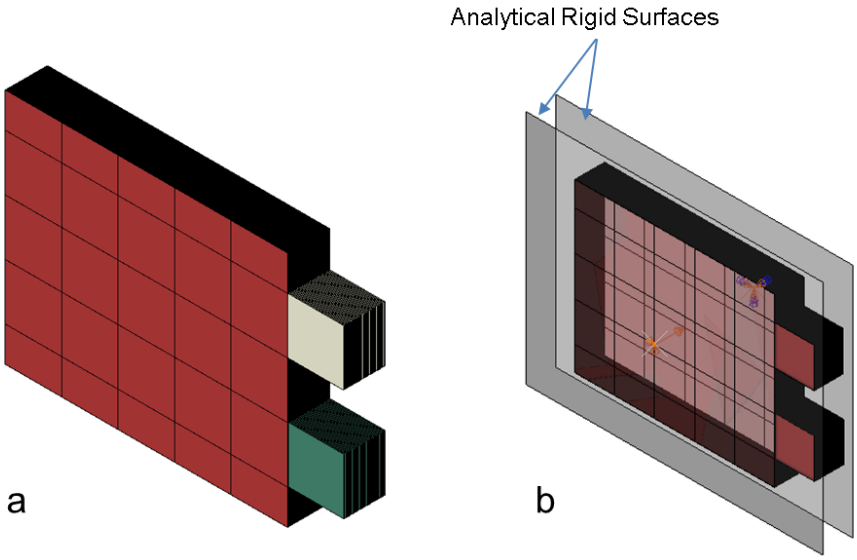

Fig 3:(a) Meshed pouch cell model, (b) pouch model with analytical rigid surfaces to apply mechanical compression load.

4. Results and Discussion

Single Cycle (CCC-CCD) Response:

The Initial simulations are carried out to study the effect of C-rate (2C, 1C, 0.5C) on the charge-discharge behavior of two cases as presented in section.3. Single cycle with constant current charging followed by constant current discharge (CCC-CCD) response of the Fix-Free cell is presented in Fig.4. The displacement of the free end is found to increase as the C-rate decreases. The Electric potential of the cell and reaction force for CCC-CCD cycle for Fix-Fix case is presented in Fig.5. It can be observed that the reaction force increases as the C-rate decreases. This observation is similar to the experimental observations carried out by Yuan[6].

Multiple Cycle Response:

The Fix-Fix and Fix-Free cases were then simulated for four cycles of CCC-CCD at 2C to understand the time behavior of the charge-discharge loading. The potential of the cells for four cycles for both the cases is presented in Fig.6. It can be observed that the time response of the cell is similar to the experimental observations seen in Fig.4 of Yuan [6] work. The reaction force for the case of Fix-Fix case has been found to increase as the cycles progress, and the temperature in Fix-Fix case was found to be relatively different from that of Fix-Free case.

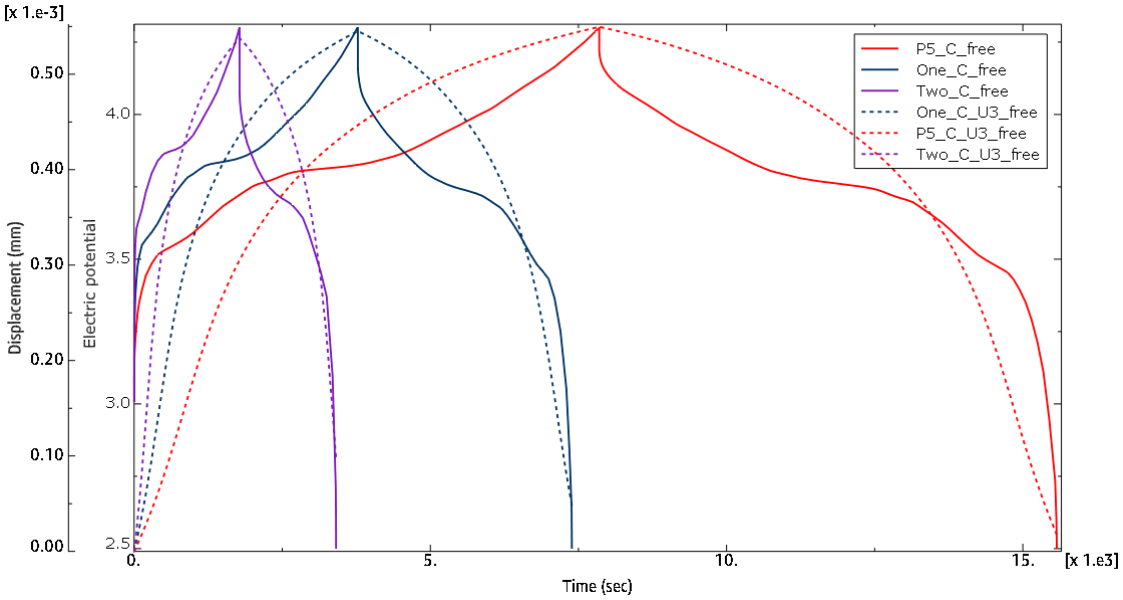

Fig 4:Electric potential and free end displacement of the Fix-Free cell plotted for C-rates 0.5C, 1C, and 2C.

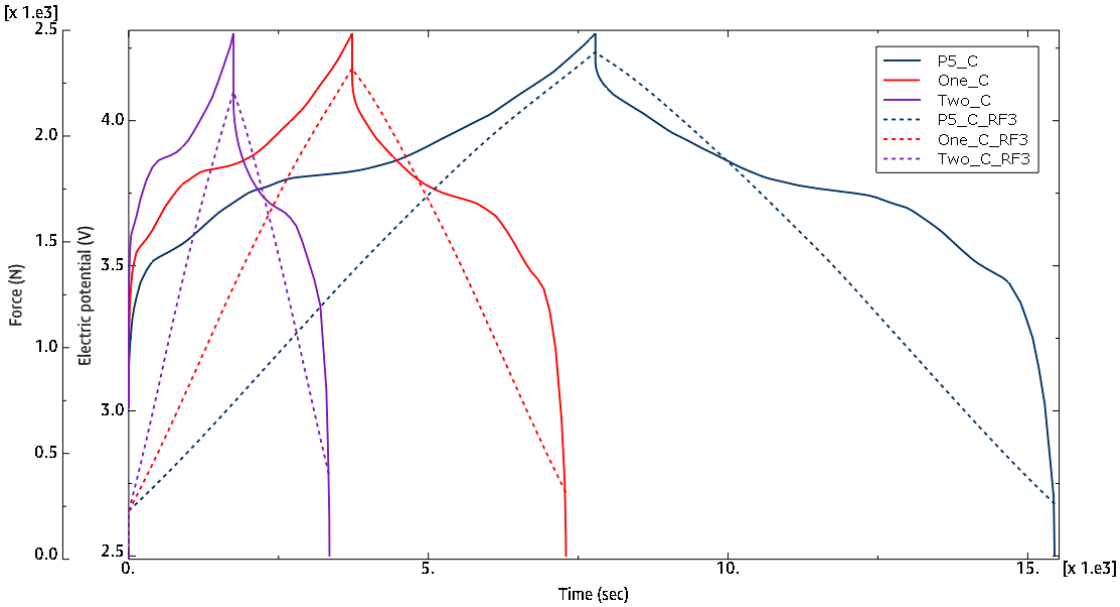

Fig 5:Electric potential and reaction force of the Fix-Free cell plotted for C-rates of 0.5C, 1C, and 2C.

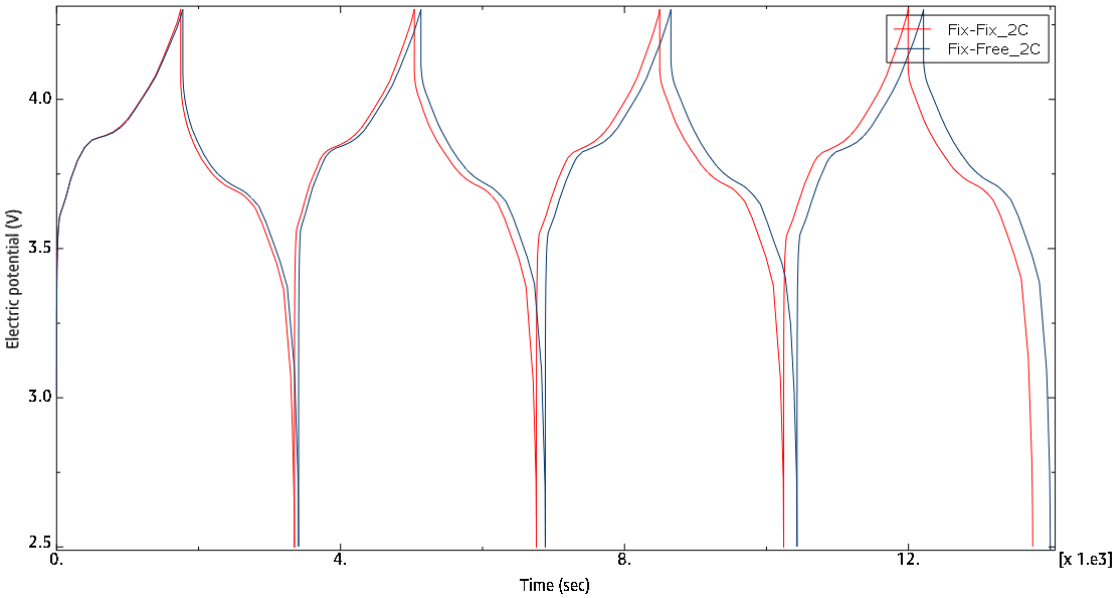

Fig 6:Electric potential of the Fix-Free and Fix-Fix case at 2C rate.

5. Conclusion

A fully coupled TECM model was used to study the effect of mechanical constraints on the charge discharge response of the battery cells. The model was found to capture the reaction force variation with respect to C-rate under Fix-Fix constraint qualitatively similar to the observations in literature. The charge-discharge time of the Fix-Fix cell was found to be lower compared to Fix-Free case as the cycles progress, these numerical cell responses were also similar to observations in literature. The fully coupled framework in ABAQUS provides insights into the interaction between various physics, helping to unravel the underlying mechanisms to design batteries tailored to specific scenarios.

References

[1] Z. Chen, D. L. Danilov, R. Eichel, and P. H. L. Notten, “Porous Electrode Modeling and its Applications to Li-Ion Batteries,” *Adv. Energy Mater.*, vol. 12, no. 32, p. 2201506, Aug. 2022, doi: 10.1002/aenm.202201506.

[2] S. Kulathu *et al.*, “A three-dimensional thermal-electrochemical-mechanical-porous flow multiscale formulation for battery cells,” *Int. J. Numer. Methods Eng.*, p. e7464, Mar. 2024, doi: 10.1002/nme.7464.

[3] J. Xu *et al.*, “Coupling Effect of State-of-Health and State-of-Charge on the Mechanical Integrity of Lithium-Ion Batteries,” *Exp. Mech.*, vol. 58, no. 4, pp. 633–643, Apr. 2018, doi: 10.1007/s11340-018-0380-9.

[4] B. Choi *et al.*, “Importance of uniformly redistributing external pressure on cycling of pouch-type Li-metal batteries,” *Korean J. Chem. Eng.*, vol. 40, no. 3, pp. 524–531, Mar. 2023, doi: 10.1007/s11814-022-1361-3.

[5] J. Xu, B. Liu, and D. Hu, “State of Charge Dependent Mechanical Integrity Behavior of 18650 Lithium-ion Batteries,” *Sci. Rep.*, vol. 6, no. 1, p. 21829, Feb. 2016, doi: 10.1038/srep21829.

[6] C. Yuan, Y. Hahn, W. Lu, V. Oancea, and J. Xu, “Quantification of electrochemical-mechanical coupling in lithium-ion batteries,” *Cell Rep. Phys. Sci.*, vol. 3, no. 12, p. 101158, Dec. 2022, doi: 10.1016/j.xcrp.2022.101158.

[7] M. Ecker, T. K. D. Tran, P. Dechent, S. Käbitz, A. Warnecke, and D. U. Sauer, “Parameterization of a Physico-Chemical Model of a Lithium-Ion Battery: I. Determination of Parameters,” *J. Electrochem. Soc.*, vol. 162, no. 9, p. A1836, Jun. 2015, doi: 10.1149/2.0551509jes.

[8] M. Ecker, S. Käbitz, I. Laresgoiti, and D. U. Sauer, “Parameterization of a Physico-Chemical Model of a Lithium-Ion Battery: II. Model Validation,” *J. Electrochem. Soc.*, vol. 162, no. 9, p. A1849, Jun. 2015, doi: 10.1149/2.0541509jes.
[9] J. Landesfeind and H. A. Gasteiger, “Temperature and Concentration Dependence of the Ionic Transport Properties of Lithium-Ion Battery Electrolytes,” *J. Electrochem. Soc.*, vol. 166, no. 14, p. A3079, Sep. 2019, doi: 10.1149/2.0571912jes.

Coupled Electro-Thermo-Structural analysis of heat coil batteries

Chetan Mahawar[1], Dharanivendhan T[2], Kazuhiro Matsuda[3]

[1] Application Engineer, ANSYS Inc., India
[2] Senior Application Engineer, ANSYS Inc., India
[3] Lead Application Engineer, ANSYS Inc., Japan
Email: chetan.mahawar@ansys.com [1]
dharanivendhant.dharani@ansys.com [2]
kazuhiro.matsuda@ansys.com [3]

Abstract

Usage of batteries for energy storage in electric vehicles, solar panels, portable devices have been increasing exponentially since decades. Performance and life of battery is heavily dependent on thermal and structural factors which in turn affects the electro-chemical behaviour and vice-versa. Non-uniform temperature distribution and structural deformation can result in an uneven electro-chemical state because of strong thermo-structural and electro-chemical coupling and ultimately leads to shorter life span of batteries. Hence, for the complete performance evaluation of battery, considering electro-chemo-thermo-structural coupling is essential. The coupling can be simplified by coupled thermal-structural simulation along with the Joule-heat generation rate which is equivalent to performing coupled electro-chemo-thermo-structural model. In this work, the thermal and structural integrity of battery is analysed by incorporating the effect of temperature dependent resistivity to calculate Joule heat generation which affects the temperature distribution of the structure. This study is performed using restart methodology in simulation on a parameterized 2D Axi-symmetric heat coil battery which reduces computation time significantly in comparison to the 3D modelled heat coil batteries. This methodology can help analyse battery performance in a more efficient manner by capturing the physics accuratel enough .

Keywords: Battery, Joule-heat, Thermal, Structural, Restart analysis

1 Introduction

The performance of batteries is highly influenced by temperature and its surrounding conditions, etc. [1], [2] and [3] as it affects the electro-chemical performance and the thermal and structural integrity of battery. Thermal stresses are generated in the battery due to thermal gradient created by Joule heat generation. The battery materials have temperature dependant properties which add to the complexity. The initial transient phase can cause a higher thermal gradient compared to steady state. Hence, it is essential to predict the contour and evolution of temperature during charging/discharging cycle as part of evaluating the coupled electro-thermal-structural performance of the battery material.

A variety of approaches for modelling the electro–chemo–thermo-mechanical problem have been proposed, see e.g. [4], [5], [6] and [7]. However, only very few models are developed based on fully coupled modelling framework of electrochemical and thermo-structural and the temperature dependant properties are not being considered. In this paper we extend a previously developed coupled electro-thermo-structural consistent computational framework of structural batteries [8], to account for Temperature dependant Joule heating using Restart methodology.

The fully coupled thermo-structural problem is solved for a simplified geometry with the temperature dependant material property and interface/boundary conditions. Numerical studies are analysed & implemented to demonstrate the capability of the Restart framework and to evaluate the effects of temperature dependant Joule heating. The axisymmetric model results are benchmarked against a full 3d model.

2 Methodology

In this section, we have described the proposed framework for simulating the electro-thermo-structural problem. The heat coil battery in 3D model consists of a spiral heat coil embedded in a hollow cylindrical substrate of same height. The current flowing in the heat coil generates heat which gets distributed in substrate through Conduction and Radiation. The heat flow leads to temperature distribution, deformation and stresses in the structure.

Equivalently, the 3D model is simulated as 2D axisymmetric model to reduce the simulation time. The section of 3D model is geometrically modelled as axisymmetric model with heat coil as rectangles adjacent to substrate. Currently Axisymmetric current cannot be given as an input to PLANE222 which is a limitation .Hence, an alternative approach, heat generation along the circumference of the coil is calculated using

commands for each turn of the spiral and applied as body loads. Even within each coil turn, the Joule heat generation will not be uniform across the cross-section as the thermal resistance vary with radial position. To account for this, element wise Joule heating has been calculated for each element in the cross-section based on its radial position. The temperature dependant properties are updated by spitting the analysis into multiple steps and the restating the analysis after each step. During each restart, the resistivity used for calculating the Joule heat is updated based on temperature of the element.

2.1 Electro-Thermo-Structural Model

The geometrical 3D model is a coupled multiphysics Electro-thermal-Structural model composed of heat coils made of copper alloy embedded in an insulator substrate, which acts as a covering to the heat coil. The heat coil considered here is 1mm thick & 5mm height spiral coil. The start face of heat coil is supplied by current of constant magnitude with the other end as grounded, resulting in the heat generation in coil. This heat generation leads to heat flux distribution & ultimately deformation & stresses in the complete structure. The number of nodes & elements for an element size of 0.5 mm is 65,311 and 14,159 respectively.

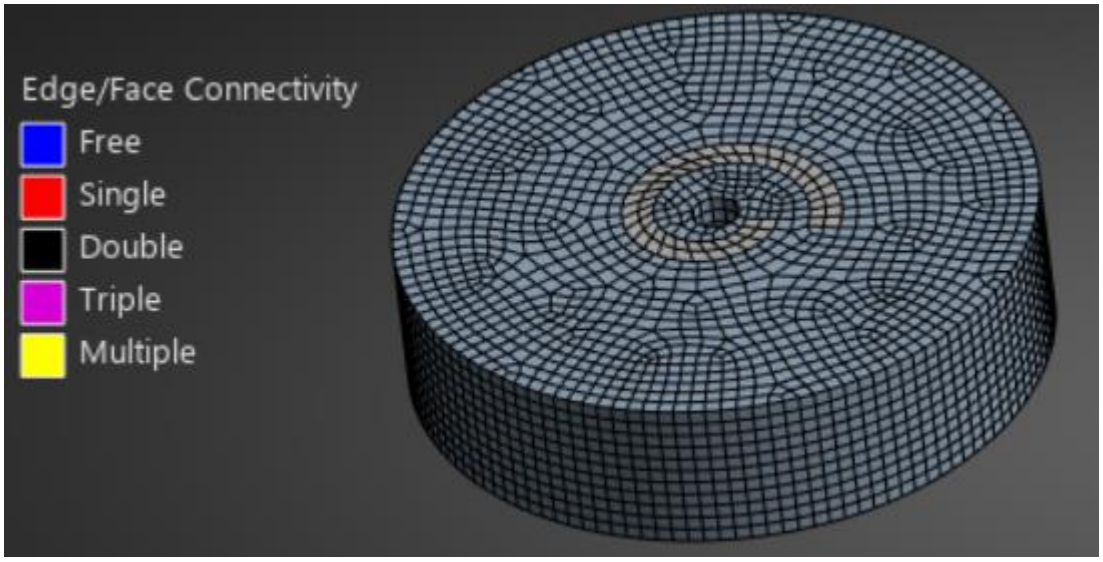

The equivalent comparison to 3D model in the purview of Concept of Simulation time is made by 2D axisymmetric model. Thus, the geometrical 2D model is made with heat coil as rectangles which is also 1mm thick and 5 mm height but is present at the mid-point of the single coil turn as that of 3D model. The heat coil is made of copper alloy material adjacent to the insulator surface, similar to 3D geometrical model.. The number of nodes & elements for an element size of 0.25 mm is 798 and 740 respectively.

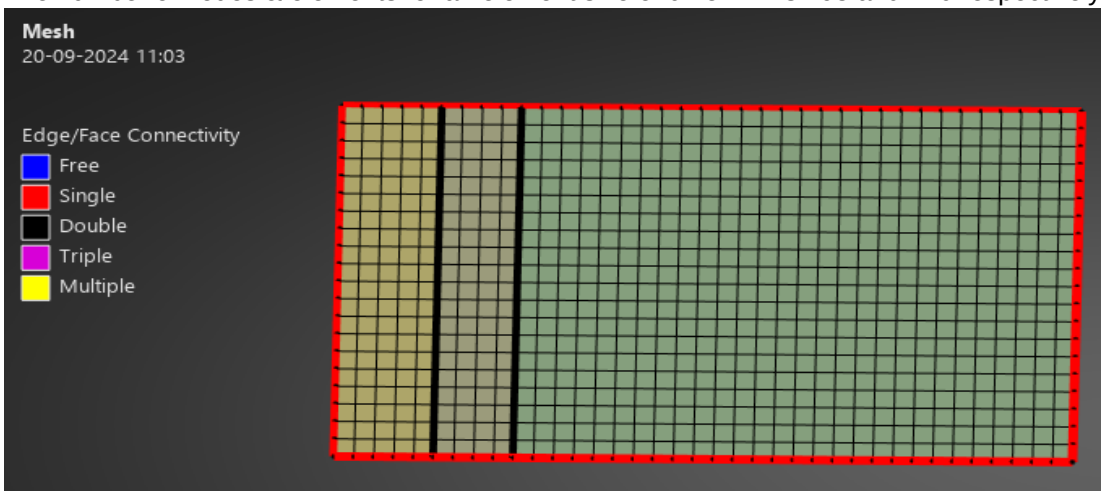

2.2 Restart analysis

The 2D axisymmetric model is a thermo-structural model instead of electro-thermo-structural coupled model as discussed above. Hence, Joule heat is applied as an alternative to the current as that of 3D model. Joule heat is the result of current and the resistance to the flow of current. Thus, in this paper we

are analysing the temperature dependent evolving resistivity which ultimately evolves the Joule heat with time. So, to account this quantitatively a Restart methodology is adopted which updates the resistivity of coil at each time step, based on temperature of the coil at the previous time step. The Restart methodology followed is explained by Restart analysis flow chart[ ] to apply Joule heat to coils, moreover, a more classified approach could be to write UPF for evolving dependent parameters.

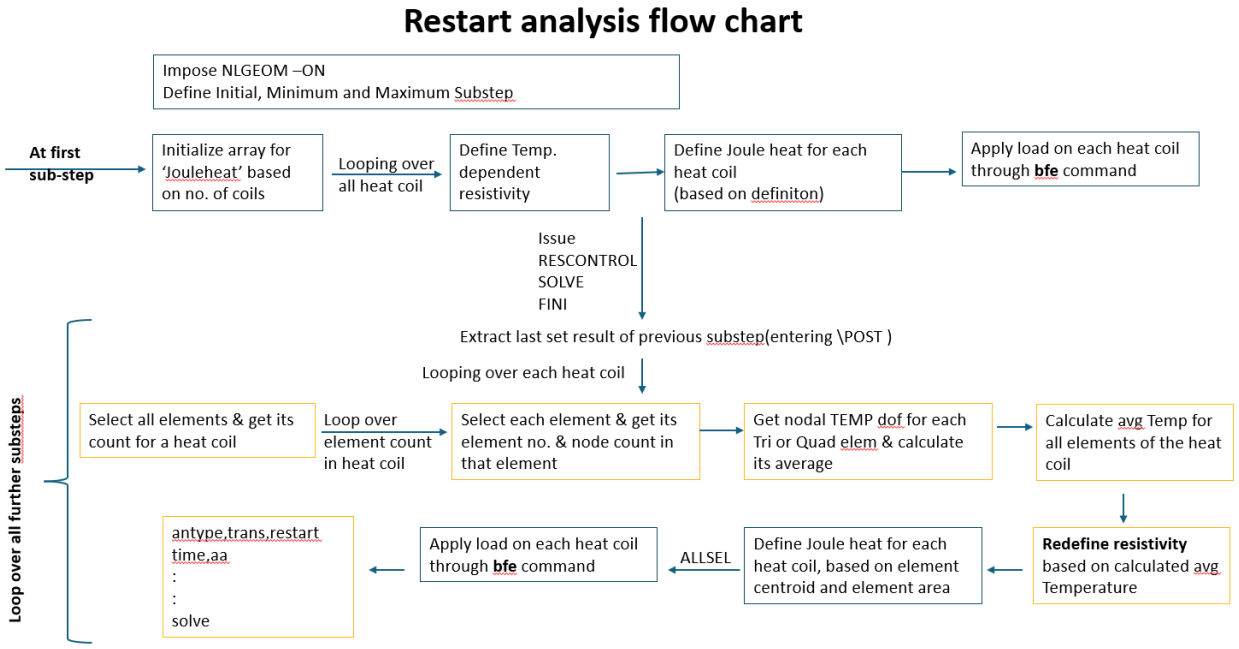

3 Results & Discussion

As mentioned earlier, that flow of current lead to Joule heat generation and thus Temperature, Deformation & Stress distribution can be studied in the structure. So, in this paper we have done study for the heat coil battery analysis considering constant resistivity and as well temperature dependent resistivity for both 3D heat coil and 2D axisymmetric model.

The results of temperature and Stress distribution for constant resistivity of copper alloy is shown in Fig.

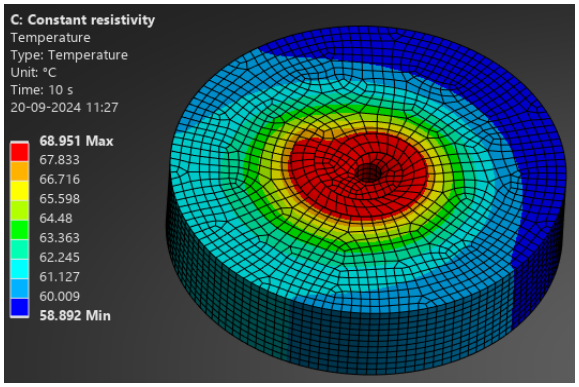

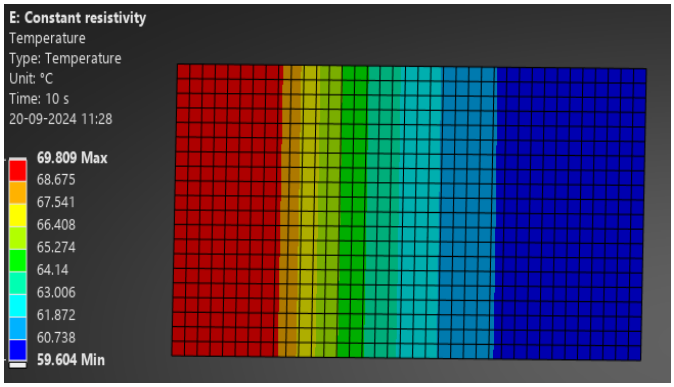

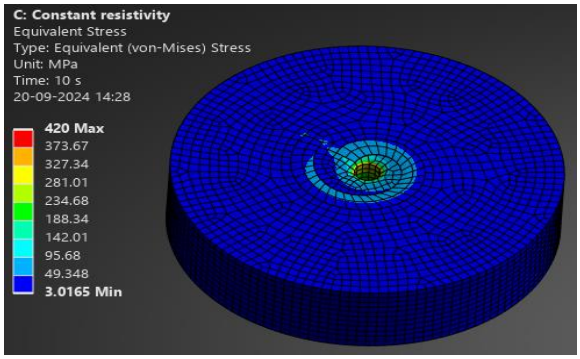

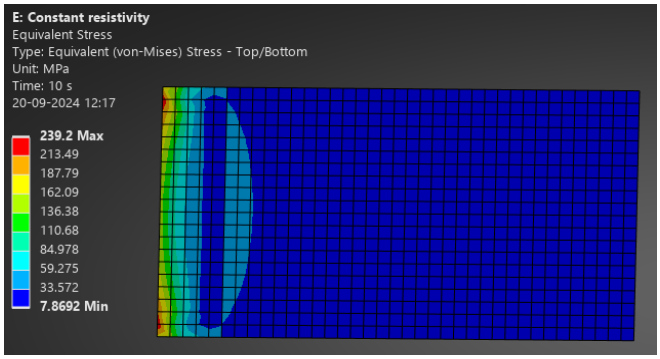

Similarly the results for Temperature dependent resistivity of copper alloy is shown in Fig.

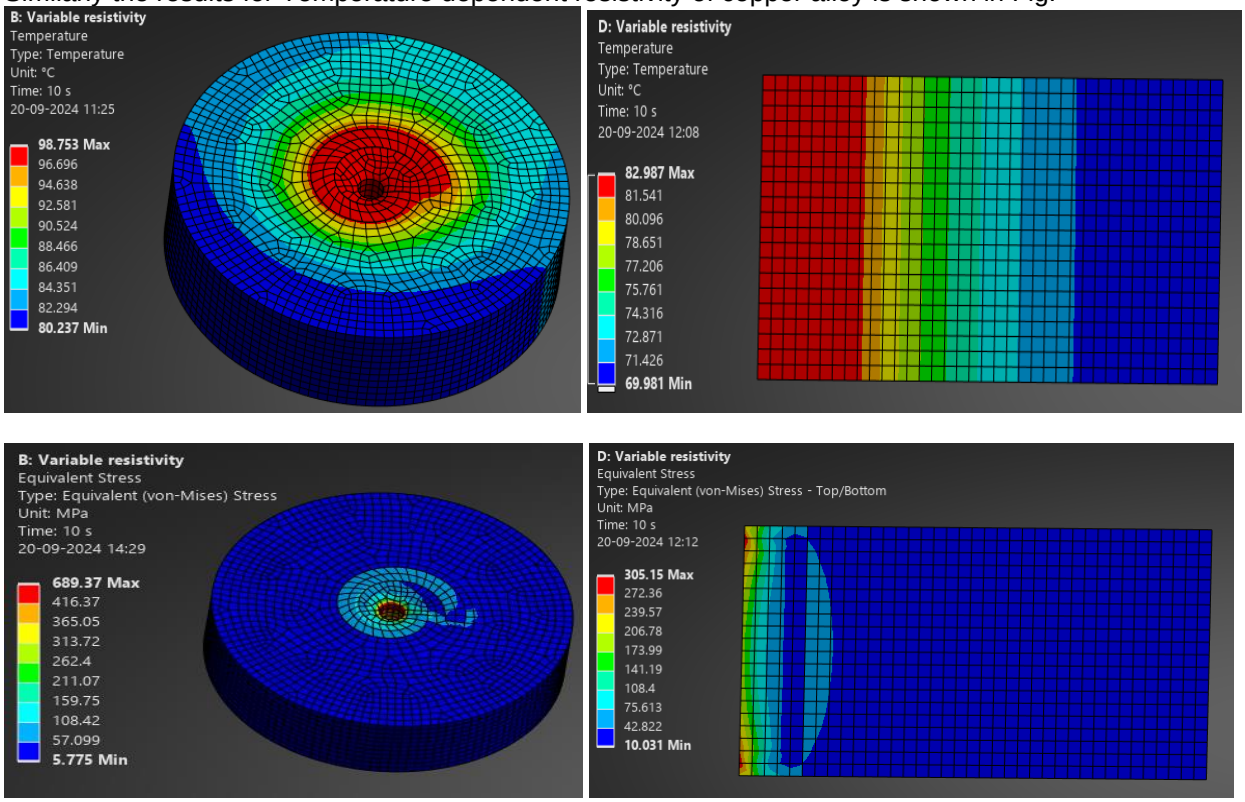

4 Conclusion

5 References

[1] Al Hallaj, S., Maleki, H., Hong, J.S., Selman, J.R., 1999. Thermal modeling and design considerations of lithium-ion batteries. J. Power Sources 83, 1–8. http://dx.doi.org/10.1016/S0378-7753(99)00178-0.

[2] Thomas, K.E., Newman, J., 2003. Thermal modeling of porous insertion electrodes. J. Electrochem. Soc. 150, A176. http://dx.doi.org/10.1149/1.1531194

[3] Forgez, C., Vinh, D.D., Friedrich, G., Morcrette, M., Delacourt, C., 2010. Thermal modeling of a cylindrical LiFePO4/graphite lithium-ion battery. J. Power Sources 195, 2961–2968. http://dx.doi.org/10.1016/j.jpowsour.2009.10.105

[4] Hu, B., Ma, Z., Lei, W., Zou, Y., Lu, C., 2017. A chemo-mechanical model coupled with thermal effect on the hollow core–shell electrodes in lithium-ion batteries. Theor. Appl. Mech. Lett. 7, 199–206. http://dx.doi.org/10.1016/j.taml.2017.09.001

[5] Zhang, X., Chumakov, S., Li, X., Klinsmann, M., Kim, S.U., Linder, C., Christensen, J., 2020. An electro-chemo-thermo-mechanical coupled three-dimensional computational framework for lithium-ion batteries. J. Electrochem. Soc. 167, 160542. http://dx.doi.org/10.1149/1945-7111/abd1f2

[6] Duan, X., Jiang, W., Zou, Y., Lei, W., Ma, Z., 2018. A coupled electrochemical–thermal–mechanical model for spiral-wound li-ion batteries. J. Mater. Sci. 53, 10987–11001. http://dx.doi.org/10.1007/s10853-018-2365-6

[7] Wang, Y., Wu, H., Sun, L., Jiang, W., Lu, C., Ma, Z., 2021. Coupled electrochemical mechanical modeling with strain gradient plasticity for lithium-ion battery electrodes. Eur. J. Mech. A Solids 87, 104230. http://dx.doi.org/10.1016/j.euromechsol.2021.104230

[8] Carlstedt, D., Asp, L.E., 2020. Performance analysis framework for structural battery composites in electric vehicles. Composites B 186, 107822. http://dx.doi.org/10.1016/j.compositesb.2020.107822.

Multiscale Coupled Electrochemical-Thermal-Mechanical Analysis for Comprehensive Battery Pack Simulation

Matias Zielonka, Youngwon Hahn, Neha Parool & Alan Tan (Dassault Systèmes)

Summary

The development of efficient and accurate simulation methods for battery systems is crucial for advancing electric vehicle and energy storage technologies. While significant progress has been made in modeling and simulating individual battery cells and modules, there remains a need for comprehensive analysis at the battery pack level. This work extends the advanced reduced order modeling technique developed in [3], validated for cell and module simulations, to enable coupled thermal-electrochemical-mechanical analysis at the pack level. We demonstrate the robustness and scalability of this approach through a comprehensive pack-level simulation, showcasing its ability to accurately predict overall battery pack performance while capturing the intricate interplay of its components across multiple scales.

Keywords

Battery pack simulation, Reduced order model (ROM), Electrochemical-thermal-mechanical coupling, Finite element analysis, Lithium-ion batteries, Pouch cells, Cell swelling, Abaqus®.

1 Background

The foundational framework for understanding and simulating the electrochemical processes within battery cells was laid by Doyle, Fuller, and Newman [1], who developed the one dimensional (1D) porous electrode theory for lithium-ion batteries.

Building upon this seminal work, Kulathu et al. [2] developed a comprehensive 3D thermal-electrochemical-mechanical-porous flow multiscale formulation for battery cells. The proposed formulation, implemented within the framework of the commercial software Abaqus® [4], extends the original 1D model, integrating electrochemical processes with poro-mechanical deformation and thermal effects, and providing a robust platform for highly detailed 3D cell-level simulations.

Leveraging this foundation, Hahn et al. [3] introduced a reduced order modeling technique that accurately capture the electrochemical/thermal/mechanical behavior of battery systems while significantly reducing computational cost. The efficiency and accuracy of this reduced order modeling (ROM) technique was demonstrated for both cell-level and module-level simulations by comparing the ROM results with a detailed model for various thermal and electrochemical performance metrics. This approach allows for efficiently scaling simulations from cell level to module level, balancing computational efficiency with model accuracy.

The current study applies this reduced order modeling technique at the pack level, demonstrating its ability to accurately predict overall battery pack electrochemical, thermal, and mechanical performance while accounting for the complex interactions between individual cells and module components.

2 Objectives

The primary goal of this research is to apply the reduced order modeling technique (ROM) introduced in [3] at the battery pack scale, and thus leveraging the coupled electrochemical-thermal-mechanical analysis capabilities of Abaqus® [4]. This approach aims to enable efficient simulation of complete battery packs while substantially reducing computational costs compared to full-fidelity cell-level models applied at the pack scale. Specific objectives include:

a) Deploy and validate the reduced order modeling technique (ROM) introduced in [3] at the battery pack scale demonstrating its ability to:
   - Capture the complex coupling between cell-level phenomena and pack-wide behavior
   - Significantly reduce computational costs compared to detailed cell-level models.
   - Maintain accuracy in predicting individual cell and module, and overall pack performance.

b) Incorporate key pack-level design components into the analysis, specifically:
   - Busbars for electrical connections between modules.
   - Phase Change Materials (PCMs) for thermal management.

c) Enable detailed analysis of individual cell behavior (Fig. 1a) within the pack context, focusing on:
   - Variations in temperature, state of charge, and charging/discharging cycles across cells,
   - Mechanical load distribution and its impact on cell performance.
   - Identifying potential hotspots or areas of stress concentration within the pack

d) Analyze the design of module electric connectors, specifically tabs, pins, and terminals, to optimize both electrical and thermal performance, focusing on geometry and material selection.

e) Investigate the impact of different thermal interface materials between cells on overall thermal performance, aiding in the optimization of thermal management strategies.

f) Demonstrate the model's ability to capture multi-scale interactions within the battery pack's hierarchical structure (Fig. 1b,c,d), specifically:
   - Component-level Interactions within each hierarchical level (e.g., between electrodes, separators, and collectors within a cell)
   - Cross-level interactions between adjacent hierarchical levels (e.g., between cells and their housing, or between module-level casings and the pack-level PCM (Phase Change Material))
   - System-wide effects and their propagation across scales: (e.g., bottom-up effects where cell-level phenomena influence module and pack-level performance or top-down effects where pack-level design choices and constraints affect module and individual cell behavior).

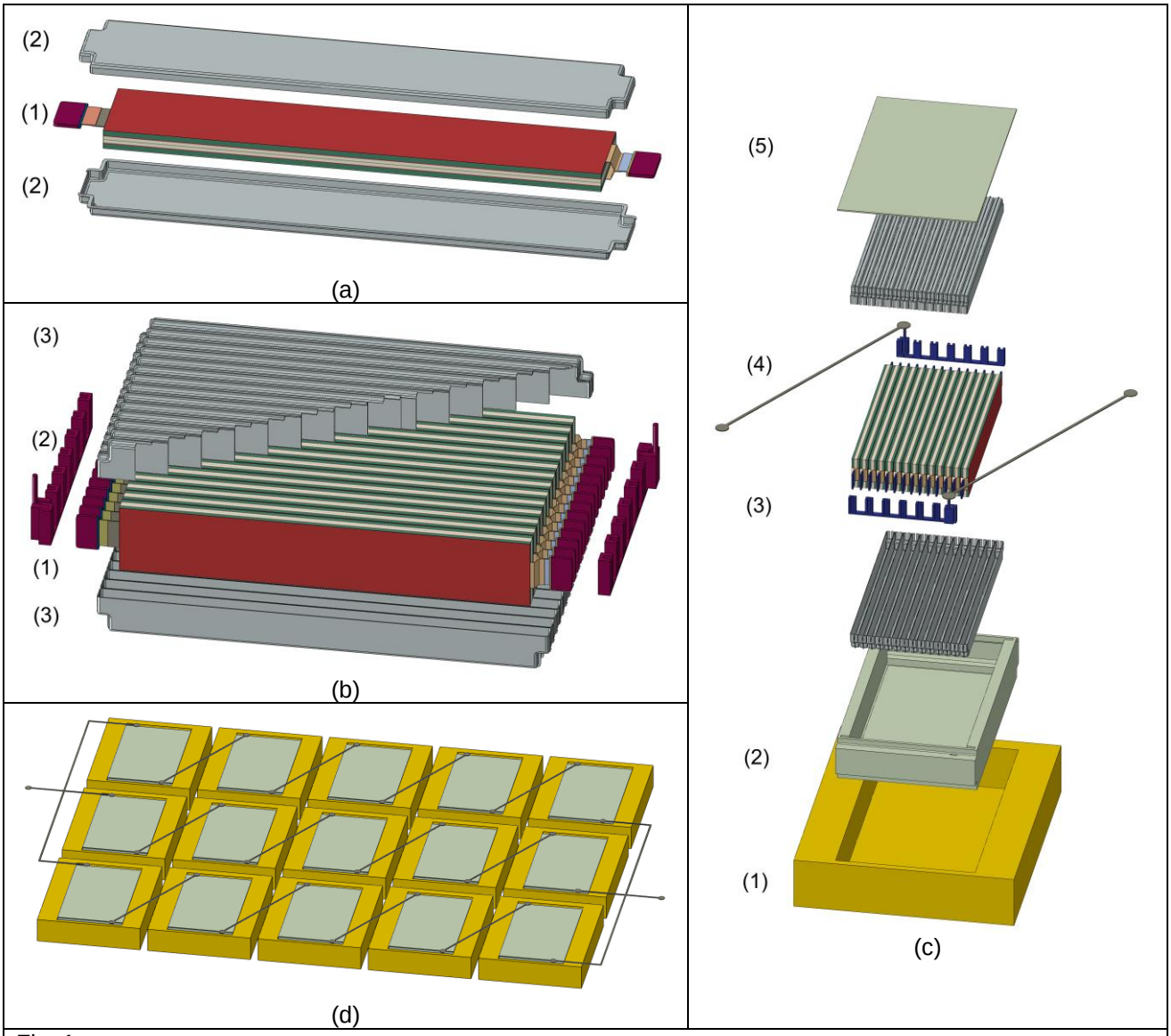

Fig. 1
(a) Reduced pouch cell (1) and cell housing (2), (b) Module assembly, showcasing cells (1), pins and terminals (2) and cell housings (3), (c) Module Assembly, showcasing PCM (1), module casing (2), pins and terminals (3), busbars(4), and module top covers (5), (d) Pack assembly with 15 modules and PCMs.

3 Methodology

The (ROM) methodology described in [3] reduces model complexity by replacing multiple stacks of thin electrode, separator, and current collector layers with a single stack of thicker layers as depicted in Fig. 2. This maintains the overall thickness of the cell while significantly reducing the number of finite elements in the model. To account for the modified layer thicknesses, the ROM methodology involves also the proper scaling of several key material properties, such as the electrical conductivity in the solid phase and the ionic conductivity and diffusivity in the electrolyte phase. We extend this ROM concept to develop a comprehensive battery pack model (Fig 1.).

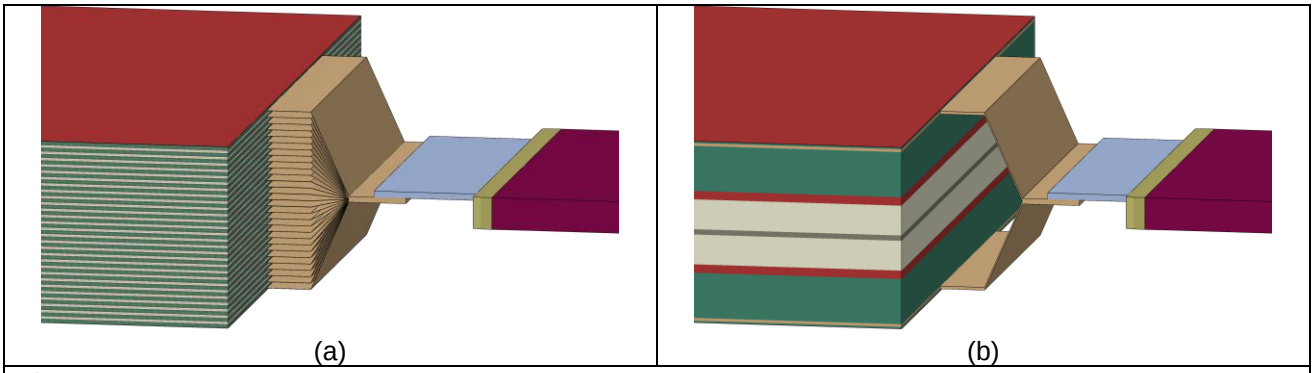

(a) (b)

Fig. 2
(a) Detailed pouch cell model featuring multiple stacks of anode/separtor/cathode/collector layers.
(b) Reduced pouch cell model featuring a single stack of thicker layers and scaled material properties.

4 Model and Scenario

Building upon the ROM methodology described in the previous section, we develop a comprehensive multi-scale model that spans from individual cell components to a full battery pack.

4.1 Model

The first step to build this model involves adding the cell housing to the cell-level ROM (Fig. 1a). We then integrate 14 of these cell models with housing into a module, incorporating module-level components such as pins, tabs, terminals, casing, and top cover (Fig. 1b and 1c). Contact interactions between cells and housing, housing and casing, considering thermal and electric conductance or insulation between components as appropriate. To create the full pack model, we replicate 15 instances of these modules (Fig. 1d). Key pack-level design elements are incorporated, including busbars for electrical connections and phase change materials (PCMs) for thermal management. Contact interactions between module casings and PCMs are also modeled. To accurately represent component interactions, friction is incorporated in all contact pairs throughout the model.

4.2 Initial and Boundary conditions

Mechanical boundary conditions are implemented to simulate realistic constraints and interactions within the battery pack. The base of all phase change materials (PCMs) is vertically constrained, representing their placement on a horizontal ground surface, while allowing for horizontal and vertical expansion due to swelling.

Electrical initial conditions are set to prevent potential short circuits. To this end, the PCMs, module casings, module top covers, and cell housings are all electrically grounded. This ensures electrical isolation between these components and the active electrical elements of the battery pack.

4.3 Loads

For this study, we simulate the following charge-discharge cycle:
- Initial state: All cells in all modules are fully discharged.
- Charging phase:
  - Constant current (CC) charging at 1C rate.
  - Constant voltage (CV) charging.
- Discharging phase:
  - Constant current (CC) discharging at 1C rate.

Throughout the entire cycle, the battery pack is air-cooled, with an ambient temperature maintained at 25°C. This cycle allows us to examine the pack's behavior under typical usage conditions.

5 Results

We present detailed results of our coupled electrochemical/thermal/mechanical analysis across multiple scales - from individual electrodes and cells to modules and the entire pack - demonstrating our model's ability to capture complex multi-scale interactions within the battery pack's hierarchical structure and pack-wide effects and their propagation across scales. These results fall into the three coupled physical processes, each representing a key factor affecting battery's performance:

- Electrochemical:
  - Distributions of state of charge (SOC) and depth of discharge (DOD)
  - Voltage and current profiles
  - Li-ion concentration gradients in the electrolyte
  - Li concentration variations in the active particles
- Thermal:
  - Temperature distributions and gradients, identifying potential hotspots
- Mechanical:
  - Swelling deformation and expansion,
  - Stress distributions, highlighting areas of potential mechanical weak points.
  - Contact interaction pressures and deformations at various interfaces.

Special attention is given to the performance of busbars, highlighting any areas of excessive heating or current bottlenecks, and on PCM's, assessing their effectiveness in managing heat across the pack during operation.

Based on these results, we provide specific insights into potential design optimization, including options to improve thermal management strategies and to enhance overall pack electrochemical performance.

6 Conclusions

We have successfully extended and validated the ROM approach described in [3], enabling efficient coupled electrochemical-thermal-mechanical simulation at the full battery pack level. This model effectively captures complex interactions between cell-level phenomena and pack-wide behavior while substantially reducing computational costs compared to detailed cell-level models.

Our multi-physics analysis yields comprehensive insights into the battery pack's multiscale behavior and reveals opportunities for enhancing thermal management strategies and overall pack design. We present detailed results on electrochemical variable distribution, thermal gradients, and mechanical stresses across individual cells, modules, and the entire pack during the entire charge-discharge cycle. This detailed examination allows for the identification of potential hotspots, stress concentration areas, and electrochemical performance bottlenecks, while also evaluating the effectiveness of electrical connections and thermal management.

This work demonstrates the viability of conducting comprehensive multi-physics analyses of battery packs with Abaqus® [4], paving the way for more efficient and accurate virtual prototyping of battery packs for electric vehicles and energy storage applications.

7 References

[1] Doyle, M.; Fuller, T.F.; Newman, J. Modeling of Galvanostatic Charge and Discharge of the Lithium/Polymer/Insertion Cell. *Journal of The Electrochemical Society* **1993**, *140*, 1526-1533, doi:10.1149/1.2221597.

[2] Kulathu S., Hurtado J., Bose K., Hahn Y., Bouzinov P., Taylor R., Oancea V., "A three-dimensional thermal-electrochemical-mechanical-porous flow multiscale formulation for battery cells". International Journal for Numerical Methods in Engineering, 2024; 125(13):e7464. doi:10.1002/nme.7464

[3] Hahn Y., Gao Z., Nguyen T.-T., Oancea V., "A reduced order model for a lithium-ion 3D pouch battery for coupled thermal-electrochemical analysis," Journal of Energy Storage, 70, 107966, 2023. doi:10.1016/j.est.2023.107966

[4] Abaqus® Analysis User's Guide. *Version 2024*. Dassault Systémes Simulia Corp; 2024.

MULTIPHYSICS METHODOLOGY FOR DETECTION OF HOTSPOTS ON PCB USING DCIR AND THERMAL SIMULATION

Priyanka R, Shruthi G S (TE Connectivity India pvt. Ltd.)

1 Introduction

Thermal analysis on PCB is often used to check the distribution of temperature on the PCB board and its components to detect hot spots. Overheating of PCBs can cause damaging effects to them.

Electronics are continuously evolving, becoming faster and more compact, which enables them to perform effectively in more demanding environments and applications. ICs and other components on PCB are smaller than ever and operate at faster frequencies and require more power. As more current is passed through these small devices, the voltage drops across these resistive elements converts power into heat, causing increase in temperature and hotspots [3].

To develop high-quality circuit boards, it is important to consider the safety and temperature of your system and design your PCB for efficient thermal performance. The layers of a PCB are highly sensitive to fluctuations in temperature, and when they get too hot or cold, they expand and contract, causing them to lose structural integrity. Excessive heat can result in circuit damage and oxidation of PCB components which is of high concern as well.

2 Methodology

Thermal analysis for PCB trace heating is a complex problem and can be simplified by coupling the same with DCIR (Direct Current Internal Resistance) simulation [4].

DCIR simulation is a branch of Power Integrity analysis which plays a crucial factor in determining the success or failure of modern electronic products that aid in capturing voltage drop, current density, via current and power losses in each trace and copper pour of PCB.

Ansys EDB file is imported into SIwave software. It consists of complete PCB Design data that includes PCB outline, layers, components, routing, assembly, silkscreen, etc. [1].

The imported Stack up provides the PCB layer information like materials used, layer thickness, dielectric, loss tangent properties, etc.

Voltage, current, and intermediate component values for the respective power nets should be assigned and the reference GND net for the PDN path needs to be provided. The PDN path is considered with the help of the Schematic Design of the PCB.

The power nets should be configured and validated before performing the DCIR simulation.

The power loss results are obtained from DCIR analysis in Ansys SIwave software, which are then imported to the classic ICEPAK software.

The MCAD which consists of PCB geometry (STEP file) should be imported into the solver. To this PCB geometry ECAD is imported for the trace and nets information.

DCIR simulation gives us power loss results which, can be imported for each layer of PCB. Power maps can be visualized to understand how temperature would vary as per power concentration.

Good quality grid needs to be generated for PCB geometry and the grid density for ECAD needs to be examined. Metal fraction can be visualized for PCB traces.

Steady state thermal analysis is then carried out considering the operating conditions [2]. This simulation gives us the temperature profile across the PCB board due to joule heating in the copper traces as per the power distribution input given.

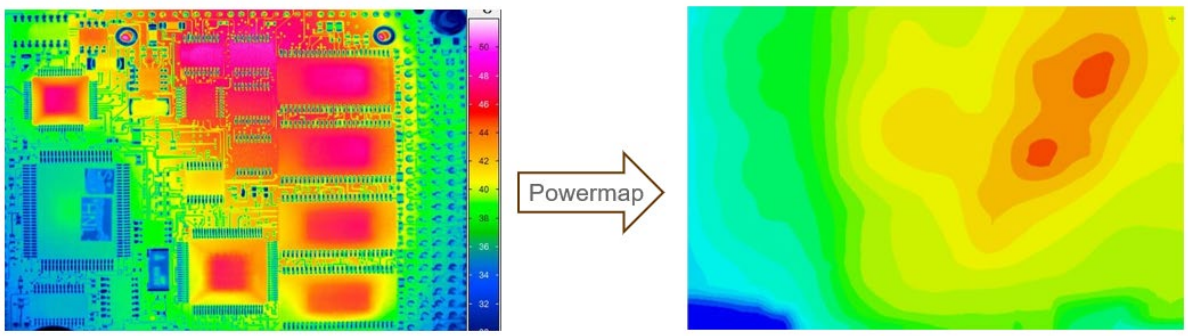

Fig. 1 - Power maps from DCIR simulation will be used as input for thermal simulation.

The methodology can be extended for module level simulations as well where multiple PCBs are modelled in the enclosure.
The results from this simulation will help us to detect the hotspots not only on the PCB board but, also on the components atop and in the overall enclosure / module. The temperature rise can be observed due to the combined heating effect of traces, copper pour and the power dissipation from the components.

Some of the challenges faced during thermal analysis are accurate modeling, complexity and effectiveness of different thermal strategies. PCB thermal management techniques depend on a number of factors including the amount of heat the components and circuit dissipate, the environment, the overall design, and the enclosure.
The complexity in the module level simulation was to include ECAD and respective power maps in all the modelled PCBs inside the enclosure.

3 Conclusions

This methodology aids in determining the thermal gradient on PCB boards due to trace heating in different layers of PCB. The correlation with physical test result was in the range of 5-15%.It also helps in identifying hotspots on PCB as per the power concentration. This method can be used wherever there is a requirement to identify thermal profile on PCBs due to heating of current carrying traces.

4 References

[1] Electronics | Signal & Power Integrity - Learning Guide (sapjam.com)
[2] Electronics | Thermal Management - Introduction into Ansys Icepak (Classic) (sapjam.com)
[3] https://www.wellpcb.com/blog/pcb-manufacturing/pcb-thermal-simulation
[4] https://blogs.rand.com/randsim/2022/05/five-easy-electronics-simulations-that-benefit-pcb-customers.html

Implementation of Digital Twin for Cathodic Protection

Zhen Qi Chee[1,2], Cheng Siong Chin[2], Hao Chen[2], Zi Jie Choong[2], JJ Chong[2], ShiLiang (Johnathan) Tan[1]*

[1]*Matcor Technology & Services Pte Ltd, Cetim-Matcor, 3 Seletar Aerospace Link, Singapore 797550, Singapore*

[2]*Faculty of Science, Agriculture, and Engineering, Newcastle University, Singapore 599493, Singapore*

**E-mail: johnathan.tan@cetim-matcor.com*

Abstract:

Procor, a Cetim in-house numerical program, utilises the boundary element method for verifying and optimising cathodic protection (CP) systems, providing effective protection for structures and applications while conserving resources. It acts as a quick decision aid and reduces maintenance through reliable evaluation of the lifetime of CP installations. This is achieved using simulations to predict current potential, anode depletion, and the required current for impressed current cathodic protection systems. With the recent growth of the Industrial Internet of Things, there has been an increase in the digitisation of processes to enhance accuracy and productivity. Applying the digital twin to a CP system allows live data to be sent to Procor, enabling real-time simulation of the CP system. The simulation results illustrate the CP potential field gradient on a 3D model (digital twin), with the 3D potential field displayed in different colours based on the potential level, aiding the user in assessing the protection level of the model. Corrective or preventive measures can then be implemented as needed. Considering these developments, there is significant interest in developing a digital twin for real-time cathodic protection diagnostics using Procor. This cutting-edge system allows Procor to function as a real-time monitoring tool capable of assessing corrosion risk, making it applicable across a wide range of systems.

Keywords: Cathodic Protection, Boundary Element Method, Procor, Digital Twin, Real-time monitoring

1. INTRODUCTION

1.1 Background

Cathodic protection (CP) systems are critical for safeguarding metallic structures from corrosion, particularly in oil and gas, marine, and infrastructure industries. Traditional CP systems rely on either Sacrificial Anode Cathodic Protection (SACP) or Impressed Current Cathodic Protection (ICCP) methods to mitigate corrosion by shifting the electrochemical potential of the protected structure [1]. While effective, these systems require regular maintenance and careful monitoring to ensure optimal performance and longevity. If poorly designed, it would be dangerous as it exposes the public to the risk of structural failure [2]. Procor, a Cetim in-house numerical program, employs the Boundary Element Method (BEM), a numerical technique particularly suited for solving problems in electrostatics and corrosion. By solving the boundary integral equations, simulating CP systems can provide a reliable means of predicting current potential, anode depletion, and the required current for ICCP systems. These simulations contribute to the accurate assessment and optimisation of CP installations, reducing the need for extensive physical testing and conserving resources [3]. BEM can accurately simulate the potential field around the protected structure, predicting the current distribution and the CP system's effectiveness. However, that would require engineers to measure on-site data for calculation. Certain risks are involved, especially when dealing with an ICCP system. [4] Hence, the recent shift toward digitisation in various industrial processes has created opportunities to enhance CP system simulations through real-time data integration. A virtual representation of the physical CP system is created by applying a digital twin concept [5,6]. This digital twin can receive live data from sensors installed on the system, allowing Procor to perform real-time simulations and continuously update the CP potential field.

The concept of digital twin technology has evolved through the years. One of the most popular concepts is Gartner's three-stage digital twin model [7]. The first level is a simple digital model, representing a physical entity of the system. The second level introduces a one-directional flow of information. This usually involves a simple monitoring system where measured data are displayed on the digital representation of the structure and includes alarms. Lastly, the third level enables two-way communication between the digital and physical systems, allowing users to change settings digitally. This also includes simulations of solutions for the system, utilising measured data to compute the electrochemical profile of the structure [8]. DT involves creating virtual representations of physical objects using the Internet of Things (IoT) to mirror their real-world counterparts in real-time. These representations are built by integrating data from diverse sources like sensors, simulations, and monitoring systems. One essential advancement DT facilitates is its ability to monitor, analyse, and interact with physical objects or systems [9]. The synergy will enhance corrosion monitoring and ensures timely intervention, thereby optimising the overall efficacy of CP measures with monitoring capabilities, facilitating continuous assessment of corrosion risks across diverse systems.

1.2 Objectives

The primary objective is to explore the integration of real-time data with Procor for enhanced cathodic protection diagnostics. This integration aims to improve the accuracy of simulations, enable real-time monitoring, and provide a more comprehensive understanding of CP system performance through a digital twin.

2. METHODOLOGY

The two test benches would cover both subterranean and subsea scenarios, focusing on the readily available carbon steel protection. The SACP would be deployed for protection of buried pipe in the soil using a magnesium anode, while the ICCP will protect a miniature offshore jacket in an improvised subsea structure employed with a mixed metal oxide anode controller with rectifier. The proposed system will integrate IoT sensors to create an innovative CP system. Key components include a network of IoT-enabled reference electrodes and sensors, a central control unit, a BEM-based simulation module for system optimisation, and a user interface for remote monitoring and control. As there are two main methods of CP, both will be integrating distinct types of IoT sensors as their environmental condition differ.

2.1 Sacrificial Anode Cathodic Protection

The SACP entails burying a carbon steel pipe in the soil to simulate an underground pipe as shown in the diagram in Figure 1. For the SACP, the physical system will focus on a protected pipe, the Sacrificial Anode, and the Zinc Reference Electrode. The system is embedded with a Raspberry Pi 5, which allows for remote monitoring with Virtual Network Computing (VNC). Currently, three sensors are used for temperature, soil moisture, and electric potential.

Figure 1: Monitoring of the SACP using Procor (Left); Arrangement of the pipe, anode, and electrode before burial (Right)

The data collected from the sensors were stored in both in a cloud database and locally on the Raspberry Pi 5. Data collected from the SACP can be seen in Figure 2. The soil moisture is in a range of 1 to 1023, where 1 is dryer soil, and 1023 is wetter soil. The potential is measured in milliVolts (mV) and temperature is in Degree Celsius (°C).

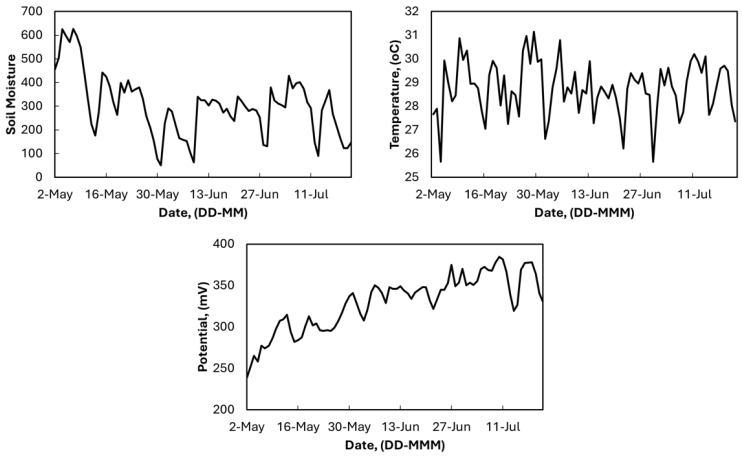

Figure 2: Soil Moisture Levels (Top Left); Temperature (Top Right); Pipe to Zinc Reference Potential (Bottom)

2.2 Impressed Current Cathodic Protection

The ICCP system comprises a carbon steel miniature jacket in a large tank filled with 3% salt water to simulate a subsea environment. The steel jacket is submerged and protected by an impressed current. For the ICCP, the physical system will focus on the Mixed Metal Oxide Anode, miniature Steel Jacket, a programmable rectifier and two Silver Chloride Reference Electrode. The system is embedded with a Raspberry Pi 5, allowing remote monitoring using VNC and control of the rectifier using RS485. Currently, five sensors are used for temperature, dissolved oxygen, pH level, Turbidity, and electric potential. This can be seen in the diagram shown in Figure 3.

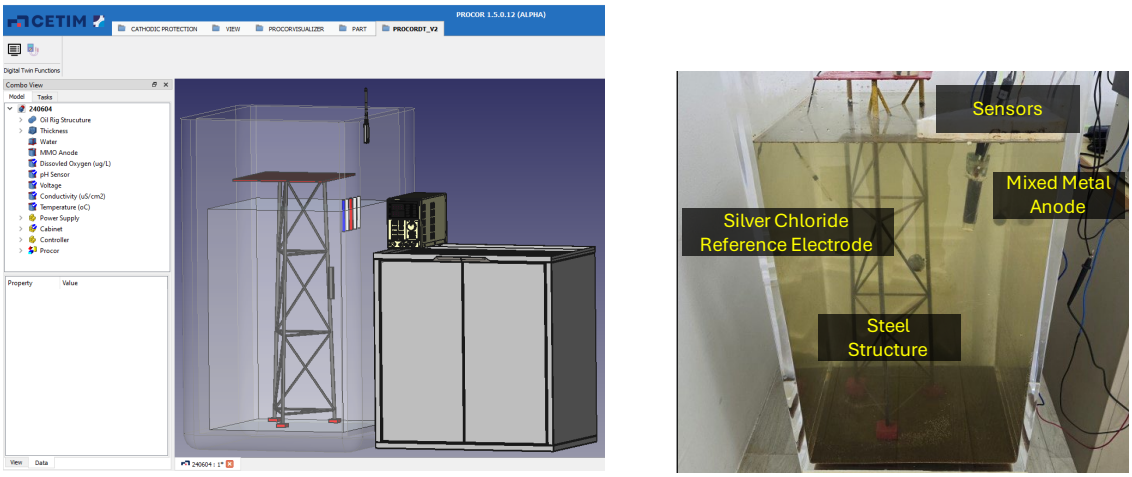

Figure 3: Monitoring of the SACP using Procor (Left); Arrangement of the pipe, anode, and electrode before burial (Right)

The data collected from the sensors were stored in both in a cloud database and locally on the Raspberry Pi 5. In addition, the rectifier voltage and current are measured and stored locally. The local data can be accessed by the Raspberry Pi 5 from an interface. Data collected from the ICCP can be seen in Figure 4. Dissolve oxygen is measured in milligram per Litre (mg/L), pH is a scale from 1 to 14 where 1 is acidic and 14 is alkaline. The potentials are measured in milliVolts (mV) and temperature is in Degree Celsius (°C).

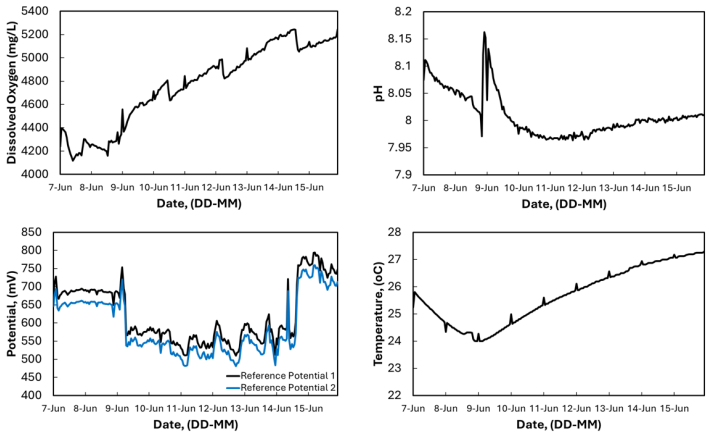

Figure 4: Dissolved Oxygen (Top Left); pH Levels (Top Right); Structure to AgCl Reference Potential (Bottom Left); Structure to AgCl Reference Potential (Bottom Right)

3. DISCUSSION

Integrating real-time data with Procor facilitates continuous monitoring of the CP system, making it possible to promptly detect changes in performance or emerging risks. This real-time simulation capability enhances the accuracy of predictions regarding current demand, anode depletion, and potential distribution. Furthermore, the digital twin concept enables a proactive approach to CP management. By analysing the simulation results, users can implement corrective or preventive measures to address potential issues before they escalate. This extends the life of the CP system, reduces maintenance costs, and minimises the risk of unexpected failures. Visualising the CP potential field in a 3D model provides valuable insights into the system's performance. The colour-coded representation of potential levels allows for easy identification of areas where protection may be insufficient, guiding decision-making for system adjustments or repairs, as seen in Figure 5.

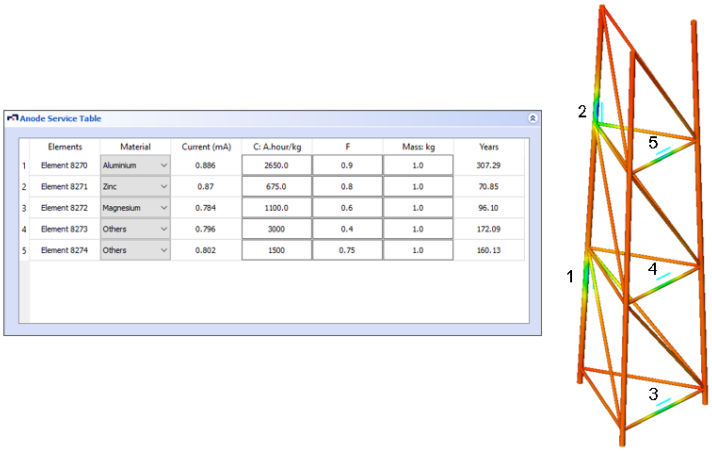

Figure 5: Protection Levels with Procor

4. CONCLUSION

By leveraging the capabilities of a digital twin, this approach enables real-time monitoring and simulation of CP systems, providing a powerful tool for assessing corrosion risk and optimising system performance. As industries continue to embrace IoT, the application of digital twins in CP systems is expected to become increasingly prevalent. With its advanced simulation capabilities, Procor is well-positioned to lead this transformation, offering a comprehensive real-time CP monitoring and management solution. This cutting-edge system enhances the accuracy and reliability of CP diagnostics and extends the operational life of CP systems across a wide range of applications. In addition, the diagnostics will assist in mitigating overprotection and under-protection. Future work will focus on refining the integration of digital twins with Procor and exploring additional applications in diverse industrial settings.

REFERENCES

[1] N. Perez, *Electrochemistry and Corrosion Science*. Cham: Springer International Publishing, 2016. doi: 10.1007/978-3-319-24847-9.

[2] U. M. Angst, “A Critical Review of the Science and Engineering of Cathodic Protection of Steel in Soil and Concrete,” *Corrosion*, vol. 75, no. 12, pp. 1420–1433, Dec. 2019, doi: 10.5006/3355.

[3] S. Aoki and K. Amaya, “Optimization of cathodic protection system by BEM,” *Eng. Anal. Bound. Elem.*, vol. 19, no. 2, pp. 147–156, Mar. 1997, doi: 10.1016/S0955-7997(97)00019-2.

[4] M. Moreau, “Testing Cathodic-Protection Systems,” *Suppl. Lustline 64*, pp. 1–5, 1995.

[5] T. Wang *et al.*, “Pipeline condition monitoring towards digital twin system: A case study,” *J. Manuf. Syst.*, vol. 73, pp. 256–274, Apr. 2024, doi: 10.1016/j.jmsy.2024.02.006.

[6] H. Liu, M. Xia, D. Williams, J. Sun, and H. Yan, “Digital Twin-Driven Machine Condition Monitoring: A Literature Review,” *J. Sens.*, vol. 2022, pp. 1–13, Jul. 2022, doi: 10.1155/2022/6129995.

[7] Gartner, “Use the IoT Platform Reference Model to Plan Your IoT Business Solutions,” *Stamford*, vol. CT, 2016.

[8] A. Andrade, “The 3 Levels of the Digital Twin Technology,” Vidya. Accessed: Jul. 09, 2024. [Online]. Available: https://vidyatec.com/blog/the-3-levels-of-the-digital-twin-technology-2/

[9] R. Kazała, S. Luściński, P. Strączyński, and A. Taneva, “An Enabling Open-Source Technology for Development and Prototyping of Production Systems by Applying Digital Twinning,” *Processes*, vol. 10, no. 1, p. 21, Dec. 2021, doi: 10.3390/pr10010021.

Singing Capacitors Secrets Simulation

Ravi Sankar Kanamarlapudi, Nopasorn Kowathanakul (Ansys)

1 Summary

Capacitors are essential for ensuring the smooth operation of electronic devices by regulating electrical flow across the printed circuit board (PCB). Among these, Multilayer Ceramic Capacitors (MLCCs) are widely used in modern electronics due to their affordability, compact size, broad capacitance range, low Equivalent Series Inductance (ESL) and Equivalent Series Resistance (ESR), as well as their excellent frequency response.

A commonly used dielectric material in MLCCs, BaTiO3, exhibits piezoelectric properties, causing the capacitor to contract and expand in response to electrical signals. This mechanical vibration, transferred to the PCB, is often referred to as the “singing” effect. To accurately simulate this phenomenon—encompassing piezoelectric characteristics, vibration behavior, and noise generation—robust multiphysics software like Ansys is required.

This work demonstrates the application of Ansys’ Coupled Field Harmonic analysis system, incorporating advanced practices in acoustic preprocessing (such as the surface wrapper and Perfectly Matched Layer (PML) extrusion layers), along with a comparison of Finite Element Method (FEM) acoustics within the Ansys Mechanical environment. The pre-built piezoelectric material database in Ansys Mechanical simplifies the selection of standard materials, with predefined matrices for anisotropic elasticity, piezoelectricity, and relative permittivity.

With these Multiphysics capabilities, developing a comprehensive simulation methodology during the early design stages is crucial to addressing noise-related issues, particularly through Harmonic Acoustics analysis driven by vibration characteristics (Modal analysis and Harmonic response). This study is particularly relevant to R&D engineers in the semiconductor industry, offering insights into system-level behavior (vibrations and acoustics) of semiconductor components.

2 Methodology Overview

2.1 Geometry Considered

- **Board Dimensions:** 190 mm x 114 mm x 2.1 mm
- **MLCC Dimensions:** 2 mm x 1 mm x 1 mm
- **Assumption:** The MLCC is represented as a simple solid with assigned piezoelectric material properties, enabling the simulation of its electrical and mechanical behavior.

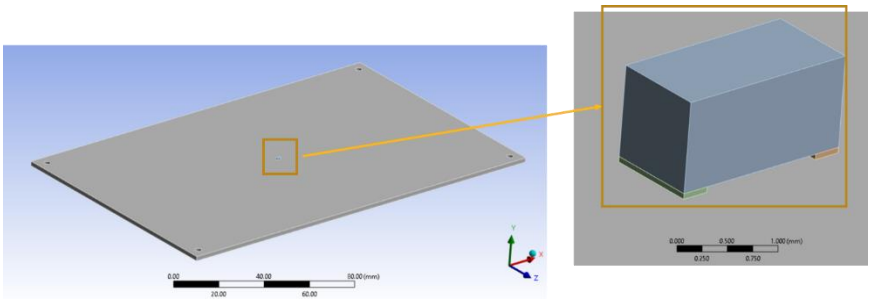

Fig. 1 Geometry of Board and MLCC

2.2 Workflow

The analysis integrates piezoelectric properties with electrical inputs through a coupled field harmonic response system. Voltage is applied as the input load, and the resulting surface velocity is transferred to an acoustic analysis to evaluate vibrational behavior.

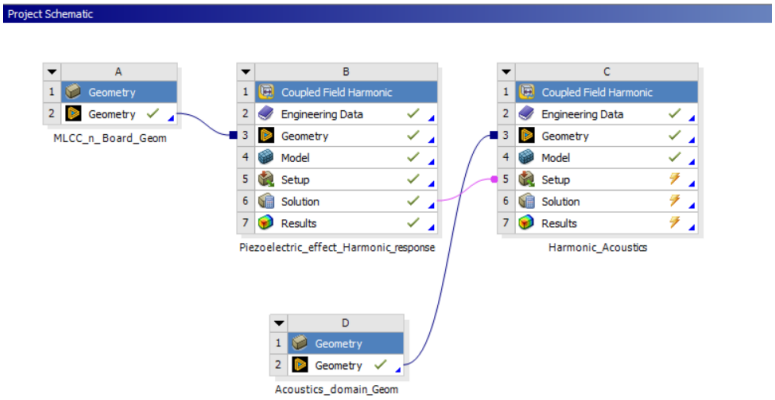

Fig. 2 Ansys workflow for the analysis

3 Vibration and Acoustic Analysis Results

3.1 Vibration Characteristics

Mode shapes and natural frequencies were analyzed to understand the dynamic response of the system.

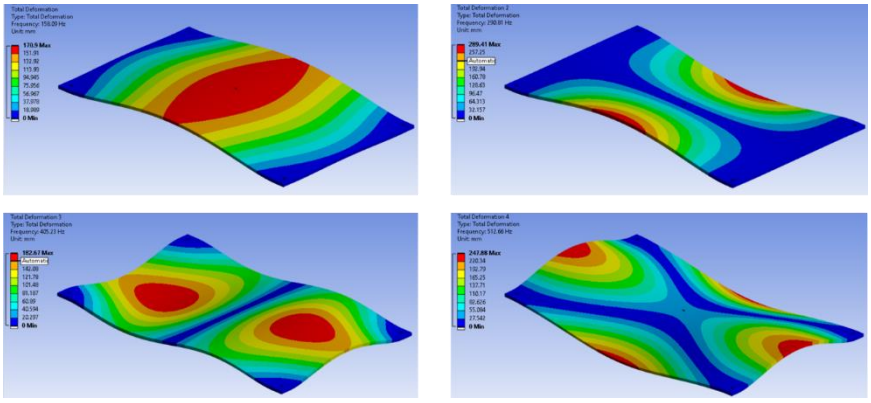

Fig. 3 Mode shapes and natural frequencies results

3.2 Harmonic Response

The harmonic response of the MLCC and the PCB was detailed.

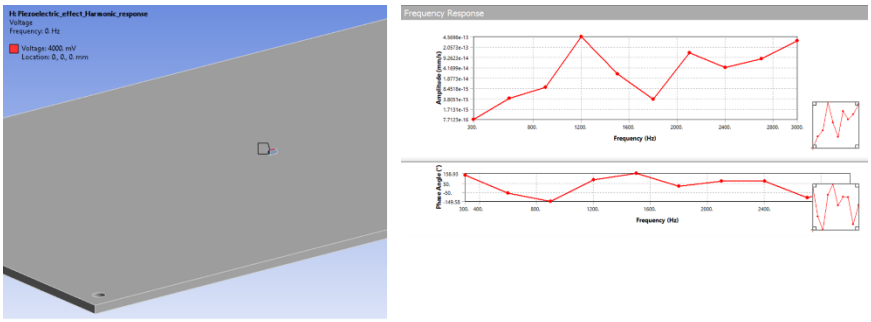

Input: Voltage Output: Freq vs Amplitude

Fig. 4 Input and output of harmonic response

3.3 Harmonic Acoustics

Acoustic analysis to understand noise generation from the system.

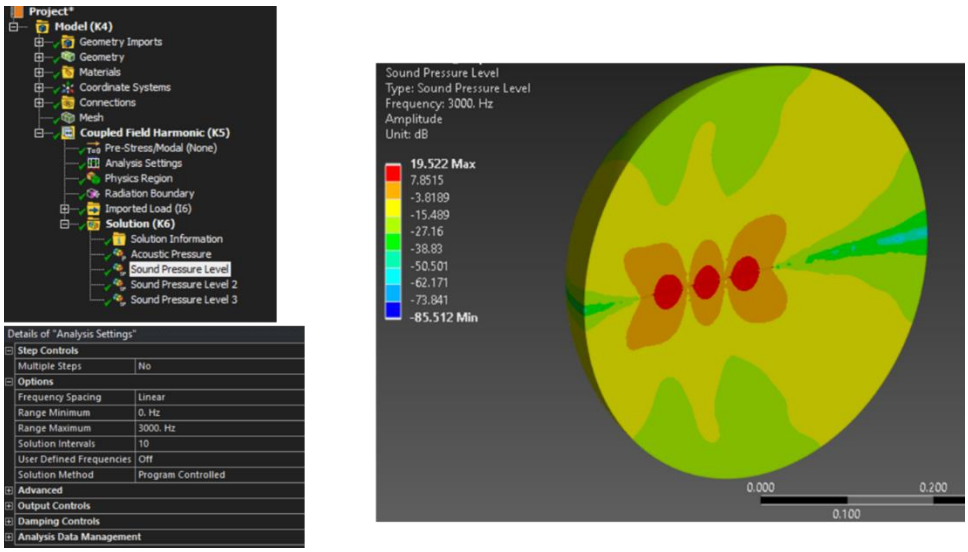

Fig. 5 Result of harmonic acoustics

4 Conclusions

This study successfully examined the piezoelectric and vibrational behavior of a generic MLCC-embedded PCB system, including:

- Piezoelectric characteristics: Contraction/expansion under voltage loading.
- Vibration characteristics: Mode shapes, natural frequencies, and vibration velocities.
- Noise generation: Source and intensity (dB) of generated noise.

5 References

[1] Ansys, Inc.: "Ansys Mechanical Help Documentation", Ansys, Inc., 2023.

Quantum-native multiphysics simulations

Invited talk

Extended abstract

V. Lahtinen, A Bastida-Zamora, Lj. Budinski, O. Niemimäki, R. Zamora-Zamora

(Quanscient Oy, Åkerlundinkatu 8, 33100 Tampere, Finland)

1 Introduction

The emergence of quantum computing holds potential in various scientific fields, including multiphysics simulations. We explore the current state of quantum computing in 2024 within the multiphysics simulation framework. We will start with an overview of how to approach multiphysics simulations with computing:

1. The traditional approach leverages quantum algorithms to speed up existing methods, such as partial differential equation solvers based on the variational method and the HHL method.
2. The so-called quantum native approach employs lattice-based methods designed explicitly for quantum architectures.

We present an overview of the pros and cons of these methods, highlighting our research findings in quantum computing for multiphysics.

Section 2 discusses the big picture of quantum algorithms in multiphysics, contrasting the traditional linear-algebra-based approach with the quantum-native approach. In section 3, we focus on quantum-native lattice-based physics simulations using the quantum lattice-Boltzann method (QLBM) and quantum lattice-gas automata (QLGA). Finally, in section 4, we draw conclusions.

2 Quantum computing and multiphysics: The big picture

The big question in applied quantum computing is how to design quantum-native and efficient algorithms for solving real-life problems. By quantum native, we mean that the algorithm encodes the physics (or other inner workings to be modeled) of the original problem, in some sense, directly into a quantum computing system. In a quantum-native algorithm, there is a clear and direct analogy between the evolution of the quantum system and the process it models.

Multiphysics simulations are ubiquitous in challenging R&D: electronics, chip design, aerospace engineering, fusion power, and the automotive industry, to name just a few. Accurately predicting a device's physical behavior is pivotal. However, if carried out accurately, these simulations are time-consuming and often impossible to carry out using classical computers. This is where quantum computing will eventually come to the rescue.

Multiphysics simulation involves discretizing and numerically solving a set of partial differential equations that model the physics involved. The usual methods unpack this process into a system of linear equations that are relatively easy to implement on a classical computer. While this approach has been successful, the computational cost of the simulations is high when applied to more complex, realistic systems at a large scale. Ideally, one would like to construct fully authentic digital prototypes and minimize the approximations involved.

Moreover, this focus on numerical methods can lead to a narrow perspective, as solving linear systems becomes paramount and the original physics problem fades into the background. This is reflected even in the state-of-the-art quantum algorithms: much focus is put on how to solve a linear system, whether directly (e.g., with some variation of the well-known HHL algorithm [1]) or by some hybrid/variational method [2]. Relying on such techniques, numerical solution methods, e.g., for elliptic partial differential equations (PDEs) and time-dependent fluid-flow problems, which are in principle suitable for quantum computers, exist. Such quantum algorithms for solving linear systems and the general quantum PDE algorithms hold promise for quantum advantage in fields such as computational electromagnetics (CEM), computational fluid dynamics (CFD), and continuum mechanics. For example, polynomial quantum speed-up is theoretically possible in finite-element-method-based simulations, growing in extent for problems with high spatial dimensionality or with specific smoothness properties [3].

However, this approach to quantum solutions has two issues. The first of them is the same as in classical computing, namely, the curse of dimensionality, which raises the computational complexity of these systems as they become more sophisticated. This is apparent in the noisy intermediate-scale quantum (NISQ) era devices, which at best can run a small variational system with rather limited success. And while the direct algorithms are clever in their use of quantum advantage, they are also forbiddingly complex to implement on these near-term devices.

The second and more fundamental problem is focusing on the speed-up and scaling of the classical method rather than rethinking the original problem in light of quantum computers' capabilities. The quantum-native approach to multiphysics addresses these problems.

In Figure 1, we summarize the two main approaches to quantum algorithms for multiphysics. In the next section, we will describe the quantum-native approach in more detail.

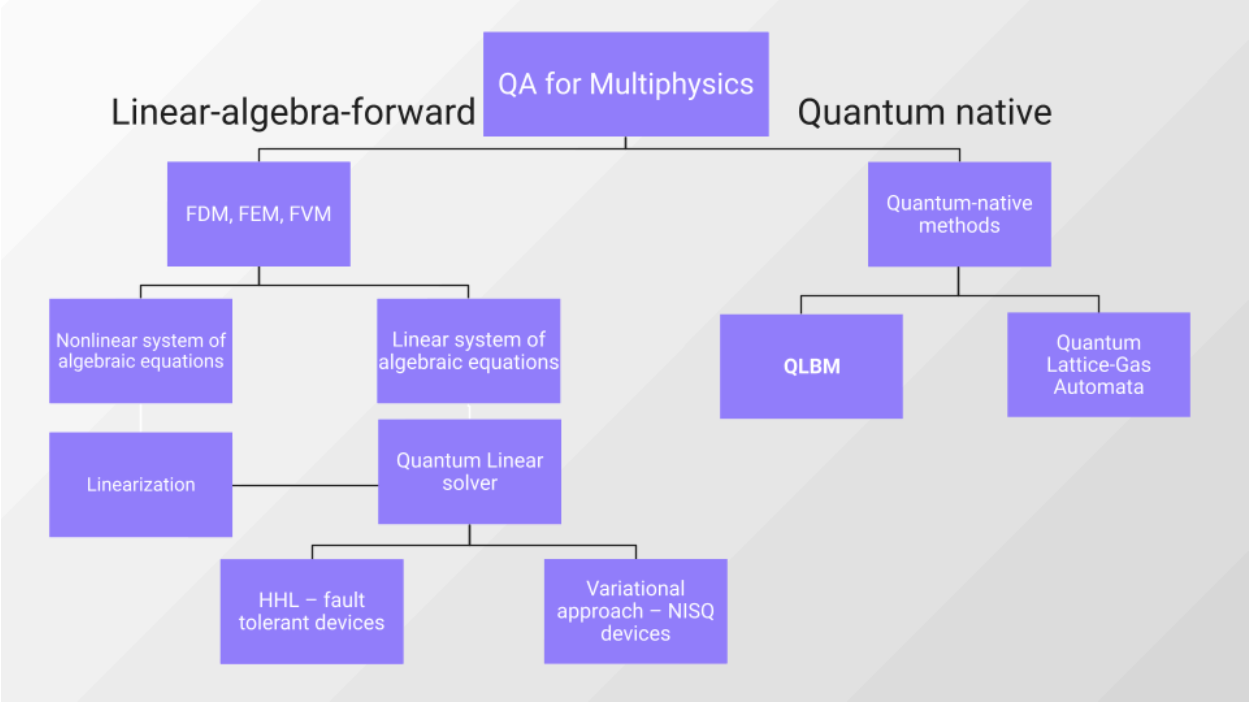

Figure 1: The big picture of quantum algorithms for multiphysics simulations.

3 Quantum-native multiphysics: quantum algorithms for lattice-based physics simulations

Now, we will turn our attention to quantum-native algorithms for lattice-based physics simulations, specifically the quantum lattice-Boltzmann method (QLBM) and quantum lattice-gas automata (QLGA).

3.1 Quantum lattice-Boltzmann Method

3.1.1. Method

The Lattice Boltzmann Method (LBM) is an alternative approach to the classical multiphysics solvers for fluid flow and partial differential equations. In terms of CFD, instead of solving, for example, the Navier–Stokes equations directly, a fluid density on a lattice is simulated with streaming and collision (relaxation) processes. Unlike “classical” CFD methods, where conservation equations of macroscopic properties are solved numerically, in the mesoscopic environment, fluid density is replaced with fictive particles that undergo a propagation and collision process over a discrete lattice covering the fluid domain.

Various lattice configurations can be utilized depending on the dimensionality of the problem being solved. For example, a two-dimensional flow can be modeled using the standard D2Q9 lattice configuration with nine vectors, shown in Figure 2. Each vector carries a corresponding density component to its neighboring site at a speed equal to one in the lattice units.

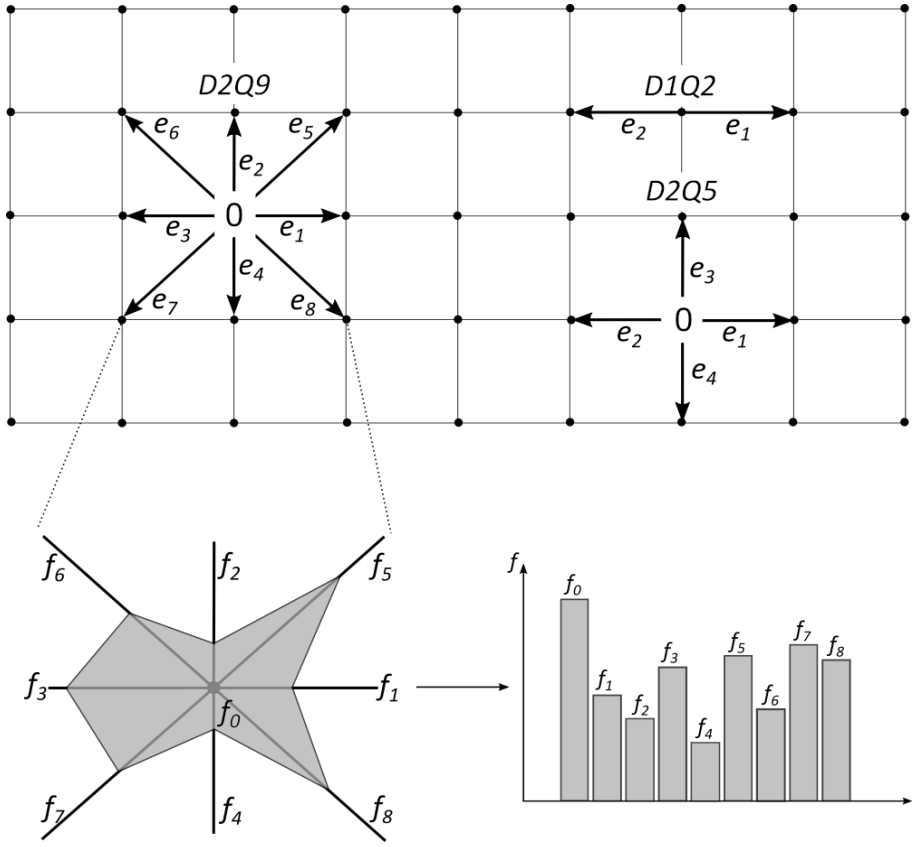

Figure 2: D1Q2, D2Q5, and D2Q9 lattice configurations for the Quantum Lattice Boltzmann Method. The probability densities f_i of particles are mapped to amplitudes of the qubits.

Comparing the mesoscopic domain with quantum (discrete form) reveals a high degree of analogy. First, the dynamical variables in both systems are related to probabilities (amplitudes of the quantum states), allowing us to implement an explicit mapping between these two systems: the components of the fluid density are encoded into the amplitudes of the quantum states. This methodology enables an exponential scaling of the lattice size with a linear increase in qubits. This formal mapping provides a solid physical connection between two systems that can be efficiently exploited in the evolution process. Second, as a direct consequence of this analogy in variables, the time evolution of the probabilities in the LBM can be mapped to the discrete quantum system used in quantum computations to carry out the simulation process on a quantum computer efficiently. Hence, in a simple linear case, the collision step can be understood as the evolution of the quantum state driven by a diagonal operator, whereas the propagation step is closely related to a quantum walk [4]. The general form of one time-step of a QLBM simulation is shown in Figure 3.

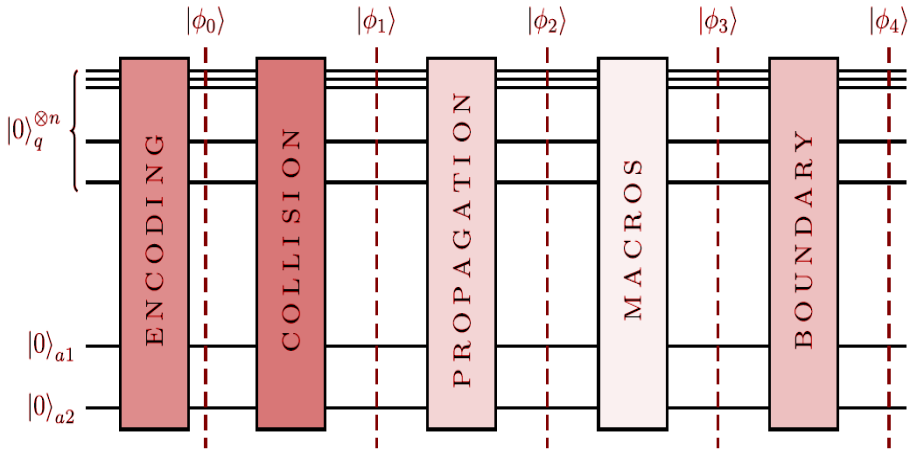

Figure 3: The general form of one time-step of a QLBM algorithm.

3.1.2. Simulation results

As a simple benchmark, easily comparable with an analytical solution, we model the movement of a Gaussian hill by solving a 1D advection-diffusion equation [5]. The results (Figure 4) match the well-known analytical results. Moreover, the results obtained for one time step on a real quantum computer give credibility to the fact that these results are reproducible on NISQ devices of today.

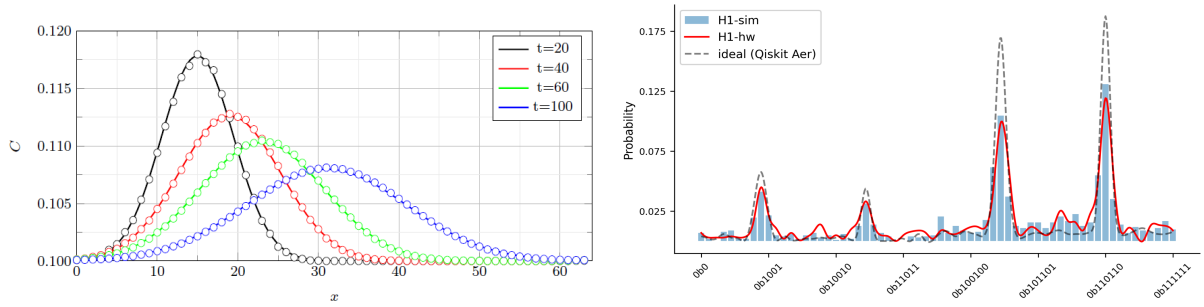

Figure 4: Solution of a 1D advection-diffusion equation using QLBM. Left: QLBM versus analytical results. Right: Results after one time step solved on Quantinuum H1-1 quantum computer (H1-hw), Quantinuum H1-1 emulator (H1-sim) and Qiskit Aer simulator (ideal).

As a more complex simulation case, we also simulate the airflow around the NACA0012 airfoil (Figure 5). This is done using the streamfunction-vorticity formulation of the Navier-Stokes equations implemented as a QLBM model, which consists of two coupled lattice-Boltzmann equations solved in superposition [6]. Furthermore, we simulate the temperature field transport using a third lattice-Boltzmann equation coupled with the flow problem. To our knowledge, for the first time, we have solved three coupled lattice-Boltzmann equations using a quantum algorithm and the superposition principle to simulate a real-world use case with complex boundary conditions.

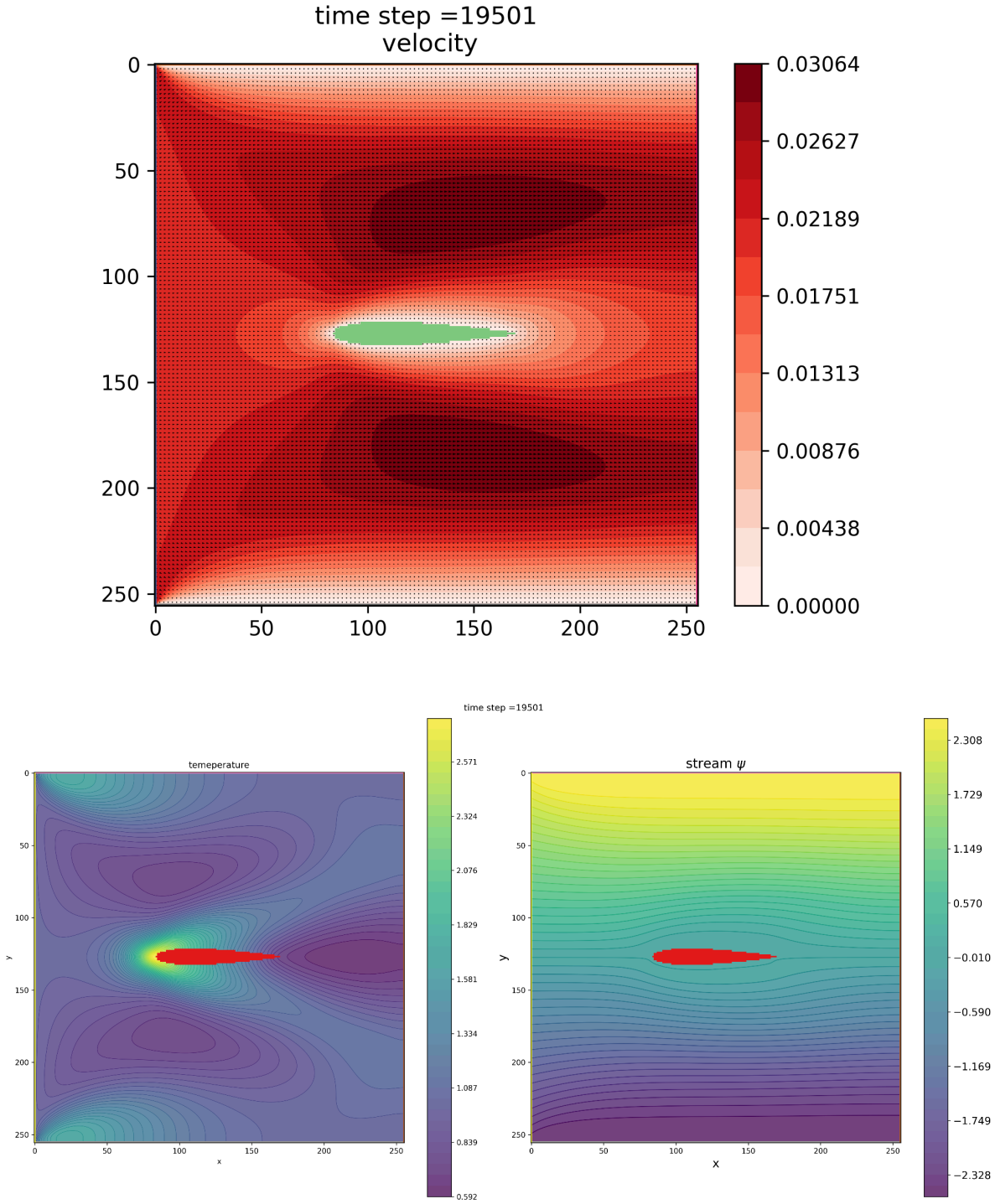

Figure 5: Airflow (stream and vorticity) and the temperature field transport around an airfoil solved using QLBM.

3.2 Quantum Lattice-Gas Automata

3.2.1 Method

The Lattice Gas Automata (LGA) is the LBM's precursor. As in LBM, particles collide and propagate over a discrete lattice. However, in this case, instead of computing the evolution of the fluid density (floating numbers), we use booleans to describe the occupancy of particles within the lattice. As in the LBM, these particles can have different directions and velocities. The boolean nature of the algorithm (exclusion principle) is imposed to guarantee that two indistinguishable particles cannot reside in the same node at the same time. If we compute the average occupancy of the particles in the lattice, we can obtain the distribution functions, which LBM works with directly. In this sense, while LBM works on the mesoscopic scale, LGA does it on the microscopic one [7,8].

Over the years, many different LGA models have been proposed. Among the most simple models, we can highlight HPP (Hardy–Pomeau–Pazzis) [9] with a rectangular lattice or FHP (Frisch–Hasslacher–Pomeau) [10] with a hexagonal lattice. These can model non-thermal fluids, where we conserve mass and momentum. However, these primitive models do not present Galilean invariance and cannot simulate fluids with high Reynolds numbers, due to the low effective rate of collision, which directly modify the viscosity. Therefore, in order to simulate highly nonlinear cases and obtain Galilean invariance, multi-speed models were proposed, where the conservation of mass is no longer linked to the momentum conservation, but independent. Additionally, different models such as FCHC (Face-Centered-Hyper-Cubic) have been proposed for their extension to 3D. Despite its initial application for computational fluid dynamics, LGA is not limited to fluid flows. In recent years, many other applications have been proposed such as biology [11], bubble formation [12], chemistry [13], and electromagnetism [14]. In Figure 6, we depict the collision rules for the FHP model.

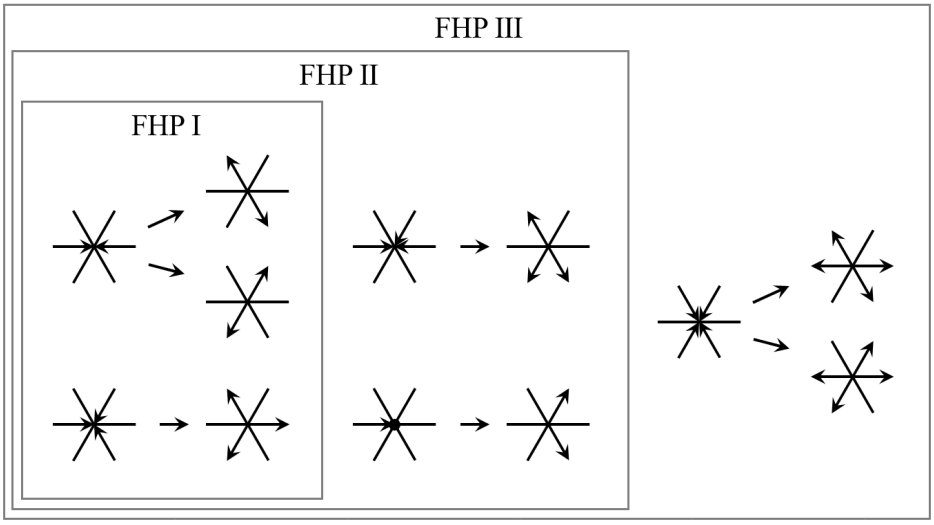

Figure 6: Collision rules for the FHP model. These are divided into type I, II, and III, depending on the number of collision rules used. Each model of increasing number also contains the collisions of the previous one.

While, historically, LGA was quickly abandoned due to the advantages of LBM (Galilean invariance, efficiency, low noise, and a direct connection between the collision rules and the differential equation to simulate), its interest has been regained in the quantum realm. In the context of quantum computing, LGA has been positioned as a very promising algorithm, as it can model nonlinear terms with a simple framework and presents noise resilience compared to other quantum algorithms that use an amplitude

encoding such as QLBM. One of the key features that make quantum LGA (QLGA) [15] a good candidate for efficient CFD simulations, is its ability to execute collision and propagation in each lattice site at the same time, as the collision rule is the same in each lattice. First, we encode which particles and in which directions are occupied in each lattice, and then we compute the collision using a certain deterministic set of rules that are identical in each lattice but depend on the occupancy of the channels. However, as the collision is based on computation on the lattice and the propagation is applied to each channel individually, an additional step (Mapping) is needed to prepare the quantum state. Then the propagation is done in the same way as for QLBM. The general form of one time step of a QLGA algorithm is presented in Figure 7.

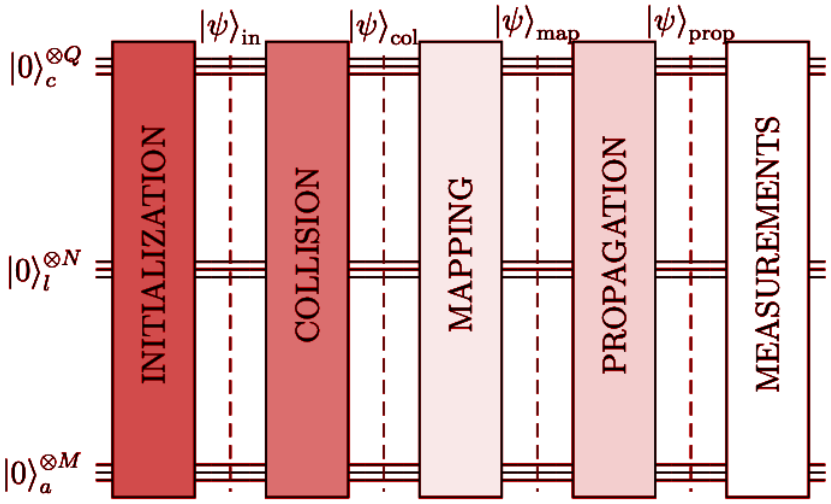

Figure 7: Steps of QLGA 1 time-step algorithm.

3.2.2. Simulation results

We use two test cases as a benchmark to verify that QLGA is capable of reproducing the same results as LGA. The first one is based on a simple 1D D1Q3 HPP LGA simulation detailed in [9, 15], where we want to reproduce the same results as in LGA for identical initial conditions. This can be seen in Figure 8, where similar results are obtained. The differences result from the random initialization but using the same parameters.

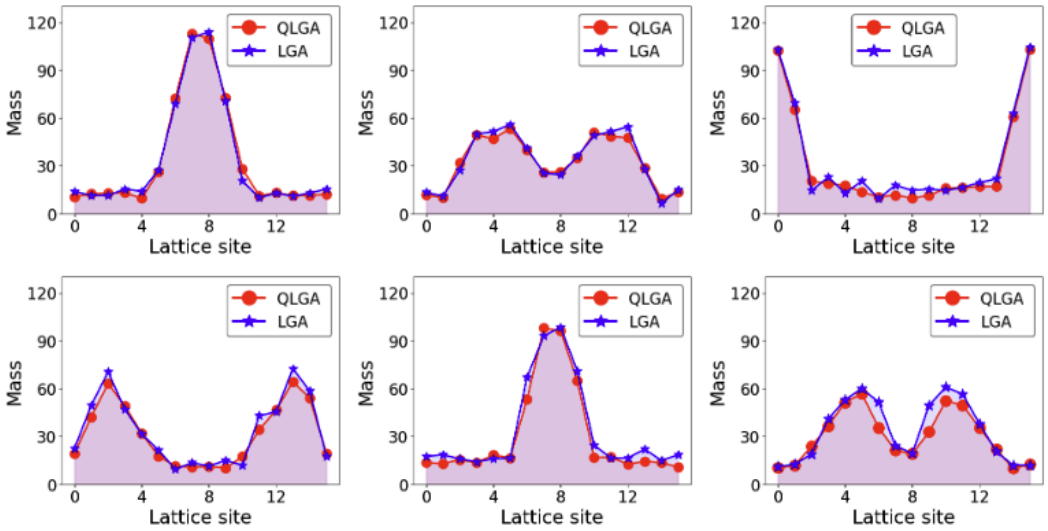

Figure 8: Comparison between LGA and QLGA for different time steps (t = 0, t = 160, t = 320, t = 560, t = 752, t = 896). [15]

Additionally, to test the model's resilience to noise, we compared it under different emulated noise levels.

Noise Level	Single Qubit Error Rate	2-Qubit Error Rate	Readout Error Rate
Low	10^{-5}	10^{-4}	10^{-4}
Mid (similar to Quantinuum H2) [16]	3×10^{-5}	2×10^{-3}	2×10^{-3}
High (similar to early quantum devices)	6×10^{-3}	2×10^{-2}	2×10^{-2}

According to this, we observe that good results (figure 9) can be obtained using modern quantum computers, which confirms the real applicability of these models, already in the non-fault-tolerant quantum era.

The other quantum case we simulated was the 2D Poiseuille flow between parallel plates (Figure 10). For this case, we used the FHP-III model with six channels (no rest particles). This is an interesting example as it shows the ability to simulate nonlinear differential equations using particle interactions. The results show that the parabolic profiles obtained with LGA and QLGA are very close to each other.

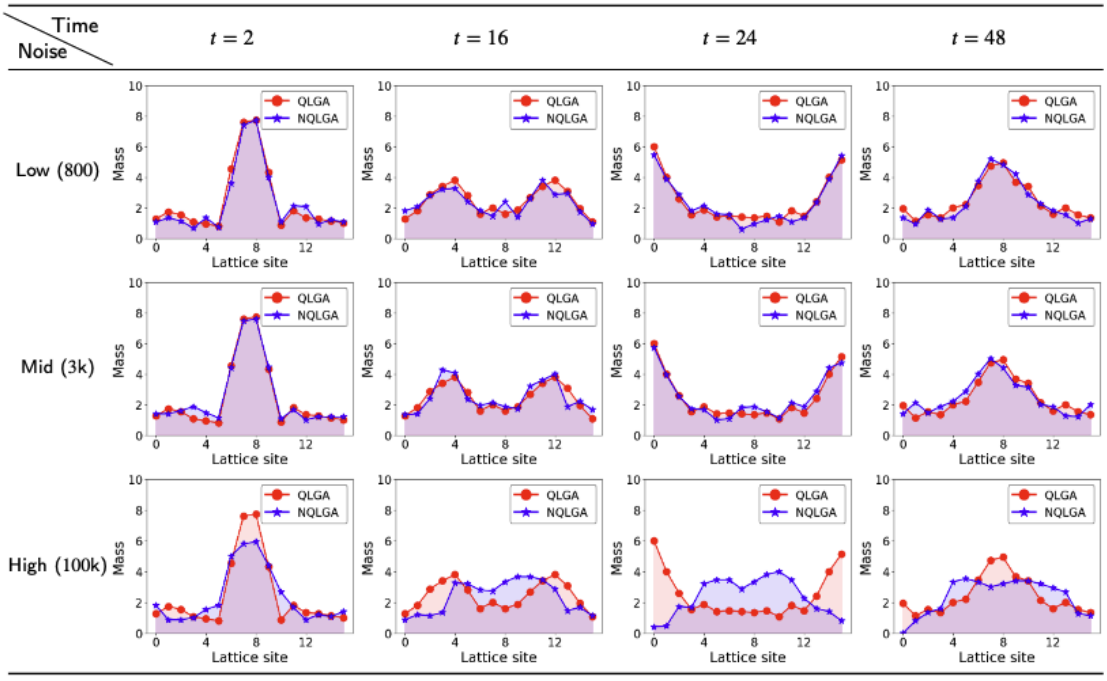

Figure 9: Comparison between Noiseless QLGA (NQLGA) and QLGA .The number of shots used appears in parentheses. The number of shots is adjusted to the minimum necessary for accurate simulations. [15]

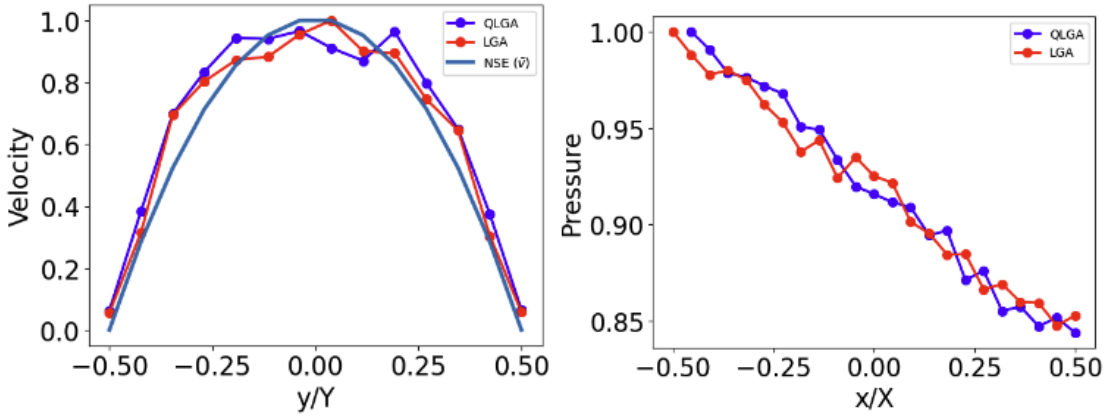

(a) Mean velocity profile respect y normalized. (b) Mean pressure respect x normalized.

Figure 10: QLGA compared to LGA for a flow between parallel plates. The NSE (blue line) is the expected result according to Navier-Stokes equations using the viscosity given by the theoretical equations.

3.2.3 Future prospects

We expect QLGA to be a useful model to simulate certain nonlinear problems in the near term. Especially given its noise resilience and simplicity to apply in new test cases. However, we are also aware of the problems yet to be solved. Specifically, the collision and propagation are applied under different encodings, and this yields the necessity of measurement for each step, with a high cost for reinitialization. Additionally, the inherent problems of classical LGA are still there, for example the control of the viscosity

and other macroscopic parameters using microscopic simple rules and the high noise resultant of its boolean nature.

4 Conclusions

Quantum-native, lattice-based physics simulations hold potential to solve multiphysics problems at immense scale. QLBM and QLGA are prime examples of this. We have shown that these methods can be implemented as efficient quantum algorithms and that simple but realistic use cases can already be run on today's quantum devices and simulators. While we have focused on simple CFD simulations as proofs-of-concept, we note that LBM in particular is a rather general method for the solution of PDEs at its heart, hence holding potential for multiphysics applications, too [17].

As quantum hardware matures, we anticipate significant advancements in simulating complex multiphysics phenomena with applications in industries from aerospace to energy and healthcare. While challenges such as hardware limitations and error correction remain, the potential rewards can be vast.

5 References

[1] A. Harrow, A. Hassidim, and S. Lloyd. Quantum algorithm for linear systems of equations, Phys. Rev. Lett. 103, 150502, 2009.

[2] M. Cerezo, A. Arrasmith, R. Babbush, *et al*. Variational quantum algorithms, Nat Rev Phys **3**, 625–644, 2021.

[3] A. Montanaro and S.Pallister. Quantum algorithms and the finite element method, Phys. Rev. A 93, 032324, 2016.

[4] Lj. Budinski, O. Niemimäki, R. Zamora-Zamora, V. Lahtinen. Efficient parallelization of quantum basis state shift. Quantum Sci. Technol. 8 045031, 2023.

[5] Lj. Budinski. Quantum algorithm for the advection–diffusion equation simulated with the lattice Boltzmann method, Quantum Information Processing 20, 2021.

[6] Lj. Budinski. Quantum algorithm for the Navier–Stokes equations by using the streamfunction-vorticity formulation and the lattice Boltzmann method, International Journal of Quantum Information 20 (02), 2021.

[7] S. Succi, The Lattice Boltzmann Equation for Fluid Dynamics and Beyond (Numerical Mathematics and Scientific Computation), ch. 2, p. Section 2.3. Clarendon Press, 2001

[8] J.-P. Rivet and J. P. Boon, Lattice Gas Hydrodynamics. Cambridge University Press, 2001.

[9] J. Hardy, O. D. Pazzis, Y. Pomeau. Molecular dynamics of a classical lattice gas: Transport properties and time correlation functions, Physical Review A 13 1949–1961, 1976.

[10] U. Frisch, B. Hasslacher, Y. Pomeau. Lattice-gas automata for the navier-stokes equation, Physical Review Letters 56 1505–1508, 1986.

[11] A. Deutsch, J. Manik Nava-Sedeno, S. Syga, and H. Hatzikirou. Bio-lgca: A cellular automaton modelling class for analysing collective cell migration. PLOS Computational Biology, 17(6):1–22, 062021, 2021..

[12] Z, Zheng, L. Lin, Z.i Chen, J. Lim, and J. Grace. A dual-scale lattice gas automata model for gas–solid two-phase flow in bubbling fluidized beds. Computers Mathematics with Applications, 61(12):3593–3605, 2011. Mesoscopic Methods for Engineering and Science — Proceedings of ICMMES-09.

[13] .T. Wells, D.R. Janecky, and B.J. Travis. A lattice gas automata model for heterogeneous chemical reactions at mineral surfaces and in pore networks. Physica D: Nonlinear Phenomena, 47(1):115–123, 1991

[14] N. Adnani, N.R.S. Simons, and G.E. Bridges. The lattice gas automata for computational electromagnetics. In IEEE Antennas and Propagation Society International Symposium. 1995 Digest, volume 3, pages 1544–1547 vol.3, 1995.

[15] A. D. Bastida-Zamora, Lj. Budinski, O. Niemimäki, and V. Lahtinen. Efficient quantum lattice gas automata. arXiv preprint arXiv:2402.16488, 2024.

[16] Quantinuum, H2, 2024. URL: https://www.quantinuum.com/hardware/h2.

[17] P. Sagaut. Classical lattice-Boltzmann methods for fluid dynamics. Von Karman Lecture Series and Events: Introduction to Quantum Computing in Fluid Dynamics - STO AVT-377. 2024.

Machine Learning Tools for Mutliphysics Analyses, Design Exploration and CAE Acceleration

Dimitrios Drougkas BETA CAE Systems

Nagananda Upadhya BETA CAE Systems

1 Summary

Machine learning tools have become increasingly prevalent in various software applications, offering numerous advantages and transforming the way we interact with technology. The challenge in the CAE-domain and Multiphysics analyses in particular, is to adapt and learn from the huge amount of Simulation data, plus demanding load cases and complex physics. The ML-workflow which involves data collection and preparation, ML-model training and evaluation, and finally Prediction.
The Prediction of scalar, 2d, 3d and Multiphysics Simulation results give us the opportunity to use Machine learning for variety of applications. Predictors as the ML-object in BETA Products enable CAE engineers to rapidly explore various design configurations without relying on time-consuming simulations. Engineers can now optimize their processes, streamline workflows and expedite the realization of innovative designs.

2 Parametric Multiphysics Optimization

This study aimed to optimize the design and manufacturing of the tailgate component of a vehicle on two fronts: manufacturing quality and ease of use. The process evolved around the specification of the gas lifter components mounting positions and force rating.

Fig.1: Tailgate with gas lifters

To optimize these two requirements, both Multi-Body Dynamic and structural analyses were essential. The goal was to maintain the deformations of the tailgate component at reduced levels resulting in optimum external appearance regarding panel gaps, while maintaining a comfortable user operation of the tailgate.

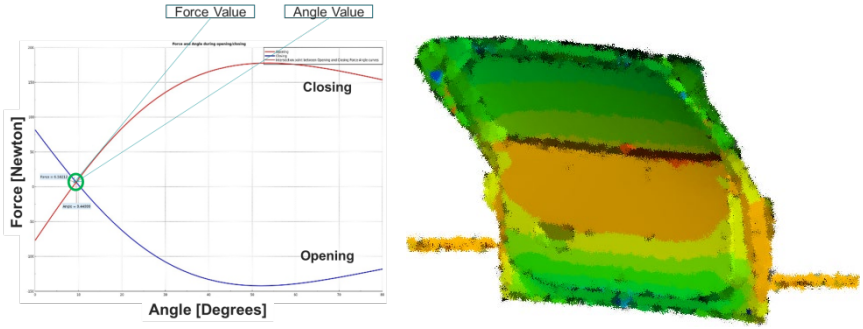

Fig.2: a. Multi Body Dynamic analysis results, b. Structural analysis results

After an initial Design Of Experiments (DOE) with 20 variations of the parametric model, Machine Learning predictive models (also refereed as predictors) were employed in order to accelerate the product design and evaluation process by predicting the two solvers results.
Continuing these predictors were updated with new DOEs created by automatic smart sampling methods, in order to improve their accuracy.

Finally these Machine Learning predictors were employed in Optimization studies, replacing the two solvers, in order to reach the optimum design in an automated and faster way, thus, improving the product development time. The objectives were to minimize the deformations of the panel and minimize the force required by the user to open and close the tailgate.

Table 1: Optimization Results with and without Machine Learning

Optimal Design	F1	S1_X	S1_Z	S2_X	S2_Z	N555914_dx	N613869_dx	Angle	Force	Time (hours)
Initial Design (reference)	600	3388.346	963.711	3218	1203	1.4573	1.4155	9.4499	6.5821	**-**
Direct Optimal	400.304	3391.47	967.006	3219.88	1201.45	1.172	1.143	17.8722	0.009097	**157.5**
ML Approach	404.939	3392.924	969.289	3219.425	1201.799	0.5519	0.5189	19.017	0.7731	**63**

3 Non Parametric Machine Learning - Body in White first torsional mode prediction

Identifying the first torsional mode of a vehicle's Body-in-White (BiW) marks a crucial stage in the product development. During product development, the BiW may undergo several types of modifications in its design and engineering specifications. These modifications may include changes in geometry (shape of parts), changes in parts thickness, and changes in materials or connection types.
Each design modification requires the creation of a new simulation model, and then a new run of a Finite Element analysis to collect the desired responses. This iterative redesign process may need to occur several times in the development cycle of a BiW.
In this work, BiW FE models from various vehicles served as input data. This Machine Learning method, also known as Feature-Based or non parametric, utilized the actual FE models and their scalar values as input, without relying on specific parameters. The method conducted automatic feature extraction, from each FE model during training and used the extracted data as input. A total of 100 different FE models were used for training.

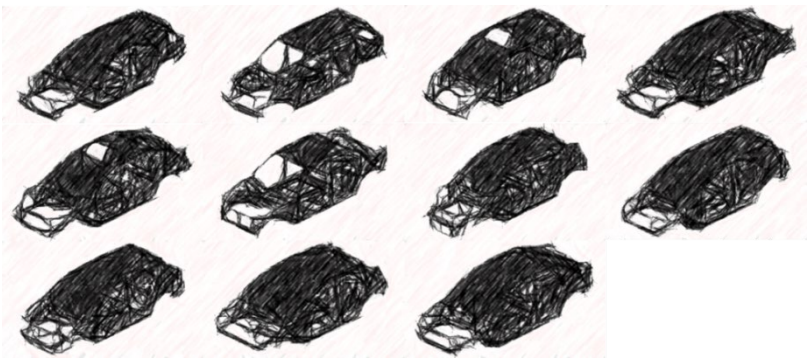

Fig.3: Various Body in White FE models used as training input

For each FE model, the frequency values corresponding to the first torsional and first vertical bending modes were identified and utilized as responses for training the machine learning predictor.

Table 2: Labelled Responses used for training

FE Model	First torsional value (Hz)	Vertical bending (Hz)
BiW_1	32.411	38.492
BiW_2	34.096	39.123
BiW_3	42.198	43.608
BiW_4	29.329	42.86
BiW_5	…	…

Once the Machine Learning model was trained, it offered insights into its accuracy and performance by means of metrics (Mean Absolute Error, etc) and Key Performance Indicator (KPI) plots.

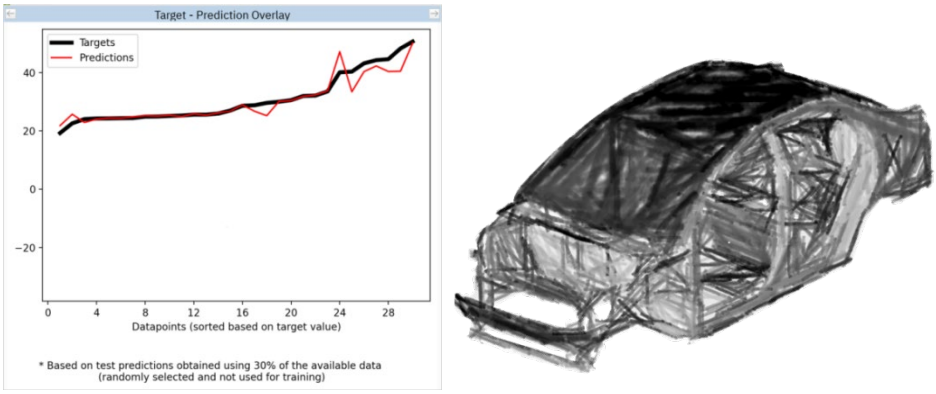

Fig.4: a. KPI Target vs Prediction overlay plot, b. New BiW FE model, unknown to the predictor

For any new BiW FE model variation, whether it belongs to a similar or different carline, the trained Machine Learning model can provide predictions for the labelled responses much faster than the respective FE analysis, along with the confidence bounds.

Table 3: Prediction Results and error

	First torsional value (Hz)	Vertical bending (Hz)
Prediction	39.74	40.88
FE Result	39.73	40.78
Abs Error	0.01	0.1

4 Mode Classification

Mode classification is a process used in structural analysis cases in order to analyze and label how structures deform under various loading conditions. This process is particularly used for NVH (Noise Vibration and Harshness) discipline, when performing normal modes analysis. The identification and classification of each mode shape is a demanding task and requires experienced engineers to work together to complete it. Machine Learning can be utilized in this domain, using legacy and history data to learn and provide automation in mode classification of new design variations.

In this study a dataset of different Body in White FE models where used as input data. For each model, a normal modes analysis was ran and a mode shape labeling was completed for 12 elastic modes.

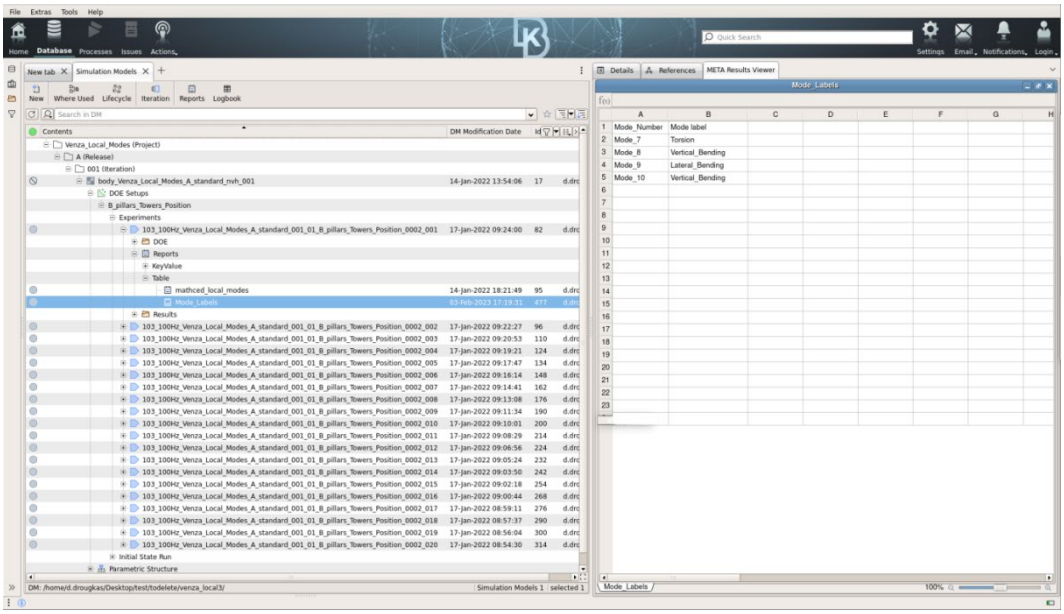

Fig.5: Training dataset for Mode classification

The trained machine learning model was used in order to predict the mode classifcation list, of new design variations, when provided with the normal modes analysis results.

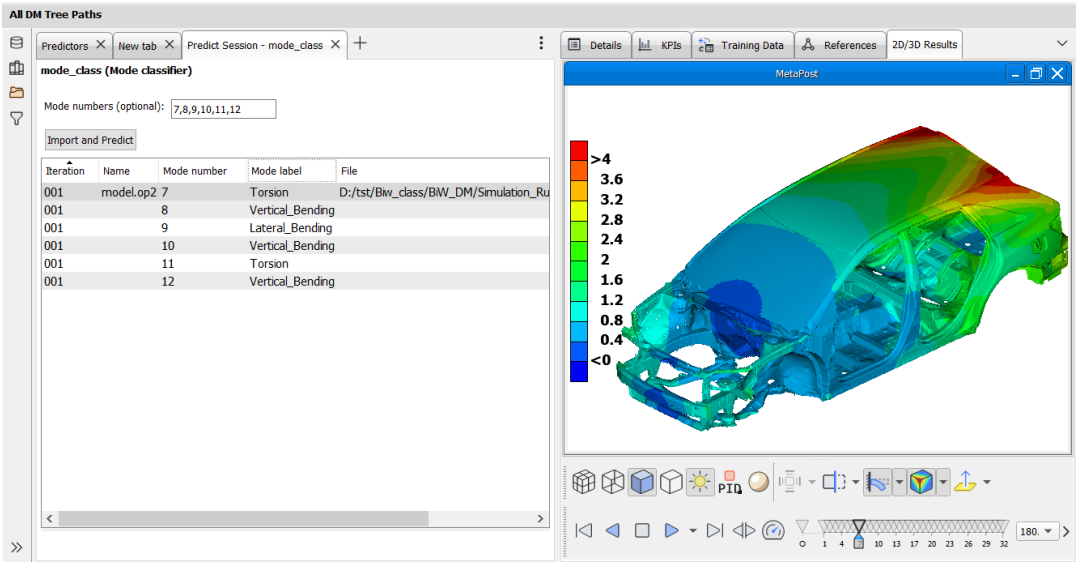

Fig.6: Mode classification prediction for new BiW variation

5 Conclusions

The potential of machine learning continues to grow with advancements in technology. Incorporating this functionality into CAE processes enhances the accuracy of simulation result predictions for "what-if" studies. When paired with optimization tools, it can lead to substantial time savings throughout product development. In this work, we explore the applications of result prediction in optimization, design variations, and mode classification.

6 References

[1] BETA CAE Systems, “ANSA User Guide,” https://www.beta-cae.com/, Dec. 23, 2022.
[2] BETA CAE Systems, “KOMVOS User Guide,” https://www.beta-cae.com/, Dec. 23, 2022.
[3] BETA CAE Systems, “Optimization with ANSA / META”, 2022

AI-Powered Multiphysics Solutions: Revolutionizing the Design of Consumer Durable Systems

Ujwal Patnaik (Altair), Nachiket Patil (Altair)

Summary

The world of consumer electronics and durable systems is evolving at an extraordinary pace, propelling product designs into new realms of complexity. This complexity arises from the necessity to integrate a diverse array of physical phenomena seamlessly, aiming to meet the increasingly stringent demands for performance, reliability, and cost-efficiency simultaneously. For instance, products as seemingly disparate as home audio speakers and washing machines: both encounter similar engineering challenges due to the convergence of various physical domains—mechanical, thermal, electromagnetic, acoustics and fluid dynamics (CFD).

As consumer demands for smaller, more powerful, and multifaceted products increase, the need to solve multi-physics challenges during the design phase has become essential. The convergence of diverse physical phenomena, compounded by product miniaturization and complex system integration, defines a tightly constrained design arena. Here, conventional engineering methods frequently fail to meet the demands, making innovative approaches crucial for success.

This paper explores how AI-powered engineering solutions offer a transformative approach to managing these design challenges. By leveraging AI, engineers can train machine learning models using any existing simulation studies including those from older design concepts, similar parts, or different programs, enabling the model to identify, learn the relationship between shape and performance for any physics. Similarly, engineers can integrate complex physics models into reduced-order models that streamline the design process, allowing for real-time simulations, rapid design iterations, and optimization. Once trained, models can deliver predictions up to 1000x faster than traditional solver simulations, enabling teams to evaluate more concepts and make better design decisions.

Thus, AI enables the seamless coupling of diverse physics, facilitating the balancing of multiple design constraints (such as cost, durability, and performance) in ways that were previously unachievable. This approach reduces the need for extensive expertise in each domain while significantly accelerating product innovation, simulation and development timelines. In this paper, we will present the utility and effectiveness of AI-powered multi-physics modeling using the case study of a Home Audio Speaker.

Case Study: Home Audio Speaker Design

Problem Definition

The contemporary audio landscape demands high-performance speaker systems that deliver exceptional sound quality while ensuring structural integrity and efficient thermal management. As speaker systems evolve, the integration of various components becomes increasingly complex. Evaluating the performance of these components in isolation is insufficient, as real-world interactions can lead to unexpected failures or sub-optimal performance. Speakers are naturally affected by the vibrations produced by their internal parts, especially when playing at high volumes. In order to clearly understand the sources of vibrations, it's essential to examine them in both isolated and integrated settings. If these vibrations are not properly managed, they can result in undesirable sounds like buzzing or rattling. The main contributors to these problems include:

- Physical contact between components, such as wires or plates rubbing together.
- Electro-magnetic interactions among the speaker's elements.
- Resonant frequencies that are insufficiently damped or controlled.

Moreover, the acoustic pressure must be analyzed both inside and outside the speaker cabinet in a room environment. By filtering the relevant acoustic responses, engineers can focus on and evaluate specific factors, such as dynamic frequency characteristics and damping effects.

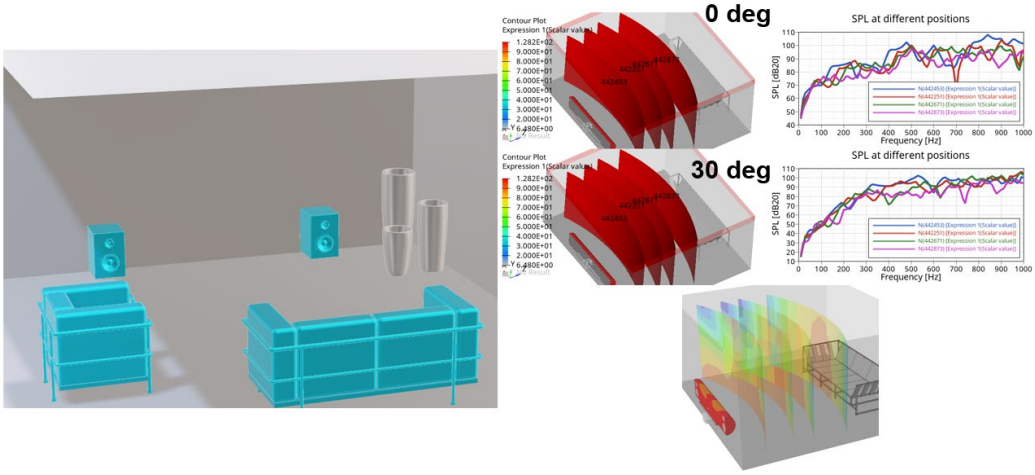

Figure 1. Acoustic Analysis of Speaker in a Room

Conventional finite element analysis (FEA) and computational fluid dynamics (CFD) techniques are often time-consuming, computationally intensive, limiting rapid prototyping and iterative design. AI-powered workflows can address these challenges by accelerating simulation processes and providing predictive insights through data-driven models.

AI-Powered Engineering Methodology

This case study employs a hybrid approach, combining traditional multi-physics simulation tools with machine learning techniques to optimize the design and performance of speaker components, such as printed circuit boards (PCB), fans, acoustic ports, and diaphragm. Data from initial simulations will be used to train AI models that can predict performance outcomes on the fly, based on varying design parameters. The iterative feedback loop between simulation and machine learning will expedite the design process, enabling real-time adjustments and optimizations.

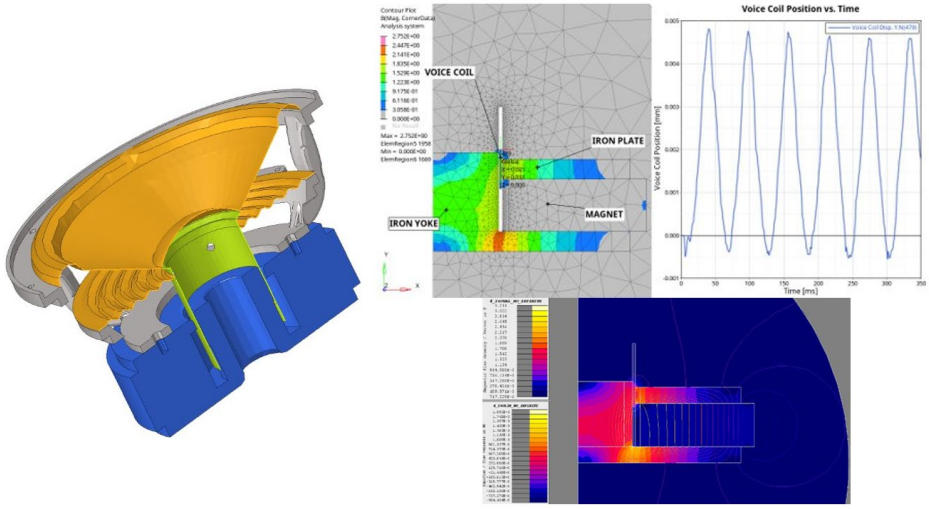

Figure 2. Multi-physics Analysis of a Speaker Membrane

At an assembly level, the speaker must be designed to withstand structural vibrations, dissipate heat from its electrical components, and maintain consistent sound quality under various environmental conditions. Hence, implementing an AI-powered multi-physics modeling approach can have a great significance, as follows:

- Material Selection and Calibration: The prerequisite for a multi-physics analysis is selection of the right material for all the components using trade-off studies. This is followed by calibration and failure characterization of the materials. AI-driven material modeling framework can help to automatically optimize the parameters of the material models, ensuring accurate simulation results.
- Structural Analysis: The structural performance of a speaker's cabinet and PCB is crucial for durability and sound reproduction quality. AI algorithms can analyze stress distribution and failure modes across materials, allowing for the identification of weak points and optimization of geometries to enhance longevity.
- Thermal and CFD Analysis: Effective thermal management and air flow are vital to maintain performance and reliability of the speaker. By integrating thermal modeling with structural and CFD simulations, AI can predict temperature distributions and identify potential hotspots, enabling

design improvements that enhance cooling efficiency through optimal fan placement and PCB layout.

- Acoustic Analysis: AI can facilitate the exploration of design variations, optimizing the acoustic properties through machine learning algorithms that correlate physical parameters with acoustic outcomes, enabling superior sound quality and responsiveness.
- Manufacturing Analysis: Leveraging AI in manufacturing of the speaker components is crucial, specifically early in the design process to predict manufacturing defects, reduce design errors and material wastage. This strategic use of AI can drive innovation, improve efficiency, and maintain a competitive edge during the manufacturing process.

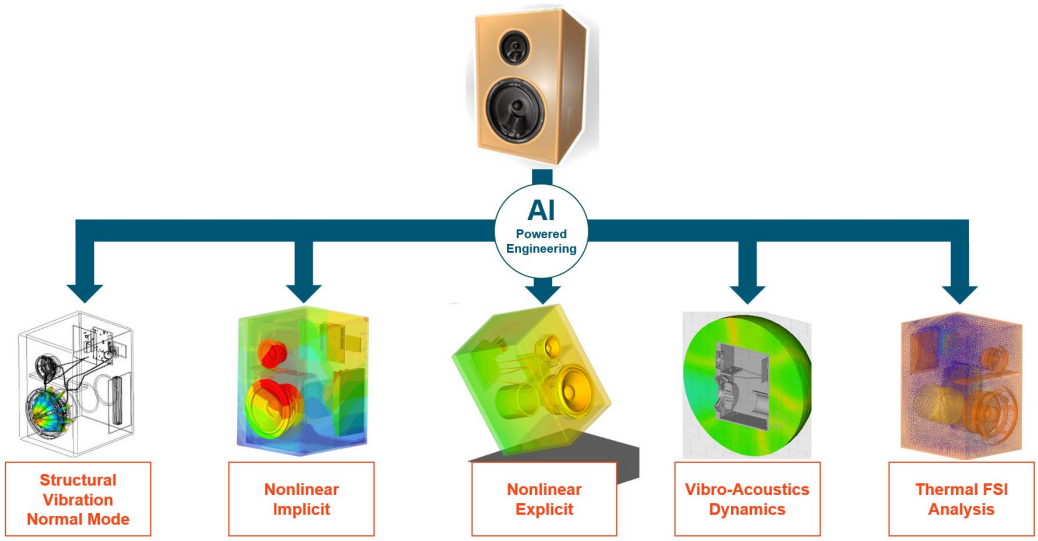

Figure 3. AI-Powered Engineering Multi-Physics Analysis of a Speaker

Results and Discussion

Preliminary findings demonstrate that AI-powered models significantly reduce computation times while maintaining accuracy in predicting structural, acoustic, and thermal behaviors. AI-powered multi-physics modeling represents a disruptive approach to speaker system design, ensuring the final design achieves performance objectives while remaining cost-effective and manufacturable at scale.

Conclusion

AI-powered engineering solutions can facilitate the convergence of multiple physics domains, allowing for a holistic approach to product design that accounts for the full range of physical interactions. The results provide engineers with actionable insights, optimizing the speaker's design towards superior efficiency and

extended service life. The ability to solve complex multi-physics problems in a reduced time frame and with fewer manual interventions has profound implications for the future of product development in consumer durables making it faster, more efficient, and more innovative. This shift ultimately results in higher-quality products that more adeptly meet the dynamic needs of consumers.

Accelerated and Reliable Predications via PINN Incorporating Field Data

Prashant Kumar Srivastava, Vineet Dravid (oorja)

Summary

Accurate and efficient predictions are essential for decision-making processes in many scientific and engineering applications. Integrating field data with physics-based models is an efficient strategy to enhance prediction accuracy while leveraging available observational information. This abstract proposes an approach employing Physics-Informed Neural Networks (PINNs) to achieve faster predictions by combining field data with underlying physical principles. The proposed methodology entails the following key steps: (1) Formulation of physics-based constraints derived from fundamental principles governing the system of interest, (2) Construction of a neural network architecture capable of approximating the system's response, (3) Training the PINN model using a combination of field data and physics constraints, and (4) Deployment of the trained model for quick predictions This abstract advocates for the adoption of PINNs as a versatile tool for accelerating predictions while harnessing the information contained within field data. Through illustrative examples of performance predictions on lithium-ion batteries, we demonstrate the efficacy of this approach in enhancing predictive capabilities and enabling informed decision-making in complex systems.

PINNs

PINN stands for physics-informed neural networks. A governing differential equation can be used to represent any physical phenomenon. To solve the governing equation using PINNs, a deep neural network is considered with spatial coordinates of the target domain (along with time if the given phenomena is dynamic) in the form of a point cloud as the input [1] (Figure 1). The outputs are the set of dependent variables that define the physical phenomena. The governing differential equation is embedded in the loss function of the deep neural network, so that for a set of domain points with appropriate boundary conditions or initial conditions, the governing equation is satisfied (figure 2). Automatic differentiation enables efficient and accurate calculation of gradients of the dependent variables at the domain points without any truncation error.

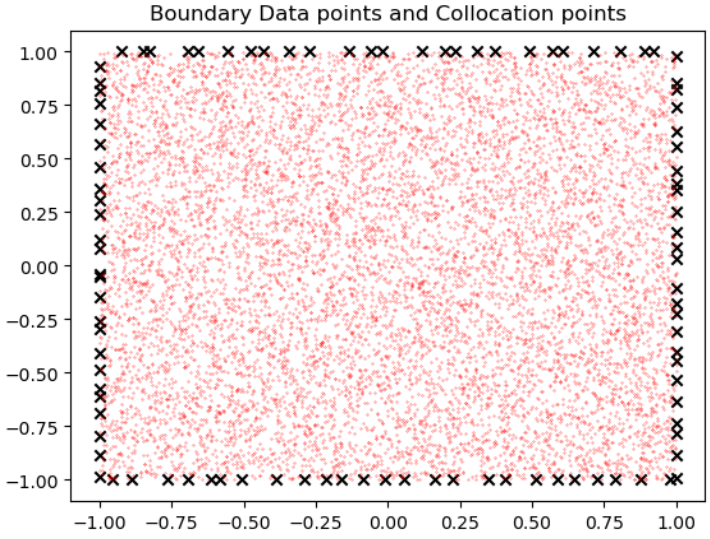

Figure 1: Input data represented as collocation points to the PINNs

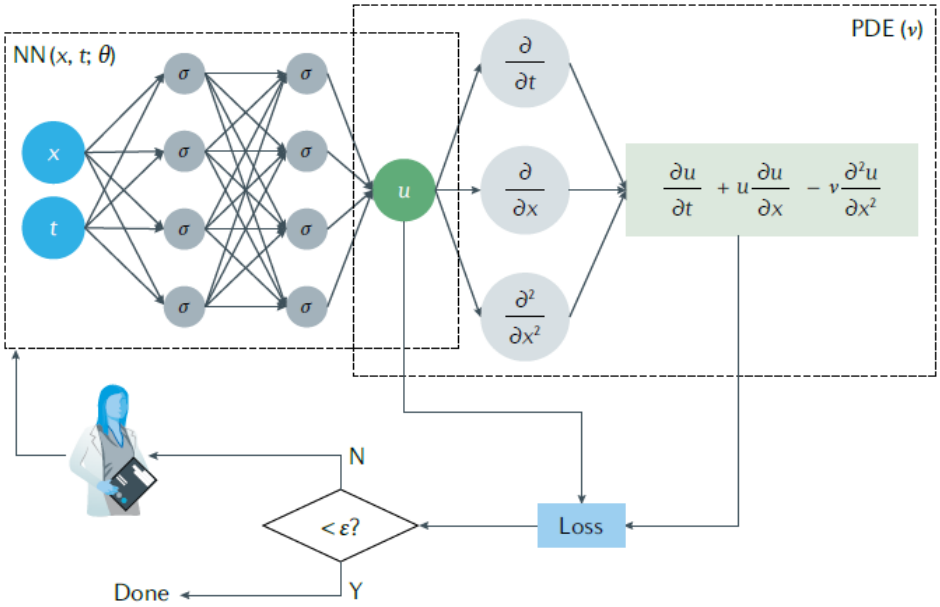

Figure 2: PINN architecture

One of the main advantages of the PINN approach to solving a differential equation is the flexibility to include multiple input nodes in the deep neural network so that a trained model captures a wider range of system parameters in the design space. For instance, when a fluid flow is modeled using PINNs, adding an input node for fluid viscosity enables training a model for a range of viscosity values to predict the flow solution in real time for different viscosity values once the model is trained. This reduces the computation time needed to create a model for a broader range of system parameters. Hence, PINNs enable accelerated predictions for engineering applications. This approach also bypasses the complex meshing process, which may be time-consuming in some complex geometries.

One of the drawbacks of using fully connected deep neural networks architecture for PINNs is that deep neural networks generally are good at approximating low-frequency functions. This phenomenon is known as spectral bias. To capture real scenarios where the geometries are complex giving rise to sharp gradients, Fourier neural networks are often used. This architecture encodes the inputs to a higher dimensional feature space through high-frequency functions [2].

Connector Optimization using PINN

The connectors in a battery pack transmit the current from the individual cells to the payload. Because of their internal resistance, they generate heat in the system. They are also welded with the cell tabs, leading to heating at the contact locations due to the contact resistance. Connectors are usually made of high conductivity and high specific heat capacity materials, which help carry the heat from the battery pack outside and reduce the heat rise rate. Due to the dual role of these components, their design is crucial to the safety of the battery packs.

In this study, we adopted the Physics Informed Neural Network (PINN) to solve the heat transfer problem in the battery pack. As discussed above, PINNs offer a distinct advantage of solving the governing differential equations with a wide range of system parameters. Multiple system parameters like battery pack input current, internal resistance of the cell, and thermal

conductivity of the connector are included in the training model to study the thermal behavior of the connectors using PINNs. Figure 3 shows the range of parameters used in the model to study the connector's thermal behavior.

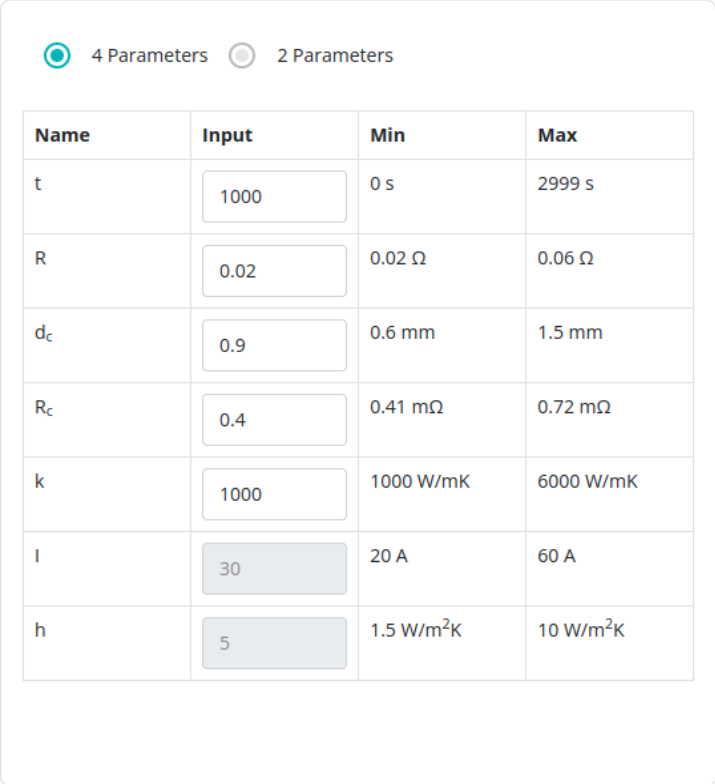

Name	Input	Min	Max
t	1000	0 s	2999 s
R	0.02	0.02 Ω	0.06 Ω
d_c	0.9	0.6 mm	1.5 mm
R_c	0.4	0.41 mΩ	0.72 mΩ
k	1000	1000 W/mK	6000 W/mK
I	30	20 A	60 A
h	5	1.5 W/m^{2}K	10 W/m^{2}K

Figure 3: Range of parameters optimised for modelling the connectors using PINNs

In this case, a deep neural network with 6 layers and 512 neurons on each layer is used with a SiLU (Signmoid Linear unit) activation function. The loss tolerance is set as 1e-5. Figure 4 shows the temperature heat map in the considered geometry.

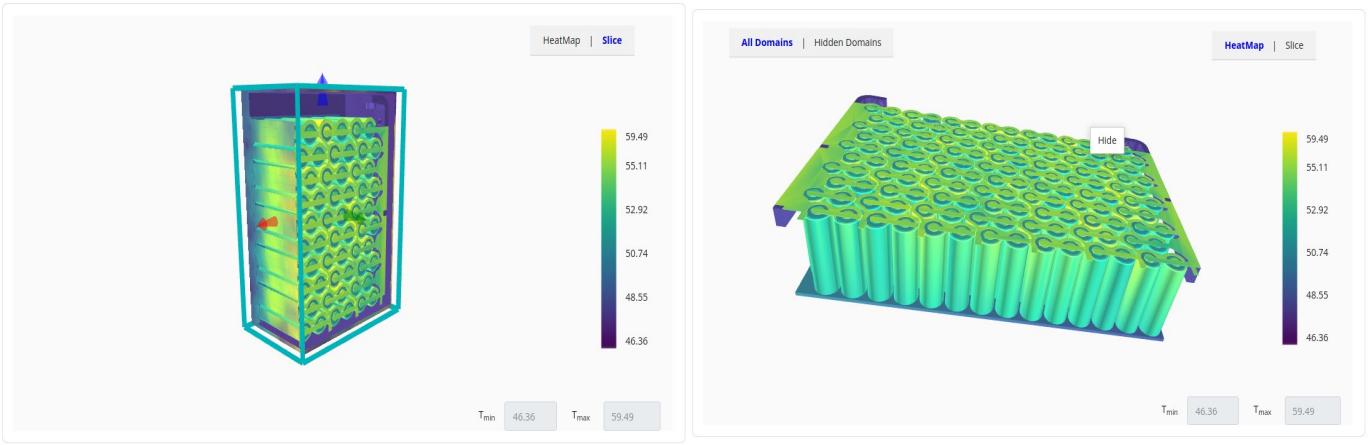

Figure 4: Temperature heat map of the battery pack computed using PINNs with multiple parameter inputs.

The prediction in Figure 4 is made for a cell current of 30 A with a cell internal resistance of 0.02 Ohms at the 1000th second. As shown in Figure 3, this approach can predict a thermal heat map for the battery pack for different configurations in real-time.

Conclusions

PINNs offer a significant advantage over traditional methods for modelling systems with multiple design parameters. It also provides a significant advantage in discretizing the physical domain under consideration in the form of point clouds. Traditional meshing techniques sometimes pose significant challenges for complex geometries. PINNs approach requires training the model only once by including the required design parameters in the neural network architecture. Once the model is trained, the solution for the governing equation is obtained in real-time. This approach is 90% faster than the traditional techniques in designing complex systems.

References

[1] Cai, S., Mao, Z., Wang, Z., Yin, M., & Karniadakis, G. E. (2021). Physics-informed neural networks (PINNs) for fluid mechanics: A review. *Acta Mechanica Sinica*, *37*(12), 1727-1738.

[2] Rahaman, Nasim, et al. “On the spectral bias of neural networks.” International Conference on Machine Learning. PMLR, 2019.

Faster design space exploration for tires using machine learning physics model

Rasika Kulkarni[1] , Girish Patil[2] , Jayant Pawar[3] , Atharv Govind[4] , Jason Barr[5] , Victor Oancea[6]

Dassault Systemes

Abstract

Tire design is crucial for vehicle safety, comfort, and performance, necessitating manufacturers to navigate complex trade-offs among key performance indicators (KPIs) while adhering to stringent industry standards. The analysis of extensive datasets to optimize tire designs poses significant challenges due to the complexity involved. Although numerous design optimization techniques exist, the substantial time investment required remains a barrier to efficiency. Recent advancements in data-driven technologies, particularly machine learning (ML), offer a promising solution to expedite the design exploration process while conserving computational resources. For passenger car tires (PCR), it is essential to achieve optimal traction and maintain a target footprint contact ratio across varying load and maneuverability conditions. Traditional nonlinear simulations often require extensive computational time and resources to explore the tire design space. To address these challenges, Dassault Systemes has developed a novel methodology that employs a parametric machine learning (ML) physics model to efficiently predict footprint contact ratio and traction across diverse load and maneuverability scenarios. This approach enhances both the speed and accuracy of tire design analysis. By leveraging a neural network-based model, the richness of 3D simulation results is maintained while significantly reducing execution time, facilitating quasi-interactive design exploration and optimization. A comprehensive finite element simulation setup is utilized as the starting point. Design of experiments (DOE) is integrated with simulation to generate data; this data is then processed to train fast-executing ML physics model. The ML physics model undergoes an optimization loop to identify the optimum tire design parameters, maximizing traction while achieving the target footprint ratio. This paper highlights the potential of combining advanced ML techniques with traditional simulation methods to achieve design optimization quickly and efficiently.

Keywords

machine learning physics model, tire design optimization, footprint contact ratio, tire traction

Introduction

In our daily encounters, the seemingly straightforward black donut known as a tire belies its true nature as one of the most intricately engineered products globally. Tires are meticulously crafted to offer paramount driving experiences characterized by safety, comfort and act as a primary suspension component. Tire comprises of various components like tread, plies, belts, sidewall and carcass. Figure 1 illustrates the tire's cross-section and its constituent parts.

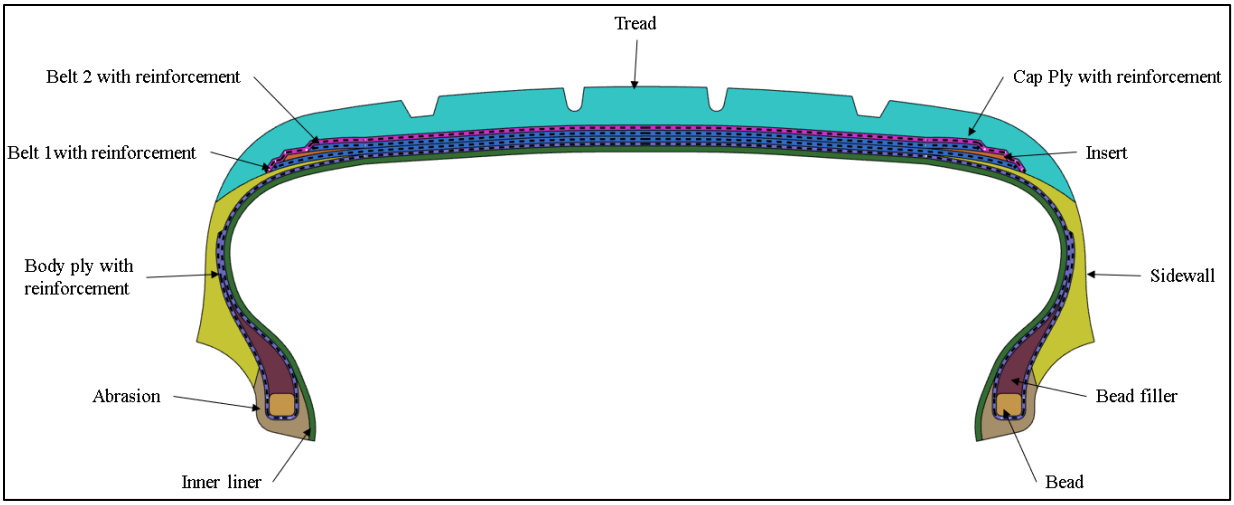

Figure 1 : Tire cross-section

Tire performance is highly sensitive to variations in design parameters. This paper focuses on three specific input design parameters: tread arc radii, bead filler height, and vehicle load. Figure 2 highlights these geometric input parameters.

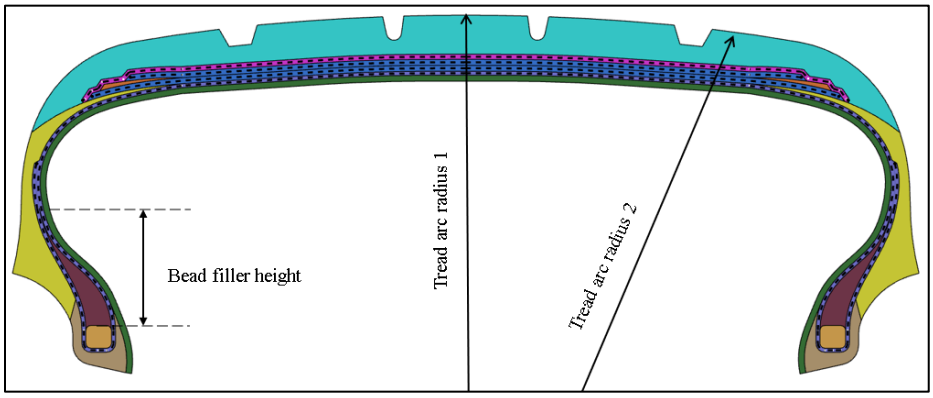

Figure 2 : Input geometry parameters

The curvature of the tread profile significantly influences the contact patch under varying load and slip conditions, while the bead filler height plays a crucial role in the tire's stiffness during lateral and longitudinal slip. A comprehensive finite element simulation is set up to analyze the baseline tire design under different testing conditions, including static footprint, lateral tire slip and longitudinal tire slip. In the static footprint test, an inflated tire mounted on a rim is held fixed at the rim and subjected to a radial load that simulates the load experienced when mounted on a vehicle. The performance of the tire during cornering is evaluated through a lateral slip test, where the tire is in a free-rolling condition and subjected to a lateral angle to mimic cornering behavior. Tire skidding is assessed during acceleration and braking conditions in longitudinal slip test by applying various slip ratios to the free-rolling tire. Tire manufacturers are keenly interested in achieving optimal road grip by attaining target contact ratios across all test conditions while maximizing traction force. Consequently, design optimization is essential to identify the best design parameters that meet these performance requirements.

Methodology

The design space for the tire encompasses over thousands of design points. Simulating each of these points to achieve an optimized design proved to be both time-consuming and computationally expensive. To address this challenge, a framework was developed to train a ML physics model using neural networks, significantly accelerating the design optimization process. From the extensive design space, very few design points representing both midrange and extreme values were selected to train the surrogate model, with 20% of the points reserved for model validation. Figure 3 illustrates the distribution of the design points selected for DOE in the design space of tread arc radius 1, the distribution is similar for all the input parameters.

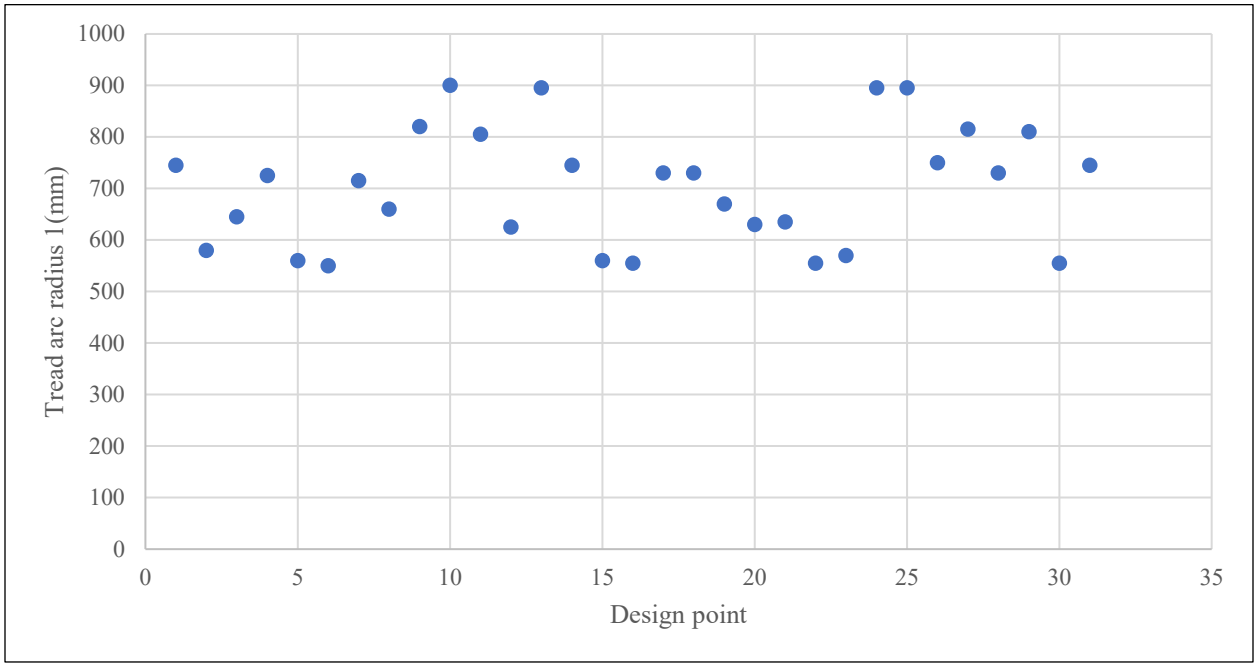

Figure 3 : Distribution of design points for DOE

Figure 4 outlines the methodology employed to generate and validate the ML physics model, as well as how it is utilized for subsequent optimization. This approach not only enhances efficiency but also improves the accuracy of design predictions, enabling more effective exploration of the tire design space. Parametric tire cross-section CAD is the initial input. The baseline cross-section is utilized to simulate key performance metrics, including static footprint, lateral slip, and longitudinal slip tests. A comprehensive design of experiments is conducted to generate the data necessary for training a machine learning model. Utilizing neural networks, the ML physics model is trained and validated, followed by an optimization loop to maximize traction force and achieve an optimal contact ratio under a fixed load percentage. This process enables the prediction of the best design parameters tailored to meet specific performance objectives.

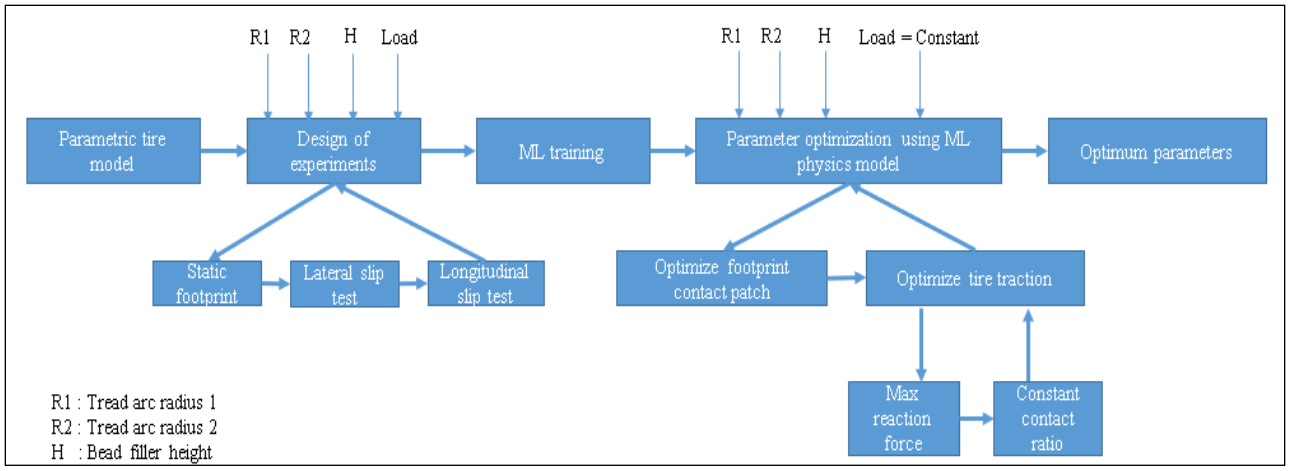

Figure 4 : Methodology

Results

The ML physics model demonstrated the capability to predict contact ratio and traction forces under various load and maneuverability conditions with an average accuracy of 94% and operating five times faster than traditional methods. Table 1 presents a comparison between the contact pressure (CPRESS) plots obtained using the Abaqus solver and those predicted by the ML model for a design point.

Tests	Abaqus result	ML predicted result
Static Footprint	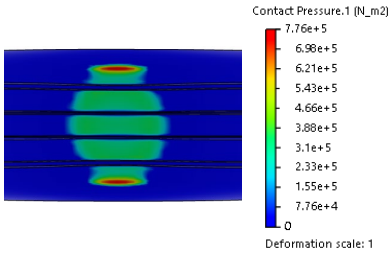	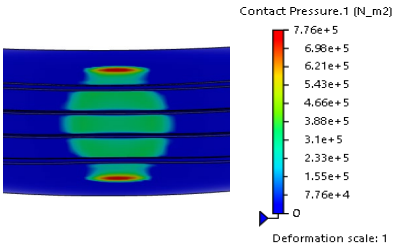
Lateral Slip Angle = +5°	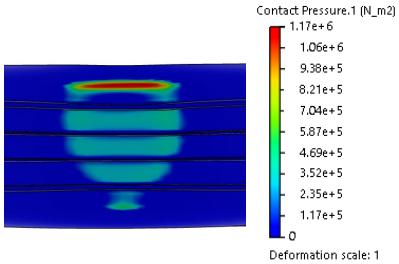	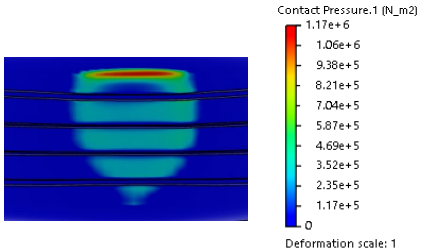
Lateral Slip Angle = -5°	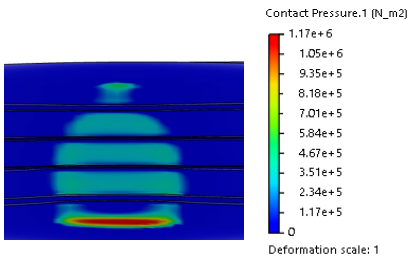	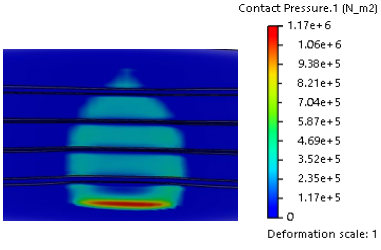

Longitudinal Slip Slip ratio = 0.55	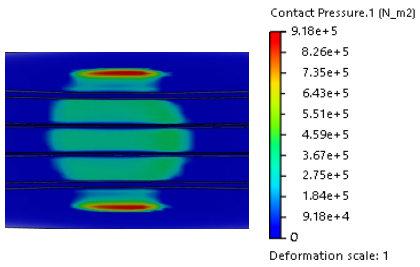	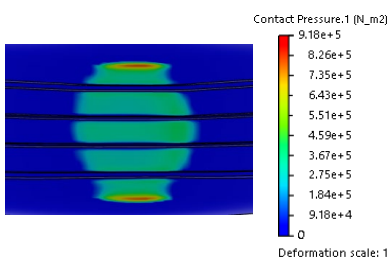

Table 1 : CPRESS comparison between Abaqus and ML predicted results

Conclusion

The entire process of data generation, surrogate model training and validation and design optimization using the ML physics model was completed within one week. This represents a significant reduction in time compared to conventional design optimization processes, highlighting the efficiency and effectiveness of the proposed approach.

References

1) Lars Greve, Bram Pieter van de Weg, “Surrogate modeling of parametrized finite element simulations with varying mesh topology using recurrent neural networks”, Array 14, April 2022, doi: 10.1016/j.array.2022.100137

FMU validation with CosiMate: Using native co-simulation to prepare and validate Multiphysics FMU-based simulation

David Balland (Chiastek France), Matthieu Jude (Alten France), Cesar Carrizo (ZF Japan)

INTRODUCTION

The industry is currently experiencing a drastic change in system design methodology. While aircraft systems are becoming smarter, complex control systems and higher safety requirements are requested, making virtual design more challenging.

Consequently, as the underlying technology, computer simulation is also growing rapidly both in fidelity and computing intensity. However, the way engineers conduct multi-physics co-simulation today can hardly keep up with the newest challenges, mainly due to the lack of collaborative virtual design platform across the supply chain. Without such tool, most suppliers can only validate their own components as opposed to the entire system. Compatibility issues are often not discovered until system integration phase, resulting in substantial cost in design change and even delayed product release. A Model-Based Systems Engineering (MBSE) approach consists in using a formal digital language to specify, design, analyse and verify a system. Co-simulation is a contributor to MBSE in the sense it helps validating a multi-component system at model level.

FMI is a standard for co-simulation at system level which can be used for such multi-component virtual testing. The CosiMate software is a platform for co-simulation that allows to instantiate both native system models and/or FMU's. Here the focus is made on the capacity offered by CosiMate to validate FMUs for a multi-physics simulation.

In this paper will be presented a strategy to set up models owned by internal and external stakeholders using different modelling tools. We will describe how to achieve the virtual design of a Power Unit by instantiating 3 models from different simulators: Simulink, GTSuite and Amesim. In this system, GT-Suite model is representing the engine, Simulink model a controller and Amesim model a sample converter. The strategy is quite simple (figure 1): a first co-simulation is built with the original models, which will be the reference platform, then we export each model, one by one, as an FMU for co-simulation.

We will discuss the benefits of native co-simulation to support the validation of FMU's and underline the advantages of FMUs for co-simulation and distributed co-simulation.

Moreover, this co-simulation platform, beyond FMU validation, also allows multi-site distribution. This capability offers the possibility to run a co-simulation using models located in different places or countries.

KEYWORDS:
Simulation, co-simulation, multi-domains, multi-physics, multi-site, MBSE, MBD, confidentiality, collaboration, FMI, FMU

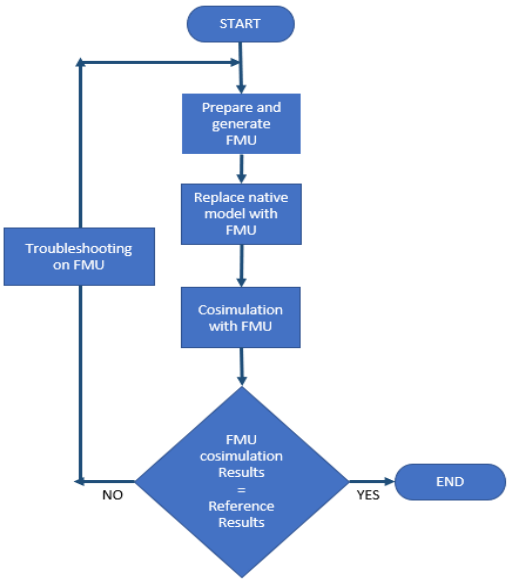

Figure 1: FMU validation algorithm

1. Reference model

1.1 Setup

This validation strategy is based on comparison of model results. It is very important to create the proper environment to prepare reference results. Then the FMU-based results will be compared against the reference. A functionality of tracing and saving the data transiting on the co-simulation platform, like CosiMate Scope, is particularly useful in this process.

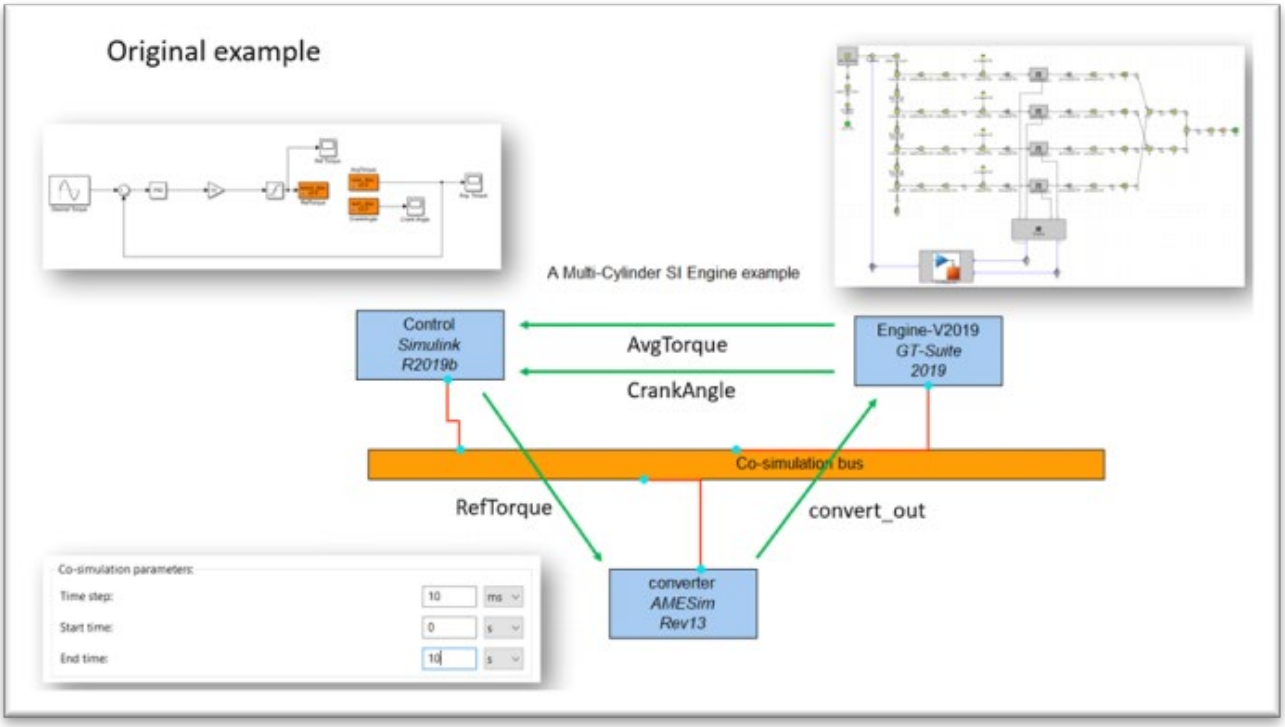

Figure 2: Reference co-simulation system

A known example is used (figure 2), based on public models that are available with the different simulation software. Those models are physically proven and allow to have a good representation of an actual system. That is why they are used are reference models.

In our case, the system is a Power Unit, where GT model is representing the engine and Simulink model a controller, Amesim model is a simple converter.

The set up to configure models before co-simulation on Amesim, Simulink and GT are very similar. First step is to create or configure model as your need, co-simulation input and output ports are available on native simulator libraries. Once model is ready, just set solver time-step and other simulation info. When model is run in standalone, a *modelname*.ixd co-simulation file is generated by CosiMate API. It is used to import model on CosiMate GUI as a co-simulation component (blue box) and contains mostly the ports information. It is the only file needed by CosiMate to run co-simulation. The end task is to configure co-simulation parameters and run the co-simulation. An option called “csv traces” shall be used to store all data transiting on the co-simulation bus. CSV files can be opened with CosiMate Scope for a graphical view. Reference results are used to compare and validate the FMU export.

In the example used, the reference co-simulation is implemented in local architecture, but co-simulation can be used using other interesting teamwork methodologies tested by partners, as distributed co-simulation or co-simulation in the cloud (see chapter 3: Alternatives).

1.2 Results

Results of reference co-simulation and FMUs shall be stored using csv option from CosiMate Bus. The csv file created during the run is stored in model folder location.

Co-simulation environment contains a scope. CosiMate Scope uses common functions of scope with colors, zoom, print, scale, etc. Save function can be used to store data with the scope.

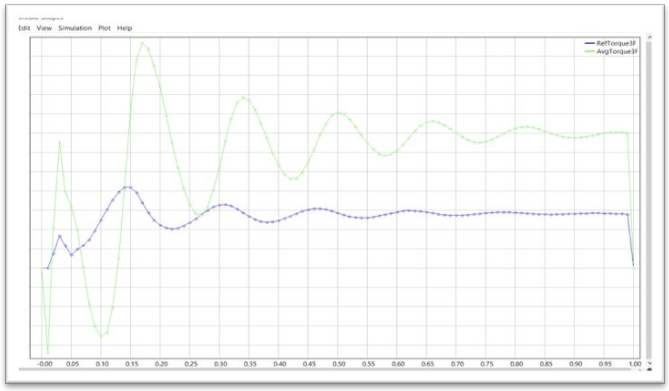

Figure 3: CosiMate Scope

The results of the reference are stored and will be used to compare against the FMU results. When the results are similar, we can assume the FMU is validated and can be used as trusted model for stakeholders.

2. FMU co-simulation

2.1 Set-up

One of the benefits of the FMI is that it is a standard for co-simulation. This means that once the FMUs are generated, they will all be set up with the same formalism (ports). The generation of FMUs depends on each simulator. To generate an FMU from a native model, one must refer to the corresponding tool's documentation.

On the co-simulation platform when the FMU is available it can be opened with FMU Connector, a CosiMate tool which is used to configure co-simulation parameters of model.

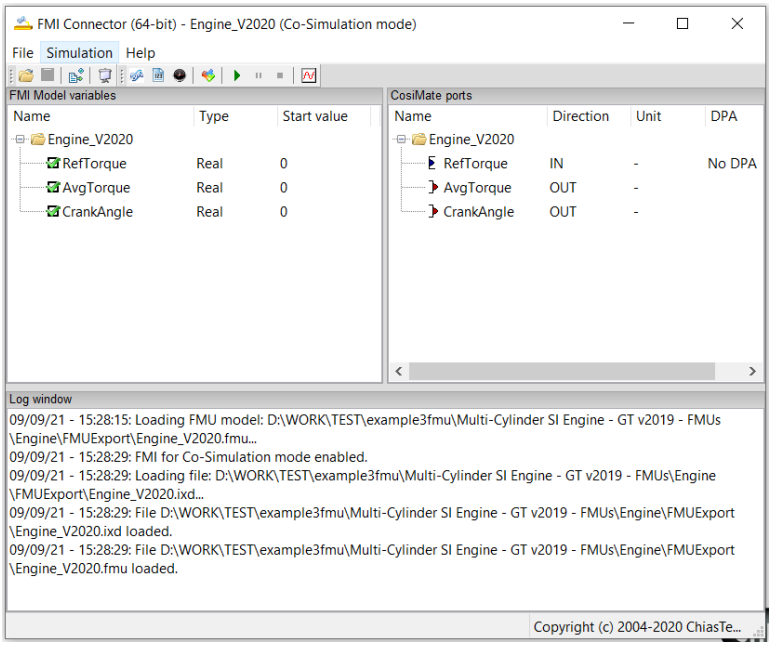

Figure 4: CosiMate FMU connector

At this point the co-simulation can be executed either in interactive or batch mode. To simply validate all FMUs, each time we have generated an FMU we replace the native model by this new FMU.

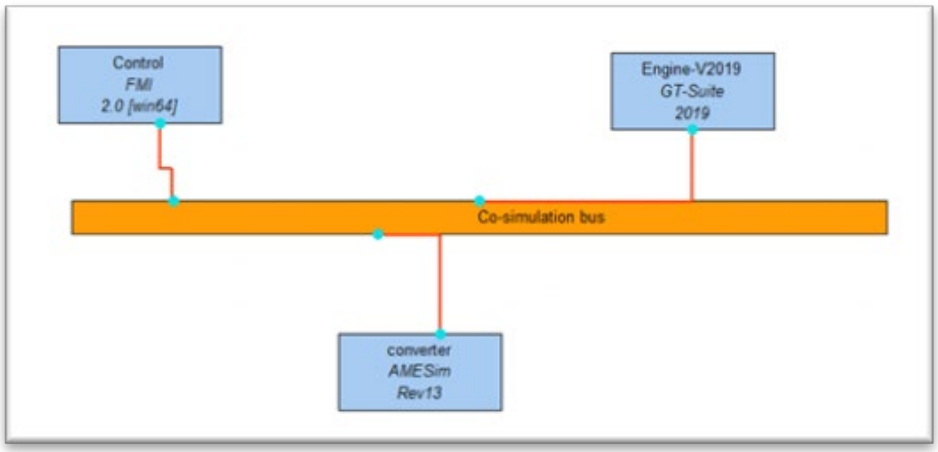

Figure 5: Co-simulation mix Native/FMU

2.2 Logs

An FMU itself doesn't have interface or log window, so the role of the co-simulation environment is to provide so. The FMI Connector contains a log area to get all live feed info, error and warning of FMU

model. A verbose mode is also available to help debugging. Log area contains FMU native's and co-simulation's information.

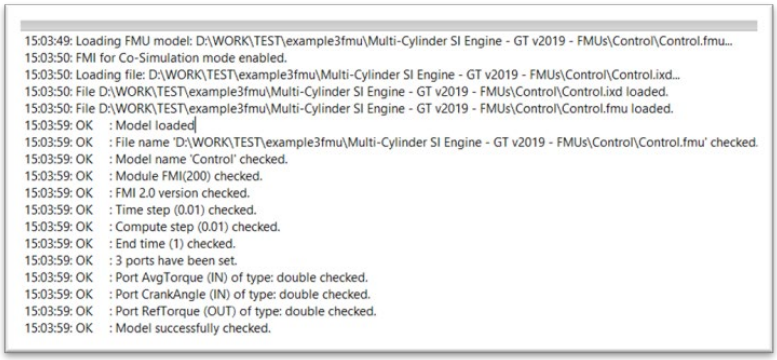

Figure 6: FMI Connector log window

2.3 Results comparison

The co-simulation results (data exchanged on co-simulation bus) are stored in csv files. There is one csv per model.
Thus, there are two ways of comparing results with the reference co-simulation platform: either graphically, using CosiScope graphical view of csv files, or any other tool managing csv (like Microsoft Excell), or by comparing directly csv files raw data, which can be automated easily by script or batch.
To validate the generated FMU, it simply requires to compare the csv files with the reference csv files.

3. Alternatives

3.1 Distributed co-simulation

The co-simulation platform allows multi-site distribution. This feature offers the possibility to run a co-simulation using models located in different places or countries. CosiMate is compatible with any VPN software. During a distributed co-simulation, models are confidential and only a description file is shared to the co-simulation host. Data are exchanged through network between the computers.

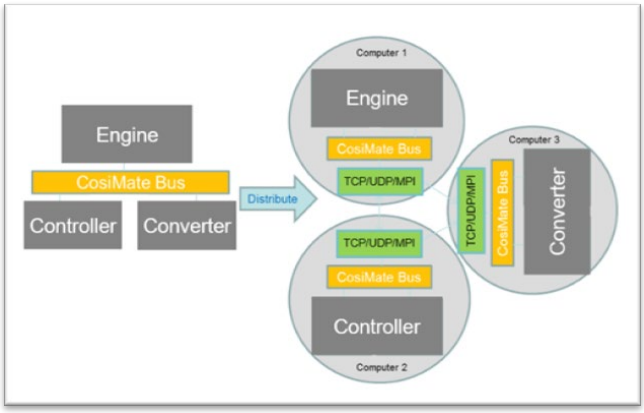

Figure 7: Distributed co-simulation

Distributed co-simulation's main advantages are time saving to run complex system and, above all, confidentiality of models and data. During a co-simulation with "csv" option activated, each model creates a file modelname.csv containing exchanged data of the model.
The objective is run each model on different computers and exchange data of co-simulation through the network. Using a VPN Software, multi-site co-simulation (different locations) is possible and very easy to set up. In Japan, Azapa, set up a co-simulation between France and Japan as a tutorial for their clients who are now deploying this usage.
With CosiMate it is very easy to create a robust reference thanks to the capability of running the original models in native mode. However, the owner of the model often cannot share the source

model. In such case, distributed co-simulation solution protect the confidentiality of model and enable the collaboration across network.

3.2 Cloud-based co-simulation

Co-simulation in the cloud is a solution used by customers to create share co-simulation platform where engineers import models and run complex systems using co-simulation template. A co-simulation template consists of the definitions of major blocks and their connection topology. Models with compatible I/O can plug-and-play without rebuilding the entire system. On the other hand, interface is also offered if the user chooses to build a new co-simulation from scratch. The user only needs to drag and drop model blocks onto the canvas, and then define their relationships by setting up connections between models. Information in each model block, such as file, simulator and launch script, also need to be entered properly.

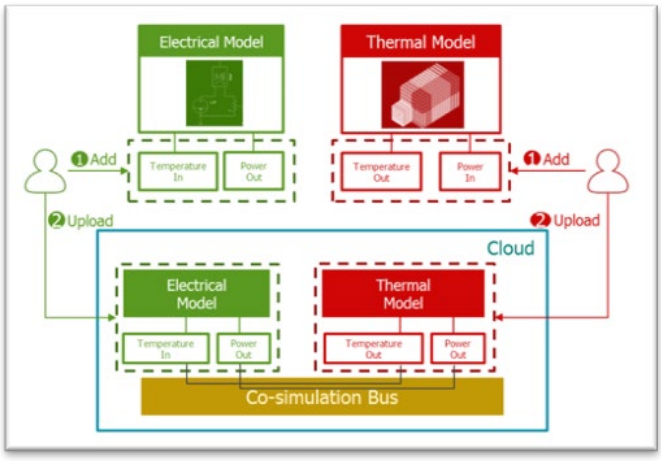

Figure 8: Co-simulation in the cloud

In 2019, Hitachi presented a platform fully cloud based to support co-simulation approach (Ref 4). The biggest innovation of this platform is the intuitive web interface that enables engineers to start collaborating on a co-simulation virtually from anywhere, without the hassle to exchange model files, assemble models by hand, or install simulation tools on the working computer. Of course, as Hitachi was implementing it on a private cloud, it could easily be implemented on Oracle Cloud Infrastructure, Google Cloud Platform, Microsoft Azure or Amazon Web Services (AWS).

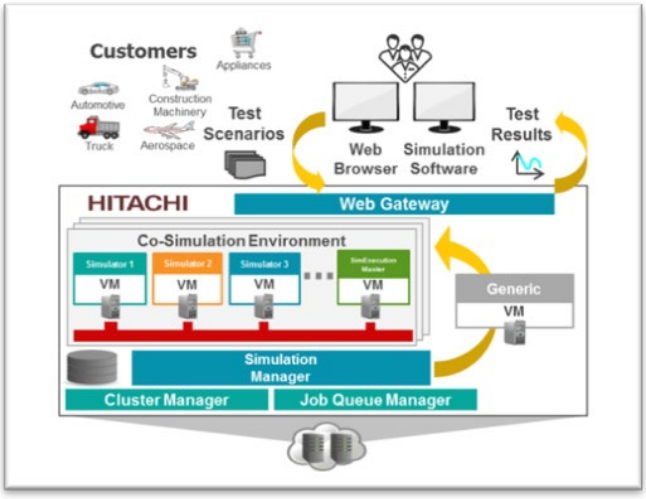

Figure 9: Architecture of a collaborative multi-physics co-simulation system

4. Troubleshooting

4.1 FMU results delay

A delay could be observed in FMUs results, this delay is expected as per the FMI 2.0 standard of co-simulation.

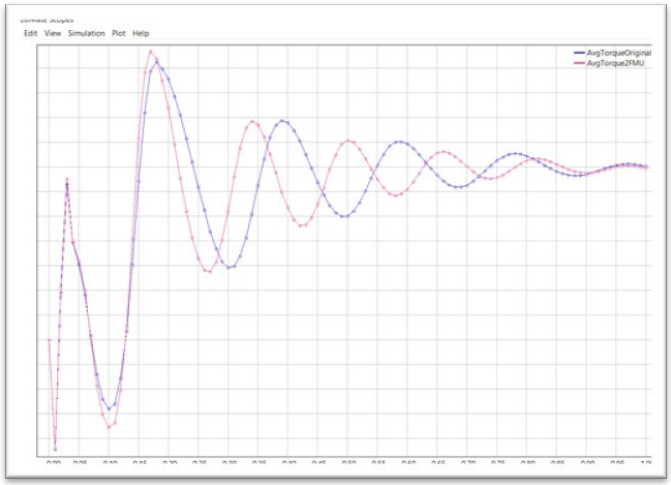

Figure 1: FMU results delay

Supports suggest introducing a tolerance when comparing the results of FMU simulation instead of working around the issue by adding a delay to the rest of the model which might not work for all models.
The workaround for the FMU delay needs to be investigated on a case-by-case basis, as it really depends on the types of blocks inside. For instance, here is the MATLAB documentation link related FMU delay:
https://www.mathworks.com/help/simulink/ug/co-simulation-execution-and-numerical-compensation.html
It gives more information about this and possible ways to compensate it using the numerical compensation feature. FMI 3.0 standard would resolve the delay in the FMU.
A possible solution could be to use a time delay for communication between the local solver of the FMU and the co-simulation tool time-step. This information is captured in an external document:
https://www.mathworks.com/matlabcentral/answers/720854-why-there-is-a-time-delay-of-one-time-step-while-co-simulating-a-fmu-in-simulink

4.2 Other investigations

They are many things to check, and we cannot be exhaustive.
Of course, you may not have access to the original model as it very often is property of the partner. In such case you can instantiate the co-simulation over a network so each stakeholder can make modification “on the fly”.
You may also want to check whether the same solver is used, whether the options of the solver are the same, whether they are limitation to the FMU export (check requisite from each vendor: some ports, blocks or options could not be supported). In most cases, an FMU (2.0) cannot be exported with variable time step solver option.

5. Conclusions

In this paper was presented a process to validate FMUs exported from different softwares using co-simulation of a controlled system. The use of co-simulation reference with native models to compare co-simulation results after FMU transformation is a strong way to validate the export and model robustness.
We presented different strategies tested by partners to instantiate reference co-simulation, analyse, and store reference results and compare FMU results to validate export.

The co-simulation with FMUs enables integration of real-time systems and simulation environments in a standardized way. A stronger relationship between virtual and real worlds demands for new methodologies in simulation and test.
One of the benefits of FMI is to share model with a black box confidentiality level, but debugging is limited to FMU execution activity and will not provide info on model content. Therefore, it is important to have a reference in order to validate the different models.
The FMI standard is constantly improved, and Software editors are adopting it. At the time of this paper test have been done with FMI 2.0, but FMI 3.0 already exists.

6. References

- G. Saikalis et al., “Virtual Embedded Mechatronics System,” SAE Technical Paper # 2006-01-0861.
- H.Chen, S.Phatak, Y.Xiao Hitachi America, Ltd., U.S.A.; Pierre Boulon Chiastek, France ; “Automated Multi-physics Co-simulation in the Cloud”, NAFEMS Technical Paper, 2019.
- J. Sinnamon et al., “Co-simulation Analysis of Transient Response and Control of Engines with Variable Valvetrains”, SAE Technical Paper, 2007-01-1283.
- S. Phatak et al., “Cyber Physical System: A Virtual CPU Based Mechatronic Simulation,” IFAC (Sep. 2010).

- FMI Standard, https://fmi-standard.org/
- ChiasTek, 2024, http://www.chiastek.com
- CosiMate https://www.cosimate.com/

Thermo-chemical-mechanical modelling of digital light processing 3D printing

Guang Liu*, David W. Rosen
Institute of High Performance Computing (IHPC), Agency for Science, Technology and Research (A*STAR), 1 Fusionopolis Way, #16-16 Connexis, 138632, Republic of Singapore
Corresponding author: liu_guang@ihpc.a-star.edu.sg

1 Summary

Digital light processing (DLP) is a type of vat photopolymerization additive manufacturing technology that has been widely used in practical applications due to its high printing resolution and high printing speed. However, the distortions and residual stresses of DLP manufactured parts are significantly influenced by the complex thermo-chemical-mechanical coupled photopolymerization process during the layer-by-layer printing. Therefore, a comprehensive understanding of the system behavior is essential to predict the cure-dependent thermal and mechanical behavior of the layer-by-layer DLP process. In this study, a thermo-chemical-mechanical coupled modelling framework is developed to simulate the layer-by-layer DLP printing process by means of finite element analysis (FEA). Specifically, four sub-models are developed: irradiation model, photopolymerization model, thermal model, and mechanical model. The curing dependent material properties are considered together with the shrinkage and heat generation caused by the chemical reaction. In addition, the progressive element activation method was implemented using the commercial FEA software ABAQUS to simulate the layer-by-layer photopolymerization in the DLP printing process. The release process to simulate the removal of the part from the build platform is also included in the framework. The capabilities of the proposed framework in predicting warpage and print-through effect have been verified with both 2D and 3D geometries from the literature.

2 Introduction, Methodology, and Results

2.1 Introduction

Additive manufacturing (AM), commonly known as 3D printing, has revolutionized the manufacturing landscape by enabling the creation of components with complex geometries, diverse materials, hierarchical structures, and even integrated functionalities [1]. Among the various AM technologies, DLP 3D printing has been widely adopted for applications such as biomedical devices, functional materials and consumer products [2]. DLP generally operates by projecting patterned light onto a photopolymer resin, curing the entire layer simultaneously, which distinguishes it from other methods like Stereolithography (SLA) that typically use a laser to trace each layer. Despite its advantages, the geometric distortions and residual stresses in DLP-fabricated parts are significantly influenced by many interacting phenomena during the printing process. These include polymerization-induced shrinkage, heat transfer, and mechanical constraints, which collectively contribute to final part distortions and residual stresses. However, most research has been focused on experimental investigations without paying sufficient attention to process modelling and simulation, resulting in an inadequate understanding of the DLP 3D printing process [3-4].

Based on our previous work [5], this research presents a comprehensive thermo-chemical-mechanical coupled modelling framework developed using the FEA method to simulate the layer-by-layer DLP process. By integrating irradiation, photopolymerization, thermal and mechanical responses, this framework aims to enable the prediction of distortions and residual stresses of DLP 3D-printed parts.

2.2 Methodology

A schematic diagram of typical DLP 3D printing is shown in Figure 1a. Parts are manufactured through a layer-by-layer process, in which UV light irradiates the top surface of the resin. During this process, the liquid resin undergoes chemical reactions to cure into solid parts, generating heat as polymerization reactions are exothermic. In addition, polymerization reactions also cause volumetric shrinkage as the distances between reacting molecules decrease. Due to the layer-by-layer nature of the printing process, previously printed layers are subjected to forces from the current curing layer, resulting in

residual stresses. To predict distortions and residual stresses of DLP manufactured parts, a thermo-chemical-mechanical framework is proposed, consisting of four sub-models: the irradiation model, photopolymerization model, thermal model, and mechanical model, as shown in Figure 1b.

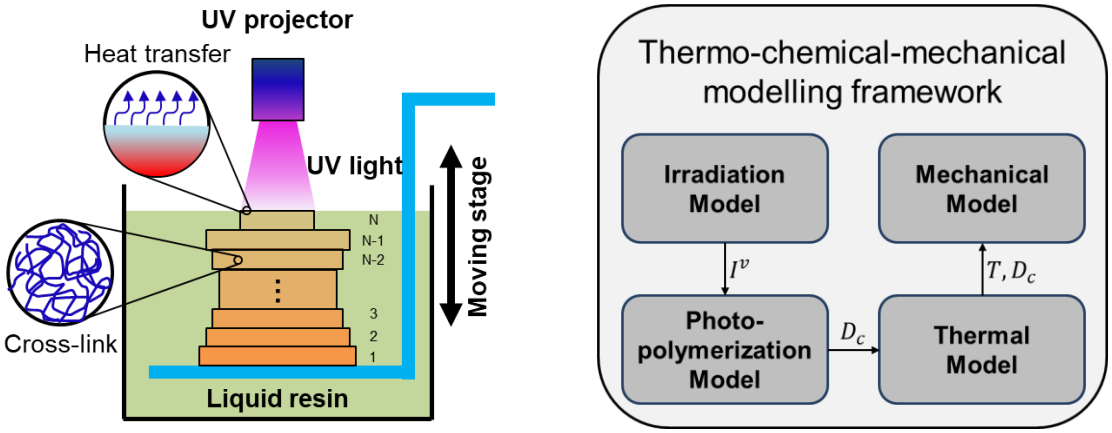

a) Schematic diagram of DLP b) Multiphysics photopolymerization process

Figure 1. Digital light processing 3D printing

- **Irradiation Model:** The Beer-Lambert law is utilized to describe the light attenuation as it propagates through the liquid resin along the layer-thickness direction.
- **Photopolymerization Model:** The degree of cure (DoC) at each material point is determined by solving a set of ordinary differential equations based on Ref [6].
- **Thermal Model:** Heat generation resulting from the exothermic chemical reactions during photopolymerization is modelled as a heat source within the thermal model.
- **Mechanical Model:** The temperature and DoC distributions are taken as the inputs for the mechanical model. The total strain is calculated as the sum of three constituent strains as $\varepsilon^{tot} = \varepsilon^{el} + \varepsilon^{th} + \varepsilon^{ch}$, where ε^{el} is the elastic strain, ε^{th} is the thermal strain, and ε^{ch} is the chemical shrinkage. Note that the elastic modulus considered here is dependent on the DoC.

The proposed simulation framework was implemented in the commercial FEA software ABAQUS, as depicted in Figure 2. For each layer, the irradiation model computes the light intensity distribution, then the photopolymerization model computes the DoC, which is then passed to both the thermal and mechanical models. Two user subroutines, UMAT and UMATHT, were utilized here. The UMAT subroutine contains three of the sub-models, and the UMATHT subroutine contains only the thermal model. Element activation was modelled using the model change module in ABAQUS to simulate the layer-by-layer printing process. In addition, the simulation framework includes a release process to simulate the removal of the part from the build platform.

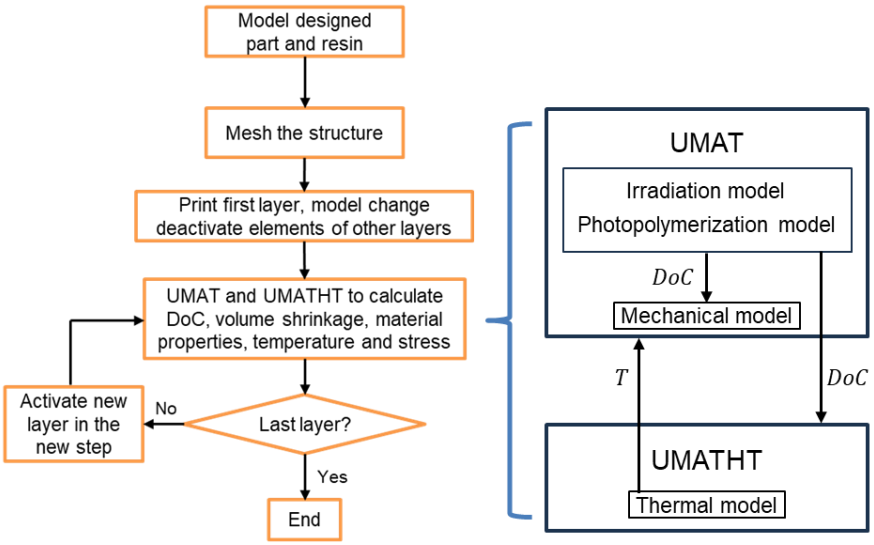

Figure 2. Implementation in ABAQUS with user subroutines.

2.3 Results

The proposed framework was validated using two examples: a 2D bridge-like part and a 3D bridge-like part. The layer thickness was set to 0.1 mm. For each layer, the UV light was turned on for 3 seconds, followed by 1 second of light off to allow for the layer transition. In addition, a cooling down period of 30 seconds was modelled after the completion of the last layer.

2.3.1 Example 1: 2D Bridge-like Part

As shown in Figure 3, the 2D bridge-like part is 8.5 x 1.6 mm in size, but the computational domain was extended to 18.0 mm in length to accommodate the surrounding liquid resin, allowing for modelling of heat transfer into the resin surrounding the designed part. With a layer thickness of 0.1 mm, a total of 16 layers were modelled. To capture the deformation at part boundaries, the mesh was adaptively refined, particularly in the corner regions. 5 elements per layer were modelled along the printing direction, resulting in 23,800 elements for the designed part and 66,560 elements for the entire model.

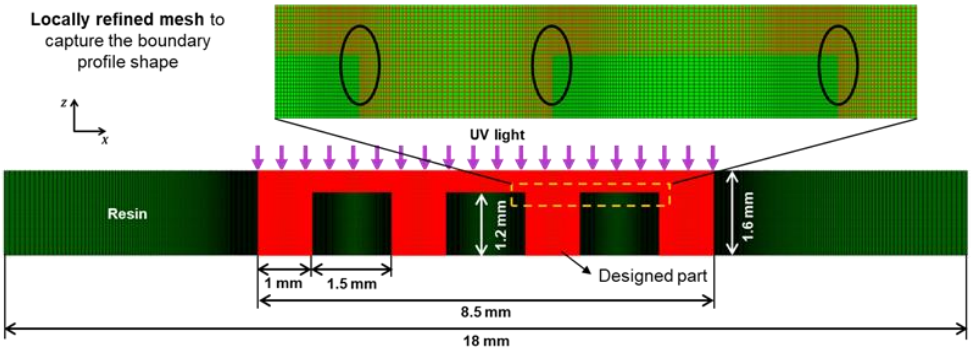

Figure 3. A 2D bridge-like part.

The results for the 2D bridge-like part are illustrated in Figure 4. Elements with DoC less than 0.15 were excluded from the results. The DoC distribution within the printed part indicates the lower regions exhibit a higher DoC while the upper regions show a relatively lower DoC, as shown in Figure 4a. This was caused by the multiple exposures to UV light during the printing process, enabling the previous layers to receive more UV light. In addition, the “print-through“ effects are observed from the overhanging areas, as shown in the centre of the part in Figure 4a. Displacements before and after removal of the part from the build plate are presented as in Figure 4b. It is evident that shrinkage occurred along the vertical part edges of the part as they are bent inwards. When the fixed boundary constraints were removed, due to the residual stresses, the released part deformed and distortion was introduced. The axial stress results are shown in Figure 4c. The tensile stress in the top region of the part largely relaxes after the part is removed from the build plate, indicating significant stress redistribution due to the release of residual stresses.

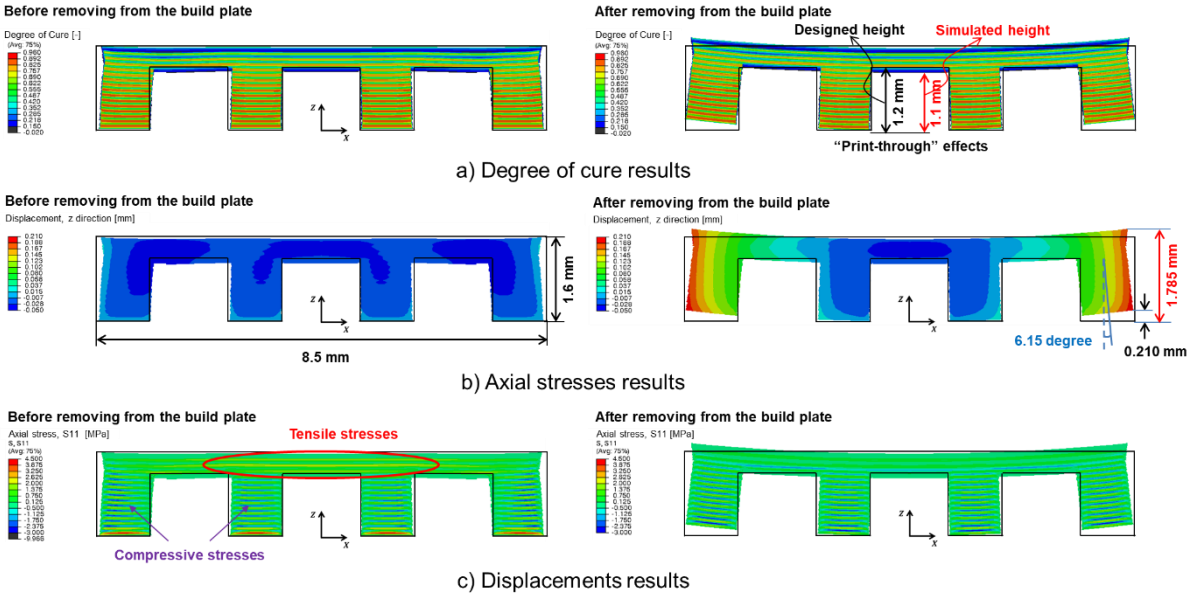

Figure 4. Results of the 2D bridge-like parts.

2.3.2 Example 2: 3D bridge-like part

Since the 3D bridge-like model can be simplified based on geometric symmetry, only a quarter model is built, as shown in Figure 5. The size of the part is 4.25 x 0.5 x 1.6 mm. Again, to account for the heat transfer into the surrounding liquid resin, the model was extended to 7.5 x 4.0 x 1.6 mm. Due to the higher computational cost associated with hexahedral elements compared to quadrilateral elements, only 2 elements were utilized for each layer in the printing direction, resulting in 25,632 elements for the designed part and 315,296 elements for the entire model.

The simulation results for the 3D bridge-like part are presented in Figure 5. For better visualization, the simulation results are shown for the middle plane (YOZ plane). Similar to the 2D example, the 3D model also successfully captured the “print-through“ effects, as evidenced by the DoC distribution. The von Mises stress results before and after part removal from the build platform are shown in Figure 5. It can be seen that the von Mises stresses significantly relax after removal from the build platform.

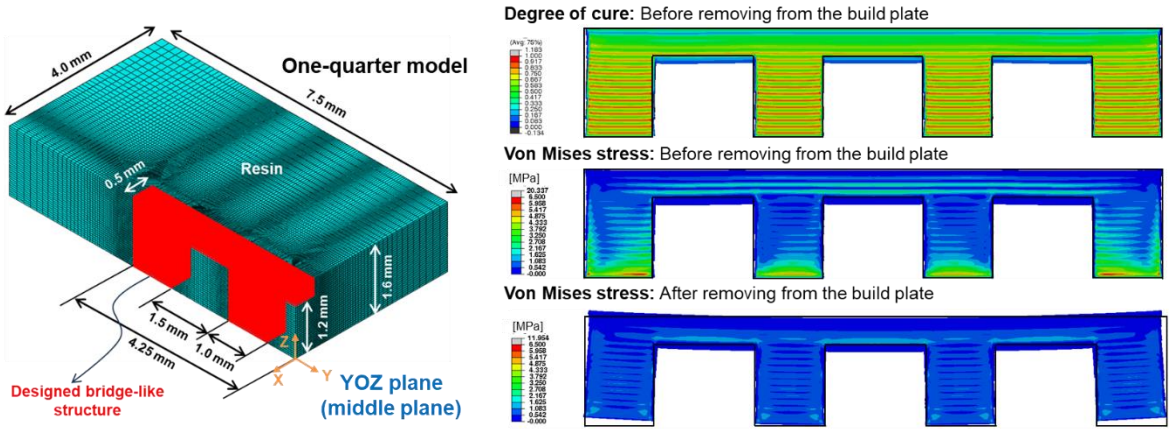

Figure 5. Results of the 3D bridge-like parts.

3 Conclusions

This research presents a comprehensive thermo-chemical-mechanical coupled modelling framework for digital light processing 3D printing, implemented using finite element analysis in ABAQUS. Four sub-models, namely the irradiation model, photopolymerization model, thermal mode, and mechanical model, were developed using the user subroutines together with model change technique. Validation with both 2D and 3D bridge-like parts demonstrated the ability of the framework to effectively predict degree of cure distributions, print-through effects, distortions, and residual stresses. The results highlight the potential of using the proposed framework as a tool for DLP 3D printing parameter optimization. Future work will focus on extending the model to include more complex material behaviour and large-scale simulation.

4 References

[1] Chaudhary, R., Fabbri, P., Leoni, E., et al. "Additive manufacturing by digital light processing: a review." Progress in Additive Manufacturing 8.2 (2023): 331-351.

[2] Zhang, F., Zhu, L., Li, Z., et al. "The recent development of vat photopolymerization: A review." Additive Manufacturing 48 (2021): 102423.

[3] Li, Y., Mao, Q., Yin, J., et al. "Theoretical prediction and experimental validation of the digital light processing (DLP) working curve for photocurable materials." Additive Manufacturing 37 (2021): 101716.

[4] Cai, R., Luo, X., Xie, G., et al. "Effects of the printing parameters on geometric accuracy and mechanical properties of digital light processing printed polymer." Journal of Materials Science (2024): 1-13.

[5] Emami, M.M., Jamshidian, M., Rosen, D.W., "Multiphysics modeling and experiments of grayscale photopolymerization with application to microlens fabrication." Journal of Manufacturing Science and Engineering 143.9 (2021): 091005.

[6] Zhang, Q., Weng, S., Hamel, C. M., et al. "Design for the reduction of volume shrinkage-induced distortion in digital light processing 3D printing." Extreme Mechanics Letters 48 (2021): 101403.

Balancing Durability and MRI Compatibility: Evaluating Hip Implant Porous Designs

Himanshu Gururani[1], Abhishek Kadri[1], Sunil Sutar[1], Anand Pathak[1]

[1]Dassault Systèmes Solutions Lab, Rajiv Gandhi InfoTech Park Phase I, Pune, MH, India

1 Introduction

Hip arthroplasty is a common surgical procedure aimed at restoring normal hip function and improving the quality of life for individuals [1]. Given the significant forces that hip implants endure daily, their durability is crucial. Recent advancements in additive manufacturing have led to the development of porous hip implants that offer a blend of durability, enhanced osseointegration, and reduced risk of osteoporosis [2]. However, the intricate lattice structures created through additive manufacturing present challenges. These structures, characterized by their mesoscale lattice cells and complex topologies, are prone to fatigue failures due to their high concentration of notches and surface roughness .

Among the various lattice structures, truss lattices are particularly problematic due to their sharp corners and the rough surface typical of additive manufacturing, which contribute to stress concentrations and crack initiation. The triply periodic minimal surface (TPMS) lattice are bioinspired [3], allows uniform distribution of cell strcuture [4], smooth interconnected architectures [5], and better load-carrying capacity [6]. The lattice structures can optimize an implant's design by reducing weight and improving porosity without compromising mechanical performance. They also mitigate the potential issues such as stress-shielding effects shown by solid implants that can lead to bone resorption and implant loosening [7].

For the implant manufacturers, adhering to ISO and ASTM guidelines is crucial to ensure that implants are strong and durable enough for in vivo conditions. Additionally, recent FDA requirements mandate that implants be labeled for MRI safety, as metallic structures can interact with MRI fields, causing image artifacts and potential heating issues [8]. This heating, influenced by the implant's geometry and its interaction with RF and magnetic fields, may create hot-spots in surrounding tissues [9]. Given these factors, the role of lattice structures in MRI-related heating of hip implants warrants careful investigation, due to thier complex topologies. A recent study indicated that RF simulations of complex geometries can be effectively replaced with simplified shapes, provided that the primary length and total volume are preserved [10]. This suggests a potential for generalized estimates of implant heating, which could streamline the safety-compliance process for orthopedic implant manufacturers. However, the study also highlighted the need for further development of parametric models to assess how implant geometry and other variables affect the accuracy of this approach [10].

In the present investigation, the purpose is to undertake a multiphysics approach combinig structural, thermal and electromagnetic simulations to assess the performace of porous hip implant. Five implant designs (one solid and four lattice) with different porous structures are created using lattice design in 3DEXPERIENCE platform and solved for durability as per ISO 7204-6. Then, the porous implant

geometries are imported in CST studio and and assessed for radio frequency induced heating as per ASTM 2182 standard. Further, a 1.5T bird-cage MRI coil system available in the component library of CST studio was used to evaluate maximum temperature rise in the implant for various MRI cycles.

2 Methods

2.1 Hip stem durability

The following section elucidates the methodolgy to evaluate durability of the hip implant according to ISO 7206-4 standard.

2.1.1 Implant model details

The CAD model of the solid implant was created on the 3DEXPERIENCE platform, Dassault Systèmes, Massachusetts, United States. A simple model with circular cross section was created with an overall length of 160 mm. The neck diameter of the implant was taken to be 13 mm. The geometrical details of the solid hip stem is shown in Fig. 1.

2.1.2 Lattice design of the implant

For creating the lattice implant, the lattice deisgner role (LTX) in 3DEXPERIENCE platform was used. The latticer designer role allows the user to automatically fill the selected volume of the body with the desired lattice. In the present study, approcimately 52 mm of the mid section of the hip stem was filled with four different types of TPMS lattices, namely, Diamond, IWP, Schwarz P and Gyroid. The unit cell size of the lattices was 8 mm with 2 mm thickness. Fig. 1 shows the lattice hip stem with diamond lattice and unit cells of other lattices.

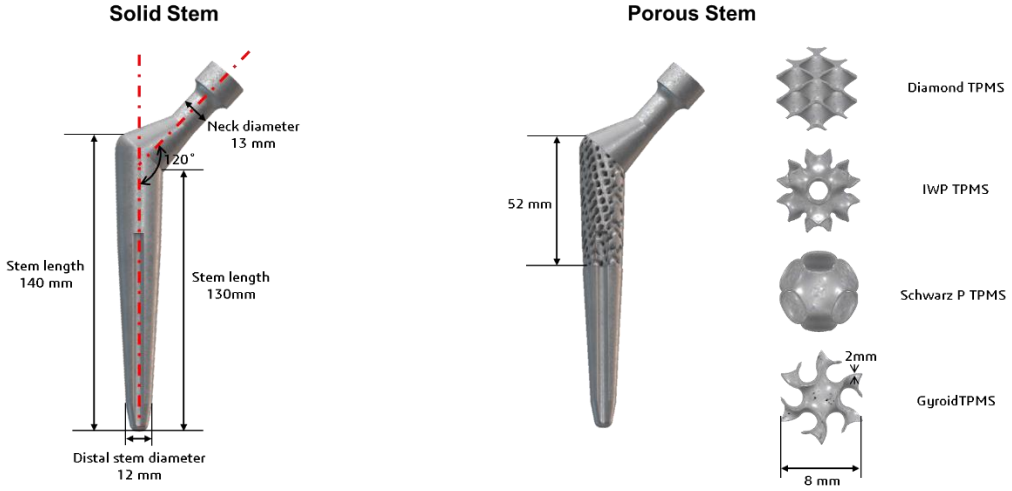

Fig. 1 An illustration of the (a) geometrical details of the solid hip stem and hip stem with three TPMS lattices

2.1.3 ISO 7206-4

The international standard ISO 7206-4 specifies the test conditions for evaluating the fatigue properties of the stemmed femoral components of total hip arthoplasty. simulates the worst case scenario of hip stem fracture. In the method, 60 % of the hip stem is embedded in a cylindrical block, which is made up of acrylic bone cement. The hip stem should be embedded to create a 10˚ adduction in the coronal

plane and 9˚ flexion in saggital plane. A schematic of the hip stem and bone cement block assembly is shown in Fig. 2.

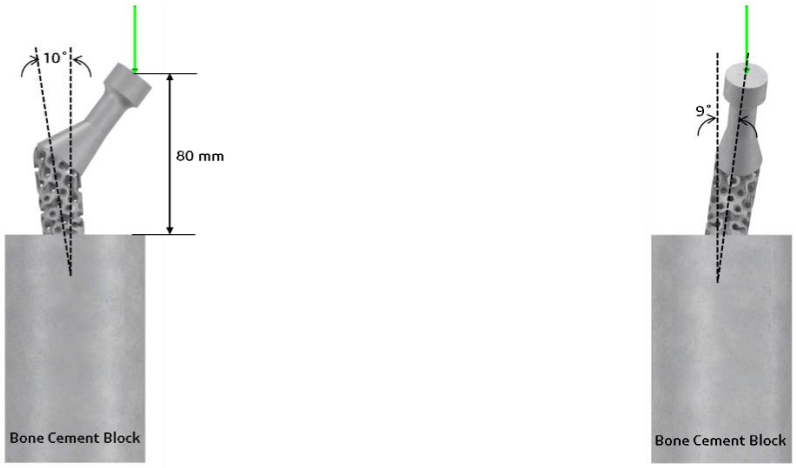

Fig. 2 The configuration of the hip stem and bone cement assembly in 10˚ adduction and 9˚ flexion

2.1.4 Finite element model of the implant

Fig. 3 shows the meshed geometry of the ISO 7204-6 assembly. The assembly was meshed with adaptive meshing capability of the lattice FEM in 3DEXPERIENCE platform with a total number of 1,84,113 four-noded linear tetraheral elements. A tie connection was defined between the inner and outer surfaces of the bone cement block and the hip stem in the embedded region. The external surfaces of the bone cement block were encastered to restrict all degrees of freedom. The material properties of the hip stem and the bone cement block are given in Table 1. The hip stem and the cement block was assigned with Ti-6Al-4V alloy and bone cement material properties.

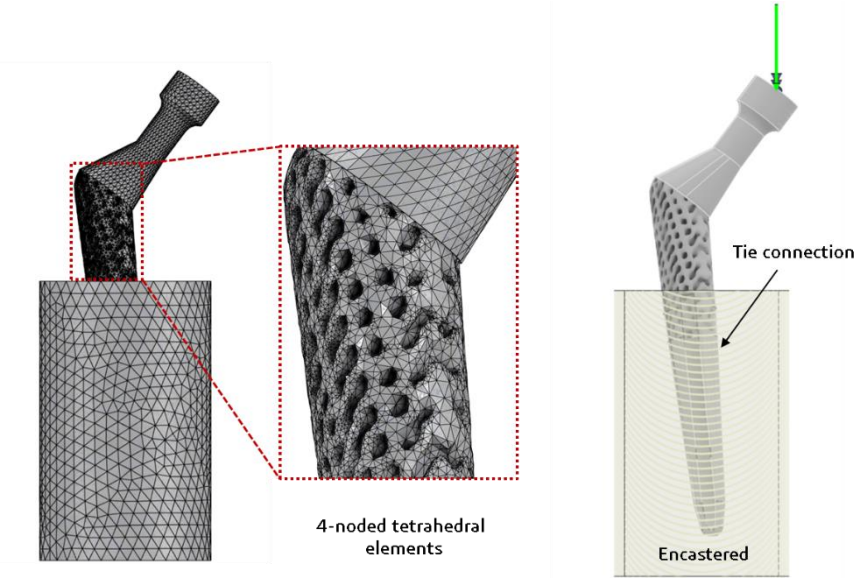

Fig. 3 An illustration of the finite element model of the hip stem-cement block assembly

Table 1 Material properties of hip stem and cement block

Material	Elastic Modulus (GPa)	Poisson's ratio
Ti-6Al-4V	112	0.3

Bone Cement	3	0.3

2.1.5 Fatigue analysis of the hip stem

In the present investigation, the hip stem design with infinite life was used to create lattice geometry. Then, the fatigue life of various lattices were evaluted using ISO 7204-6 standard. The von-Mises stress-based fatigue algorithm with goodman correction was used for the fatigue analysis with the factor of safety of 2. As per the ISO 7204-6 standard, the hip system was loaded with the maximum loaad of 3000 N and a stress ration of 0.13 was used for evaluating the fatigue life of the implant.

2.1.6 Design of MRI coils

CST Studio's component library consists of an MRI Coil example which contains the empty RF coil of a 1.5T MRI system. It is basically a cylindrical shield and a typical bird-cage coil, as shown in Fig. 4. Lumped capacitors are used to tune the coil to the required 64 MHz. The coil is driven by two discrete ports positioned at a 90° angle, which excites the required rotating field. This simplified example does not consist of GC coils. It only takes into account the RF behaviour of the MRI and uses the transient solver of CST Studio.

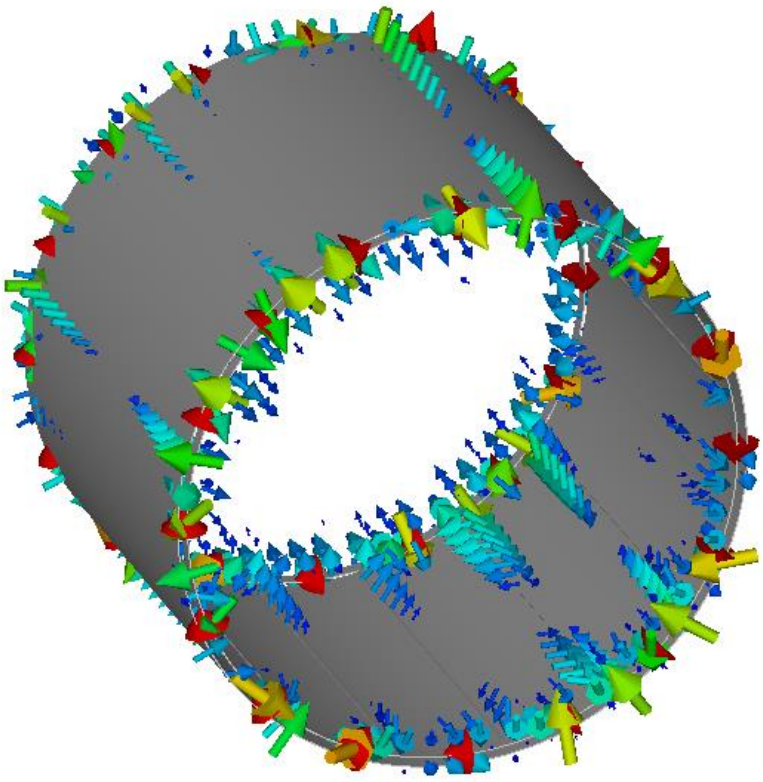

Fig. 4 An illustration of a cylindrical shield and a typical bird-cage coil

2.1.7 Interaction of RF with solid and lattice

The interaction of electromagenic radiation and the lattice surface is crucial to understand the overall MRI heating of the hip implant. In this section, the auhors simulated the behavior of electromagnetic radiation with a simple cubic solid with and without the lattice. An incident wave with E-field along y-axis was allowed to propogate along the z-axis from far left. The objective of the study was to understand how the lattice structure affects ambient EM waves. Fig. 5 shows the scenario setup used in CST to

model this interaction where the red surface is the excitation port, the transparent block is a section of human bone, the gray cube is the section of PEC without lattice (top) and with lattice (bottom). The blue line indicates the path along which E-field is to be analyzed.

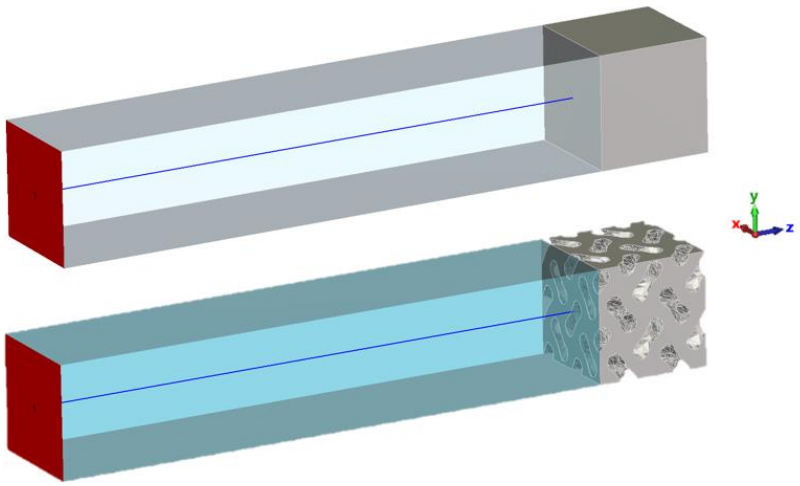

Fig. 5 The scenario setup used in CST to model this interaction where the red surface is the excitation port, the transparent block is a section of human bone

2.1.8 Interaction of RF with solid and lattice hip implant

It is important to observe the performance of the full implant in an MRI coil, as the volume, shape and material of the implant can significantly affect its performance. Hence a second study was performed where the full 3D implant with diamond TPMS lattice was placed in a container filled with a gel mimicking human tissue, after performing the durability analysis is 3DEXPERIENCE platform. The material properties for the gel were defined as per ASTM-F2182-19e2, and the implant model was modeled with Ti-6Al-4V alloy properties. This aparatus was then placed in the MRI coil model described in section 2.1.6. The study was performed for both solid and lattice implant and the results were studied Fig. 6 shows the setup as seen in CST Studio. In addition to the transient electromagnetic simulation a transient Thermal simulation was also performed to observe the change in temperature of the implant and the gel around it

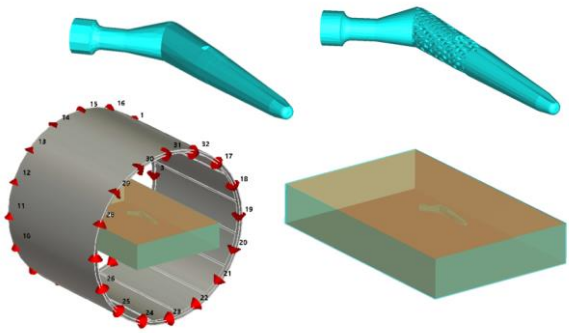

Fig. 6 The MRI setup to evaluate hip implant heaitng in CST Studio as per ASTM-F2182 standard

3 Results and Discussion

3.1 Structural behavior of implant

Fig. 7 shows the von-Mises plots and the fatigue life plots of the solid and the lattice implant in the lateral and medial neck region of the implant. It can be seen that the maximum von-Mises stress for both the solid and the lattice implant design is well within the yeild strength of the Ti-6Al-4V alloy. It has been

shown earlier that the addtitively manufactured Ti6Al4V can last 50 million cycles at 357 MPa with the given material properties used in the present investigation. Therefore, the fatigue life obtained in the present investigation, as shown in Fig. 7 is of 10^7 cycles, as the maximum von-Mises stress during the loading conditions as per ISO 7204-6 is within this value.

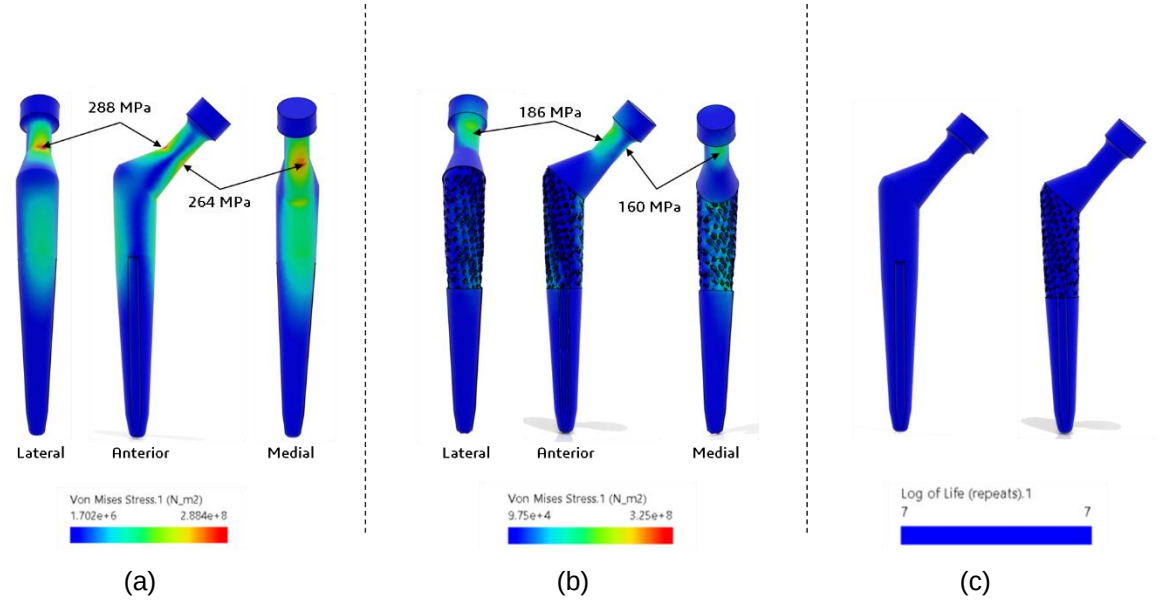

(a) (b) (c)

Fig. 7 Von -mises stress and the fatigue life distribution in the (a) solid,(b) lattice implant and their (c) fatigue life prediction

Table 2 gives the von-Mises stresses and the implant stiffnesses for the various lattice designs evalutaed from the force vs displacement plots. It is intresting that the lattice stems exhibits higher stiffness as compared to the solid one. This could be attributed to the structural stifness arising from the simultaneous out of plane bending, torsion and compression of the hip stem in the loading scenario defined under ISO 7204-6.

Table 2 von-Mises distribution in the various implant geometries

Stem Type (Cell size, thickness in mm)		**Porosity (%)**	**Lateral Neck von Mises (MPa)**	**Medial Neck von Mises (MPa)**	**Stem Stiffness (kN/mm)**
Solid			288	264	4.3
Diamond TPMS (8, 2)		14.15	186	160	10.3
IWP TPMS (8, 2)		17.07	189	180	9.4
Schwarz P TPMS (8, 2)		21.96	208	174	8.3
Gyroid TPMS (8,2)		18.51	207	164	9.1

Intrestingly, the implant stifnesses were found to be different for varying lattice types despite having same lattice parameters (cell size: 8 mm and thickness: 2 mm), as shown in the Table 2. This can be attributed to the varying porosity levels of the lattice implants. The swchwarz P structure shows minimum stifness amongs the lattices with 21% porosity, which is an essential parameter of osseointegration. And the diamond lattice exhnited maximum stiffness with14% porosity.

Despite exhibiting infinite fatigue life for all the lattice implant designs, the differences in the implant stifnesses indicates the importance of lattice structure in determining the transfer of stresses around the proximal femur to avoid stress-sheilding and restore natural stress distribution in the femur [11]. A futher investigation is underway to study the stress-shielding and assiciated bone loss for various lattice structures designed in the present investigation.

3.2 MRI-induced heating of implant

Fig. 8 shows the 3D results for the block simulation study described in section 2.1.7. The upper two plots show the e-field at 64 MHz along the cutplane x=0. The lower two plots show the same e-fields in a dB scale to give better insights on the fields within the lattice structure.

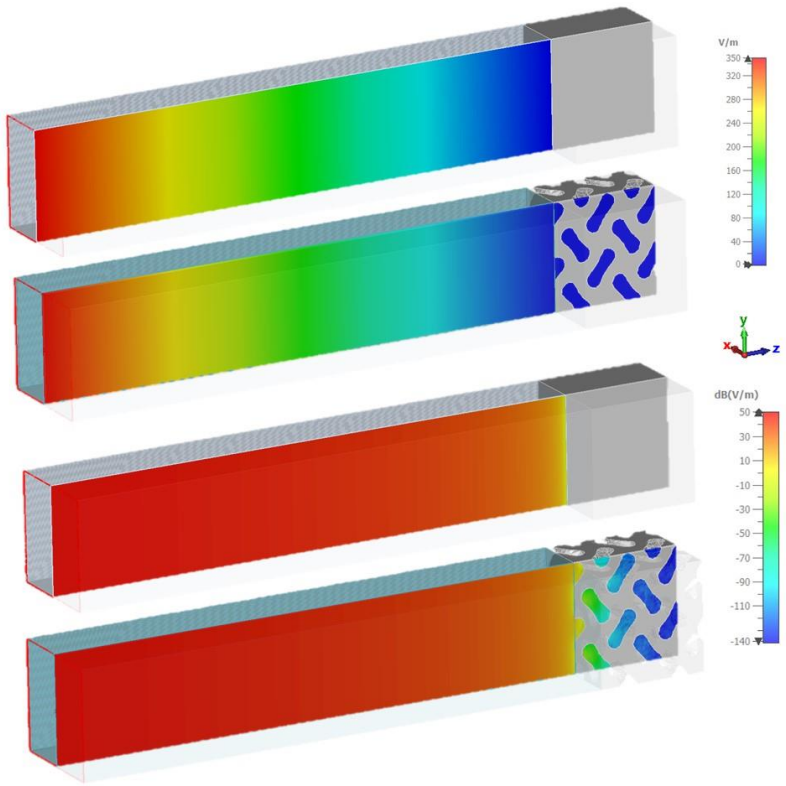

Fig. 8 2D electric field at 64 MHz for PEC blocks

In case of the non-lattice cube, the EM field attenuates as it travels through the section of bone and upon reaching the surface of the cube it drops down to zero as incident and reflected fields cancel each other out. This suggests that the cube does not absorb any field, neither does it allow any field to pass through it. In the case of the lattice cube, the holes in the cube act as pathways for EM waves to travel.

But since the dimensions of these holes are too small compared to the wavelength of the RF field of the MRI at 64 MHz, the strength of EM waves that are able to enter these holes is negligible.

The fields plotted in dB show the degree to which the fields have been attenuated. Fig. 9 shows the same fields in a 1D plot on a linear and dB scale. Hence it can be said that the lattice cube behaves similar to a solid cube, and that the lattice structure creates very lttle effect on the EM waves at 64MHz.

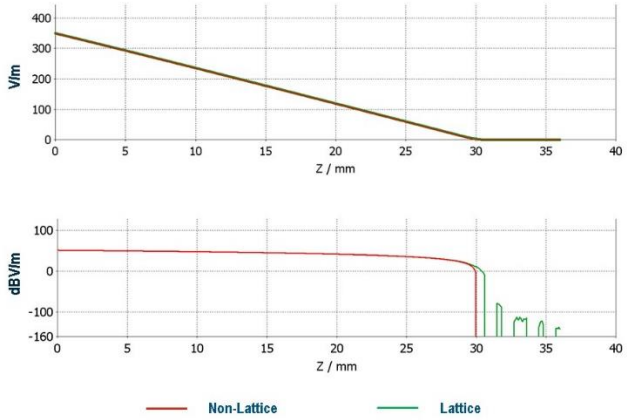

Fig. 9 1D electric field at 64 MHz for PEC blocks

Fig. 10 shows the results of the transient electromagnetic simulations giving insights into the electric field distribution across the implants which seem to be quite similar. Fig. 11 shows the results for the transient thermal simulations after 15 minutes of continuous exposure to MRI fields. Both the lattice and non-lattice implants seem to have similar thermal performance with the lattice implant being slightly hotter (40.8 degrees Celsius) compared to the non-lattice implant (40.63 degrees Celsius).

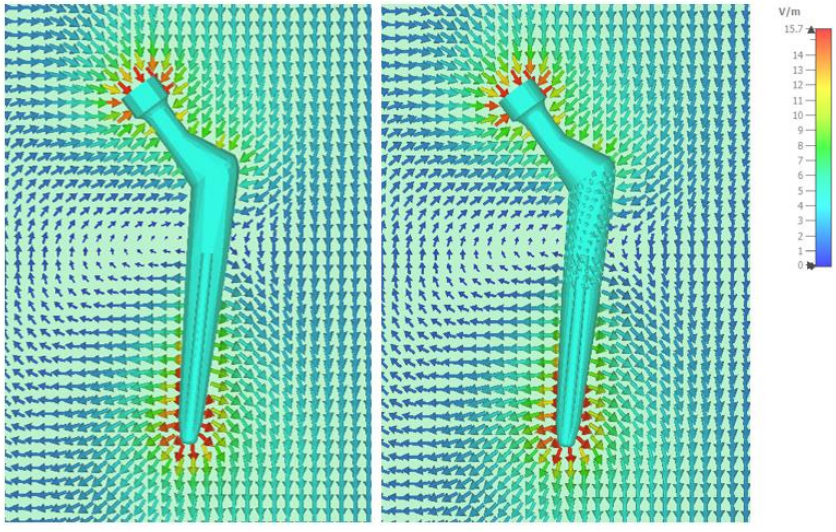

Fig. 10 3D electric field at 64 MHz for full implants

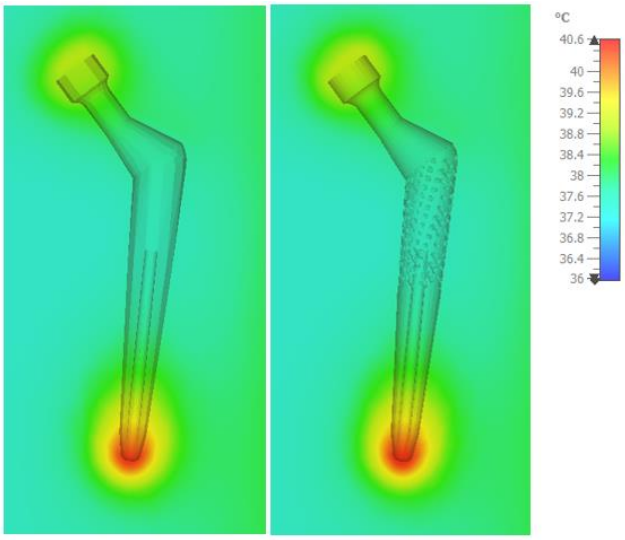

Fig. 11. 3D temperature results for full implants

Further studies were carried out to study the temperature rise in the implants when excited with different ON/OFF cycles. Fig. 12 shows the results for a flat 1 hour MRI exposure compared to three ON/OFF cycles :a. ON for 2 minutes, OFF for 18 minutes, b. ON for 5 minutes, OFF for 15 minutes, c. ON for 15 minutes, OFF for 5 minutes.

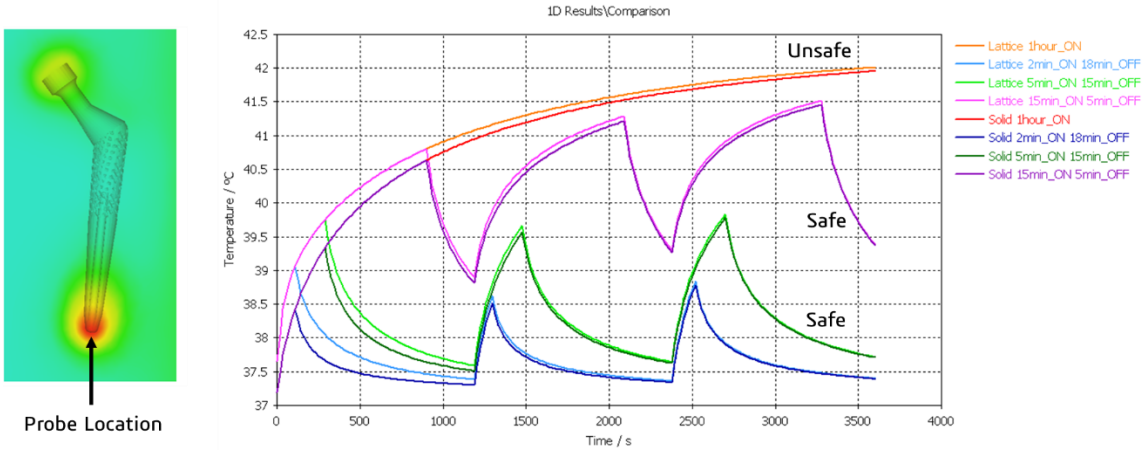

Fig. 12 Full implant temperature 1D results with various MRI cycles

Although titanium alloys are paramagnetic, sufficienly long exposure to MRI may induce implant heating. Therefore, the labelling of these implants indicating the conditions under which they are safe, is a crucial aspect for the implant manufacturer. It can be seen in the Fig. 12 that the both the lattice and the solid implant heat upto 42˚C under the continous 60 min MRI cycle. However, the implant heaitng is significantly reduced for the other cycles.

These results give us insights about how a specific lattice design compares to a traditional non-lattice implant. Further studies need to be performed to study how different lattice designs affect both the durability and termperature of the implant. Also, in addition to placing a single temperature probe at the most critical point on the implant, placing these probes at other non-critical locations can help us understand how the overall temperature distribution around the implant is influenced due to the presence of the lattice structure.

4 Conclusions

In conclusion, the present study explores the interplay between the structural integrity and MRI safety of hip implants through a multiphysics approach. In this study, the authors evaluated various porous implant designs for their durability and MRI safety. The findings reveal that the lattice structure significantly influence the implant stiffness indicating their role in determining the transfer of stresses around the proximal femur to avoid stress-sheilding and restore natural stress distribution in the femur. While the results indicate that lattice design does not significantly affect implant heating during MRI scans, the number of MRI cycles plays a substantial role in temperature changes. These findings underscore the importance of further research to clarify the balance between implant durability and MRI safety across different designs, ultimately contributing to the optimization of hip implant performance.

5 References

[1] L. Okafor and A. F. Chen, “Patient satisfaction and total hip arthroplasty: a review,” Dec. 01, 2019, *BioMed Central Ltd*. doi: 10.1186/s42836-019-0007-3.

[2] J. M. Dias, F. S. C. P. da Silva, M. Gasik, M. G. M. Miranda, and F. J. F. Bartolomeu, “Unveiling additively manufactured cellular structures in hip implants: a comprehensive review,” Feb. 01, 2024, *Springer Science and Business Media Deutschland GmbH*. doi: 10.1007/s00170-023-12769-0.

[3] J. Feng, J. Fu, X. Yao, and Y. He, “Triply periodic minimal surface (TPMS) porous structures: From multi-scale design, precise additive manufacturing to multidisciplinary applications,” Jun. 01, 2022, *IOP Publishing Ltd*. doi: 10.1088/2631-7990/ac5be6.

[4] C. Pan, Y. Han, and J. Lu, “Design and optimization of lattice structures: A review,” Sep. 02, 2020, *MDPI AG*. doi: 10.3390/APP10186374.

[5] Z. Chen, Y. M. Xie, X. Wu, Z. Wang, Q. Li, and S. Zhou, “On hybrid cellular materials based on triply periodic minimal surfaces with extreme mechanical properties,” *Mater Des*, vol. 183, Dec. 2019, doi: 10.1016/j.matdes.2019.108109.

[6] Z. H. Lin, J. H. Pan, and H. Y. Li, “Mechanical Strength of Triply Periodic Minimal Surface Lattices Subjected to Three-Point Bending,” *Polymers (Basel)*, vol. 14, no. 14, Jul. 2022, doi: 10.3390/polym14142885.

[7] S. A. Naghavi *et al.*, “A novel hybrid design and modelling of a customised graded Ti-6Al-4V porous hip implant to reduce stress-shielding: An experimental and numerical analysis,” *Front Bioeng Biotechnol*, vol. 11, Jan. 2023, doi: 10.3389/fbioe.2023.1092361.

[8] CDRH, “Testing and Labeling Medical Devices for Safety in the Magnetic Resonance (MR) Environment Guidance for Industry and Food and Drug Administration Staff Preface Public Comment.” [Online]. Available: https://www.regulations.gov.

[9] G. M. Noetscher *et al.*, “An in silico testbed for fast and accurate MR labeling of orthopedic implants,” vol. 12, p. 90440, 2023, doi: 10.7554/eLife.

[10] J. Wooldridge *et al.*, “Gradient coil and radiofrequency induced heating of orthopaedic implants in MRI: influencing factors,” *Phys Med Biol*, vol. 66, no. 24, Dec. 2021, doi: 10.1088/1361-6560/ac3eab.

[11] S. A. Naghavi *et al.*, “A novel hybrid design and modelling of a customised graded Ti-6Al-4V porous hip implant to reduce stress-shielding: An experimental and numerical analysis,” *Front Bioeng Biotechnol*, vol. 11, Jan. 2023, doi: 10.3389/fbioe.2023.1092361.